DISSERTATION FOR THE DEGREE OF DOCTOR OF PHILOSOPHY (PHD)

The role of DRP1-a mitochondrial fission protein- in mitochondrial morphology rearrangement during neuronal differentiation

by Marvi Ghani

UNIVERSITY OF DEBRECEN

DOCTORAL SCHOOL OF MOLECULAR MEDICINE

DEBRECEN, 2024

DISSERTATION FOR THE DEGREE OF DOCTOR OF PHILOSOPHY (PHD)

The role of DRP1-a mitochondrial fission protein- in mitochondrial morphology rearrangement during neuronal differentiation

by Marvi Ghani

Supervisor: Dr. Tar Krisztina

UNIVERSITY OF DEBRECEN

DOCTORAL SCHOOL OF MOLECULAR MEDICINE

DEBRECEN, 2024

Table of contents

List of Abbreviations

AD	Alzheimer's disease
AKAP1	A-kinase Anchoring Protein
Anti/Rot	Rotenone/Antimycin A
ANXA1	Annexin A1
ATP	Adenosine triphosphate
Aβ	Amyloid-β
BDNF	Brain-derived neurotrophic factor
BPA	Bisphenol A
BSA	Bovine serum albumin
CAMK1α	Ca^{+2}/calmodulin-dependent protein kinase 1α
CCCP	Carbonyl cyanide m-chlorophenyl hydrazone
CDK	Cyclin-dependent kinase
cGMP	Cyclic guanosine monophosphate
dbcAMP	Dibutyryl cyclic-AMP
DC NPC	Down's syndrome adult mice
DDC	Dopa decarboxylase
DDIT4	DNA damage-inducible transcript 4 protein
DEGs	Differentially expressed genes
DMEM	Dulbecco Modified Eagle Media
DNM1L	Gene name for DRP1
DRP1	Dynamin related protein 1
DS	Down's syndrome
DSP	Dynamin superfamily
DUSP1/6	Dual specificity phosphatases 1 and 6

EDTA	Ethylenediaminetetraacetic acid
EPHA8	Ephrin type-A receptor 8
ERK1/2	Extra signal-regulated protein kinase 1 and 2
FAD	Flavin adenine dinucleotide
FBS	Fetal bovine serum
FCCP	Carbonyl cyanide-p-trifluoromethoxy phenyl hydrazone
Fis1	Fission protein 1
FLRT1	Leucine-rich repeat transmembrane protein
GAPDH	Glyceraldehyde-3-phosphate dehydrogenase
GED	GTP effector domain
GFP	Green fluorescent protein
GO	Gene ontology
GPM6A	Neuronal membrane glycoprotein M6-a),
GRIP1	Glutamate receptor-interacting protein 1
GTP	Guanosine Triphosphate
H_2O_2	Hydrogen peroxide
HBBS	Hanks' Balanced Salt Solution
HCA	High content analysis
HD	Huntington's disease
HES1	Transcription factor HES1
HES7	Transcription factor HES-7
HRP	Horseradish peroxidase
ID2	DNA-binding protein inhibitor ID-2
ID-4	DNA-binding protein inhibitor ID-4

IL33	Interleukin 33
IMM	Inner mitochondrial membrane
IMS	Intermembrane space
INSM1	Insulinoma-associated protein 1
iPSC	Induced pluripotent stem cells
JNK	c-Jun NH2-terminal kinase 1 and 2
LIMK2	LIM kinase 2
MAPK	Mitogen-activated protein kinase
MD	Middle domain
MDGA1	MAM domain-containing glycosylphosphatidylinositol anchor protein 1
Mff	Mitochondrial fission factor
Mfn1	Mitofusin-1
Mfn2	Mitofusin-2
MHtt	Mutant Huntington protein
MiD49/51	Mitochondrial dynamic proteins of 49 and 51 kDa
MITOL	A mitochondrial E3 ubiquitin MARCH V
MMP	Mitochondrial membrane potential
MMP	Matrix metaloproteases
mtDNA	Mitochondrial DNA
NAD+	Nicotinamide adenine dinucleotide
NES	Gene for encoding nestin protein
NeuN	Neuronal nuclear protein
NEUROG2	Neurogenin 2
NO	Nitric Oxide

NPCs	Neuronal progenitor cells
NRP1	Neuropilin-1
NSC	Neural stem cells
OCR	Oxygen consumption rate
OGA	O-GlcNAcase
OGT	O-GlcNAc transferase
OMM	Outer mitochondrial membrane
Opa1	Optic atrophy 1
PBS	Phosphate buffer saline
PD	Parkinson's Disease
PDI	Protein disulfide isomerase
PI	Propidium iodide
PI3K	Phosphoinositide 3-kinase
PINK1	PTEN-induced putative kinase 1
PKA	Protein kinase A
PLXA4	Plexin A4
PMSF	Phenylmethylsulphonyl fluoride
PolyQ	Polyglutamine
PPIA	Peptidylprolyl isomerase A
PQ	Paraquat
PTM	Post-translational modification
RA	Retinoic acid
RARα	Retinoic acid receptor alpha
RIPA	Radio immunoprecipitation assay
ROBO2	Roundabout homolog 2

ROS	Reactive oxygen species
SDS-PAGE	Sodium dodecyl-sulfate polyacrylamide gel electrophoresis
SENP5	Sentrin/SUMO- specific protease-5
siRNA	Small interfering RNA
SNAP25	Synaptosomal-associated protein 25
SOK1	Serine/threonine-protein kinase 25
SOX2	Transcription factor SOX-2
SRB	Sulphorhodamine B
SUMO	Small ubiquitin-like modifier
Sv2	Synaptic vesicle protein 2
SYN1	Syanpsin1
TCA	Tricarboxylic acid
TEM	Transmission Electron Microscopy
TH	Tyrosine 3-monoxygenase
TrkB	Tropomyosin receptor kinase B receptors
TRP	Tetracopeptide repeat
TUBβ3	Tubulin beta-III
Tuj1	Class III β-tubulin
VD	Variable domain

1. Introduction

Mitochondria divide during cell division to be distributed to the daughter cells. Even quiescent cells show mitochondrial division during cellular differentiation and cell growth or in response to external signals. The processes of mitochondrial division and fusion must be closely regulated, as the survival of a cell relies on maintaining a sufficient number of mitochondria within it. The mechanisms behind these processes are probably quite intricate due to the double membranes of mitochondria, which pose unique topological and energetic challenges (E. Smirnova, L. Griparic, D. L. Shurland, & A. M. van der Bliek, 2001). The three GTPases, Mitofusins (MFN1, MFN2) and OPA1, are vital in mitochondrial fusion (H. Chen, Chomyn, & Chan, 2005). In contrast, dynamin-related protein 1 (DRP1) and Fis1 have been recognized as fission machinery. (E. Smirnova et al., 2001). DRP1 is part of the dynamin superfamily (DSP). Dynamins are a family of large GTPases. Dynamin, the classical member of this family, coils around the endocytic vesicles and aids in separating them from the cell membrane (Hinshaw, 2000).

DRP1 contains four distinct regions. At the protein's N-terminus, there is a large GTPase domain vital for the binding and hydrolysis of GTP. After the GTPase domain is the middle domain necessary for the self-assembly of the DRP1 protein. Next is a variable domain with a B insert specific to DRP1 (Michalska, Duszyński, & Szymański, 2016). At the protein's C-terminus end, an effector domain (GED) is associated with GTP hydrolysis (Sesaki, Adachi, Kageyama, Itoh, & Iijima, 2014). Human fibroblast 5756-Ti cells modified to express a dominant negative form, DRP1 (DLPS39N), exhibited large, networked peroxisomes due to decreased GTP affinity (X. Li & Gould, 2003). X-ray structural analysis established that the S39 amino acid plays a crucial role in DRP1’s interaction with the α-phosphate of GTP. This residue is essential for GTP function as it is situated within the phosphate binding loop, also known as the P-loop. The sequence pattern (GSQSSGKSS) containing the underlined S39 residue is widely preserved. S39 plays a role in binding to the α-phosphate through hydrogen bond interaction via its backbone. Still, it does not interact with β-phosphate, unlike the corresponding serine residues in dynamin-1 at that position (Wenger et al., 2013).

Endogenous DRP1 is found in cell cytosol and, in certain stimuli, moves around the mitochondria and is vital in mitochondria division. Time-lapse imaging of cells transfected with DRP1 fused with green fluorescent protein showed assembly at specific sites of mitochondrial

division. Like the dynamin family, DRP1 wraps the mitochondria by forming a ring around it (E. Smirnova et al., 2001). Any imbalance in the mitochondrial fusion and fission cycle leads to various abnormalities, contributing to different neurodegenerative diseases such as Huntington's disease (HD), Alzheimer's disease (AD), and Parkinson's disease (PD). And also, in other diseases like cancer, cardiomyopathies, and several metabolic disorders (Oliver & Reddy, 2019; Reddy et al., 2011). The mutant huntingtin protein (Htt) binds with DRP1 and raises its enzymatic activity, which leads to excessive fragmentation and abnormal distribution of mitochondria in HD neurons. The abnormal interaction of mutant Htt and DRP1 causes mitochondrial damage and synaptic degeneration (Shirendeb et al., 2012). In Alzheimer's disease, DRP1 interacts with monomers and oligomers, and these atypical interactions advance as the disease progresses. Loss of neuronal branches and degeneration were observed in neurons containing Aβ oligomer aggregates, suggesting a potential link between oligomeric Aβ and neuronal degeneration (Manczak, Calkins, & Reddy, 2011). In Parkinson's Disease, mutated α-synuclein interacts with spectrin, a cytoskeleton protein causing alteration in F-actin dynamic. This altered dynamic causes dysfunctional mitochondria by relocating DRP1 (Ordonez, Lee, & Feany, 2018). There is still a lack of understanding about the cause of PD, but there are many indications that various disease mechanisms are linked to its development**.** These include α-synuclein misfolding and aggregation, neuroinflammation, excitotoxicity related to glutamate signaling, oxidative stress, and neuron cell death. Alongside these factors, mitochondrial malfunction is suggested as a critical process in PD as it plays a part in preserving cellular equilibrium and operation (Franco-Iborra, Vila, & Perier, 2016).

DRP1 plays a critical role in neurons' development, function, and viability. Mice with a specific deletion of *DRP1*$^{-/-}$ died soon after birth due to nervous system development issues (Ishihara et al., 2009). DRP1-perturbations displayed brain development defects, indicating the necessity of DRP1-mediated mitochondrial fission for neuronal development. In developing chick motor neurons, mitochondria became shorter over time alongside an increase in DRP1 expression (S. Y. Choi et al., 2013). Blocking DRP1 activity led to longer mitochondria, suggesting that increased DRP1 expression contributed to adjusting mitochondrial length during development. Conversely, cultured mouse cortical neurons are known to experience gradual elongation of mitochondria. A significant change occurs in mitochondrial structure during the conversion from somatic cells to induced pluripotent stem cells (iPSC). During reprogramming, the pro-fission factor DRP1

undergoes phosphorylation, and both its knockdown and inhibition hinder mitochondrial fragmentation and iPSC cell formation (Prieto et al., 2016). DRP1 is crucial in developing human iPSCs into cardiac mesodermal cells. Blocking DRP1 activity enhances the differentiation of induced iPSCs in cardiac cells, shifting mitochondrial behavior towards fusion and altering energy production from glycolysis to oxidative phosphorylation (Hoque et al., 2018).

Our findings highlight that shDrp1 displays a fused mitochondrial structure. DRP1/DNMIL (gene name for DRP1: UniprotKB) knockdown leads to an increase in genes related to the development of the nervous system. High-Content Analysis determined enhanced growth and formation of nerve cell projections, segments, and extremities in differentiated shDrp1 cells. This study sheds light on the process of neuronal differentiation linked to a decrease in ERK1/2 phosphorylation independent of dual specificity phosphatases 1 and 6 (DUSP1/6) in shDrp1 cells. Our research demonstrates that control cells undergo change in mitochondrial shapes while shDrp1 cells maintain highly fused mitochondria during differentiation. We also mention that control and shDrp1 cells exhibit similar responses to specific triggers for programmed cell death. We also show that reducing DRP1 leads to a decrease in huntingtin protein aggregate formation under experimental conditions. Our findings indicate that DRP1 plays a crucial role in neuronal differentiation. Knockdown of DRP1 leads to extensive changes in gene expression. It enhances RA-BDNF-induced neuronal differentiation in SH-SY5Y human neuroblastoma cells by enhancing longer neurites and more roots, neurite segments, and extremities by increasing cellular bioenergetics during differentiation. We also highlight the importance of the DRP1 GTPase domain and its role in maintaining mitochondrial morphology.

2. Review of Literature

2.1. Brief Overview of Mitochondria

Mitochondria are essential for maintaining cellular homeostasis as they undergo continuous fusion and fission cycles. Mitochondria are subcellular structures with a double membrane. They are crucial for intracellular signaling, apoptosis, and intermediary metabolism involving amino acids, lipids, cholesterol, steroids, and nucleotides. Their role is of utmost importance in cellular energy metabolism, encompassing fatty acid oxidation, the urea cycle, and the respiratory chain (a critical pathway for ATP production) (Chinnery & Schon, 2003). All eukaryotic cells contain mitochondria, which is an essential organelle. They play a significant role in cellular energy production, resulting in cell death. It is widely thought that they evolved from symbiotic predecessors and preserved a genetic code (mtDNA) containing 13 essential proteins for respiratory chain activity. Mitochondria contain inner and outer membranes and maintain a distinct aqueous region – the intermembrane space and the matrix–contributing to various critical cellular processes such as calcium signaling, cell growth, differentiation, regulation of cell cycle, and apoptosis. Fusion, fission, biogenesis, and autophagy processes carefully control the shape and positioning of mitochondria to maintain a stable population of mitochondria. Mitochondrial malfunctions have been associated with metabolic disorders, age-related diseases, neurodegenerative conditions, and heart and brain ischemic injuries (Osellame, Blacker, & Duchen, 2012).

The mitochondrial structure is defined as two lipid bilayers containing proteins. It consists of an external outer mitochondrial membrane (OMM), an intermembrane space, and a matrix surrounded by the inner mitochondrial membrane (IMM). The IMM undergoes extensive folding into cristae, significantly expanding the surface area of the membrane (Kotiadis, Duchen, & Osellame, 2014). Mitochondria was discovered in the late 19^{th} century. The function of providing energy by the chemiosmotic process of oxidative phosphorylation was established in the 1960s. Mitochondria have multiple crucial functions, such as synthesizing phospholipids and heme, maintaining calcium homeostasis, activating apoptosis and cell death, transmitting metabolic and stress signals, and combating the reactive oxygen species (ROS). Mitochondria form ATP by oxidizing proteins, fats, and sugars, catabolizing them into acetyl-CoA, and then entering the mitochondrial matrix for the TCA cycle. Sugars first go through glycolysis in the cytosol and convert into pyruvate, which is then converted into acetyl CoA by the enzyme

pyruvate dehydrogenase. Various enzymes convert amino acids into pyruvate, acetyl-CoA, or citric acid cycle intermediates. However, beta-oxidation converts fatty acids into acetyl CoA inside the mitochondria (Chan, 2006b).

2.2. Functions of mitochondria

In the tricarboxylic acid (TCA) or citric acid cycle, two carbon acetyl groups combine with four carbon oxaloacetates to form citrate, a six-carbon compound. Through seven subsequent enzymatic steps, citrate is oxidized back to oxaloacetate while releasing excess carbon in the form of two molecules of carbon dioxide and transferring electrons to cofactors, such as nicotinamide adenine dinucleotide (NAD^+) and flavin adenine dinucleotide (FAD). This process frees up oxaloacetate for further participation in the cycle, whereas NADH and $FADH_2$ carry away liberated free energy to the mitochondrial electron transport chain.

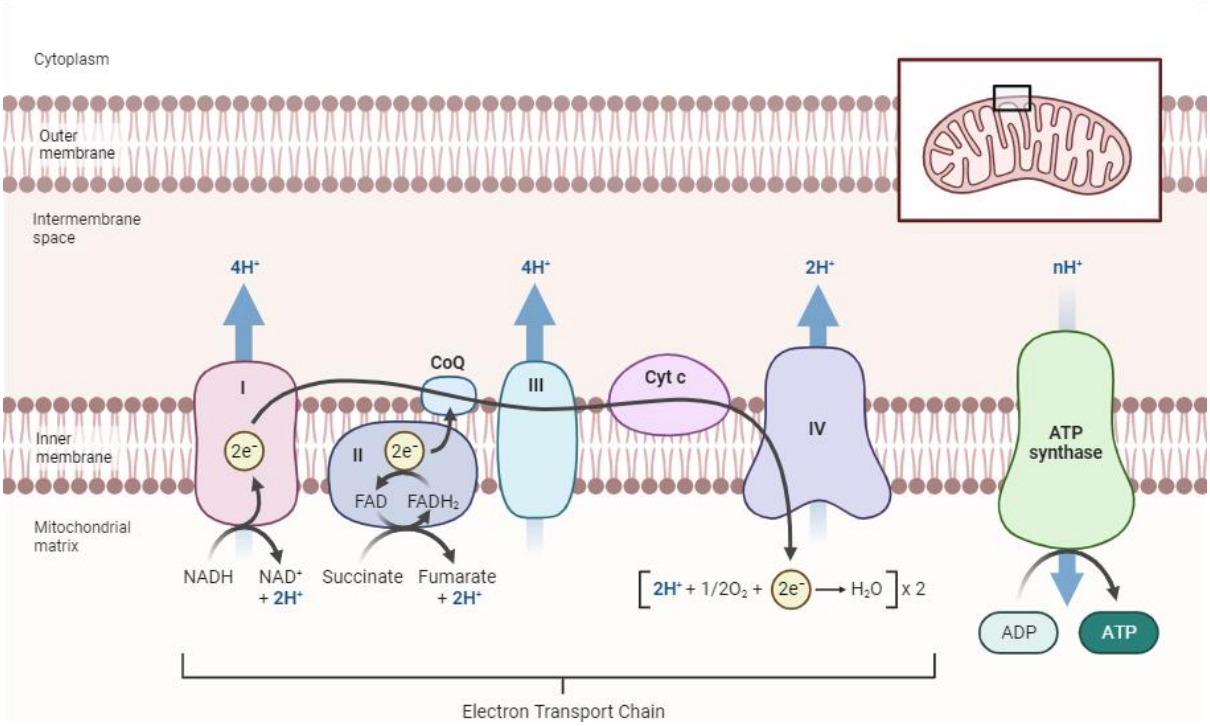

Fig. 1: ***The schematic representation of Electron Transport chain****. $NADH_2$ and $FADH_2$, formed during the breakdown of carbohydrates, fats, and proteins in intermediate metabolism, transfer electrons to complex I and complex II. Electrons move through the complexes along an electrochemical gradient, transported by ubiquinone and cytochrome c via complex III and IV. ATP synthase or complex V forms ATP in the last stage of ETC.*

The electron transport chain, the respiratory chain, consists of multiple subunit protein complexes embedded in the inner mitochondrial membrane. The mitochondrial electron transport chain comprises five enzyme complexes (**Fig. 1**) (Biorender). Complex I is the largest complex containing 40 polypeptide components. The electrons extracted from the citric acid cycle through NADH and $FADH_2$ fuel the transport of protons from the matrix to complexes I and II. These electrons are then transferred to complexes III and IV through the mobile carriers ubiquinone and cytochrome c, respectively. The proton gradient in the intermembrane space creates a voltage gradient across the inner mitochondrial membrane. ATP-synthase eventually utilized this voltage gradient to generate ATP in the final stage. This process is oxidative phosphorylation (Osellame et al., 2012).

2.3. Mitochondrial dynamics

Mitochondrial dynamics indicate the dynamic processes of fusion, fission, and movement in the mitochondria. The dynamic nature of mitochondria, including fusion, fission, and distribution, is closely associated with mitochondrial function and inheritance. Mitochondria can form complex networks within the cells, ranging from interconnected threads to smaller fragmented structures. Fission produces smaller organelles, which is crucial for the efficient movement and organization within cells to ensure the inheritance of a population of mitochondria. Fusion allows the material to mix between organelles to maintain a more functional and structurally uniform network. Kinesin and dynein motor proteins move the mitochondria along the microtubule network across the cytoplasm to deliver ATP to the organelle and to processes where ATP is needed, such as calcium homeostasis. Other processes associated with mitochondrial dynamics include quality control, metabolic state, and cell stress or disease state (Kraus, Roy, Pucadyil, & Ryan, 2021).

Mitochondria are dynamic organelles that appear as small spheres, long or short tubules, or interconnected tubules controlled by fusion and fission processes. The selective removal of dysfunctional mitochondria ensures a healthy population. Mitochondrial dynamics encompasses fusion, fission, selective degradation, and transport through the cytosol via the cytoskeleton (Chan, 2020).

Another aspect of mitochondrial dynamics is that they can form extensive tubular networks within a cell that facilitate the rapid exchange of mitochondrial contents or divide into individual rod-like mitochondria for deep penetration into the short diameter of neurites (Chan, 2006a).

Neurons, highly polarized and energy-demanding, require excessive energy for normal synaptic functions, axonal transport, and calcium homeostasis. Healthy mitochondria are transported to the synaptic region through anterograde movement via kinesin for these processes. However, damaged mitochondria are supplied back to the soma via retrograde movement with the help of dynein (Hollenbeck & Saxton, 2005; Z. Li, Okamoto, Hayashi, & Sheng, 2004).

This dynamic balance of mitochondrial fusion and fission is crucial in controlling mitochondrial morphology, length, size, and number and regulating mitochondrial function and distribution. Therefore, it is unsurprising that mitochondrial fusion and fission changes significantly affect neuronal function. The prevalence of neuronal diseases associated with mutations in genes related to mitochondrial fusion/fission highlights the importance of a functional relationship between neuronal function and mitochondrial dynamics (Chan, 2006a).

2.4. Description of components of the mitochondrial machinery

2.4.1. Fusion proteins

Mitochondrial fusion involves tethering and fusion of the neighboring mitochondrial outer membranes, followed by inner membrane fusion. This process allows components within different mitochondrial sub-compartments to mix, promoting mitochondrial health and uniformity (Meeusen, McCaffery, & Nunnari, 2004). It enables mtDNA maintenance, genetic exchange, complementation, and compensation for the depletion of metabolic substrates (H. Chen & Chan, 2009). Fusion proteins MFN1, MFN2, and OPA1 are essential components that regulate mitochondrial fusion. MFN1 and MFN2 are transmembrane GTPases located in the outer mitochondrial membrane. These proteins facilitate the fusion of the outer mitochondrial membrane by tethering adjacent mitochondria together and promoting the fusion of their outer membranes, enabling the exchange of contents and bioenergetic complementation. In contrast, OPA1 is an inner mitochondrial membrane protein involved in the fusion of the inner mitochondrial membrane. It regulates cristae structure within the mitochondria, which is critical for the integrity of the mitochondrial inner membrane and optimization of oxidative phosphorylation efficiency (Jodi Nunnari et al., 1997).

Hyperfusion of the mitochondrial network is considered a protective mechanism during mild stress as it increases ATP production (Tondera et al., 2009), blocks mitophagy, and delays cell

death (Gomes, Benedetto, & Scorrano, 2011). Stress-induced hyperfused states are observed under oxidative stress and nutrient depletion, where oxidized glutathione promotes hyper-fusion (Shuttt, Geoffrion, Milne, & McBride, 2012).

2.4.2. Mitofusins

Proteins responsible for mitochondrial fusion were initially discovered in 1988 (H. Chen et al., 2003). Subsequent advancements in crystallography revealed that the crystal structures of MFN1 and MFN2 share a similar topological structure with an identity sequence of over 80% (Cao et al., 2017). MFN1, MFN2, and OPA1, which are GTPases from the dynamin family, mediate mitochondrial fusion. The process begins with membrane tethering facilitated by OMM, followed by IMM joining (**Fig.2**) (X. Zhou et al., 2021). *Mfn1* or *Mfn2* deficient mice die during mid-gestation.

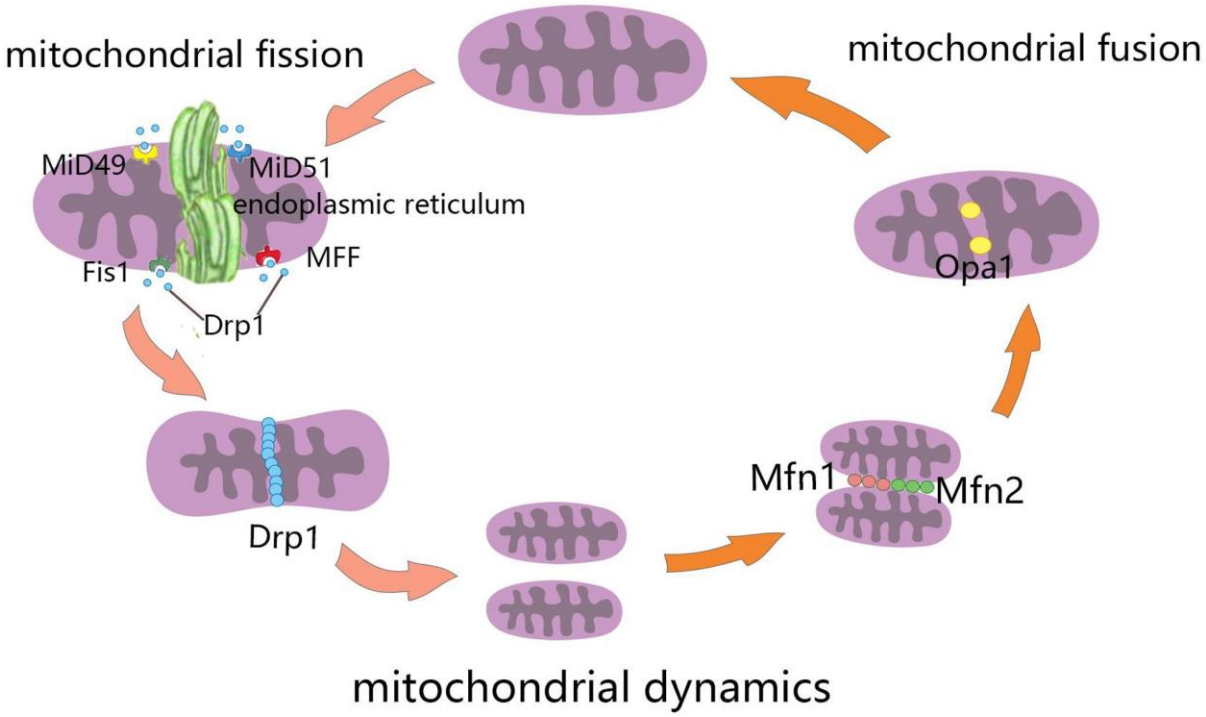

Fig. 2: ***Mechanism of mitochondrial dynamics.*** *DRP1, the most essential component of mitochondrial fission machinery, divides mitochondria into two daughter organelles. Four transmembrane receptors, MFF, MiD49/51, and Fis1, are required on OMM to recruit DRP1. Mitochondrial fusion is mediated by Mfn1 and Mfn2, which join OMM while Opa1 fuses IMM.*

Mfn1 deficient giant cells exhibited typical characteristics, in contrast to the specific and severe disruption observed in the placental trophoblast giant cell layer of MFN2 mutant embryos. Cells

lacking either MFN1 or MFN2 exhibit fragmented mitochondrial networks and stochastic loss of membrane potential in some mitochondria (H. Chen et al., 2003). However, overexpression of either of the MFNs induces mitochondrial aggregation around the nucleus (Eura, Ishihara, Yokota, & Mihara, 2003).

2.4.3. OPA1

Mitochondrial OPA1, a large GTPase related to dynamins, is situated on the inner membrane, facing the intermembrane space. OPA1 has eight splice variants that are initially produced as precursor proteins. To aid the sorting of this protein into IMM, the precursor protein contains a mitochondrial localization sequence at the N-termini along with hydrophobic stretches that are eliminated by mitochondrial processing peptidases during import into the mitochondria. This generates the L-forms of OPA1 (Ishihara, Fujita, Oka, & Mihara, 2006). This form is embedded in the IMM facing the intermembrane space (IMS) with a GTPase domain, where it is further processed to generate S-forms either in IMS or in the matrix, depending on the splice variant (Duvezin-Caubet et al., 2007). The GTPase domain exposed to IMM participates in OPA1's tetramerization and higher-order self-assembly. Both L- and S-forms maintain a balance between these forms, which is critical for sustaining proper mitochondrial function within cells. GTP hydrolysis plays a crucial role in mitochondrial fusion activity, as fragmented mitochondria are linked to mutations in the GTPase domain. OPA1 is associated with autosomal dominant optic atrophy caused by haploinsufficiency. Numerous OPA1 mutations associated with dominant optic atrophy have been identified in the GTPase domain. This condition leads to the degeneration of retinal ganglion cells and optic nerve atrophy (Delettre et al., 2000). Moreover, OPA1 facilitates the fusion of the inner mitochondrial membranes and influences cristae morphology. As a result, it plays a key role in regulating crucial mitochondrial functions such as apoptosis and respiratory capacity through stringent cellular control mechanisms.

2.5. Mitochondrial fission proteins

2.5.1. Understanding DRP1: An introduction

DRP1, a dynamin-related protein, is a regulatory protein that plays a crucial role in mitochondrial dynamics. Its primary function is to promote mitochondrial fission, which involves the division of the mitochondria into smaller units. DRP1 is a cytosolic protein that translocates to the mitochondrial outer membrane in response to specific signaling events.

DRP1's involvement in mitochondrial dynamics significantly affects cellular function and health. Its role in regulating mitochondrial fission is essential for maintaining the balance between mitochondrial fusion and fission, which is critical for the overall mitochondrial function (Bleazard et al., 1999). In addition to its physiological activities, DRP1 has also been implicated in various pathophysiological processes, such as cardiovascular and neurodegenerative disorders. This highlights the importance of understanding the intricate regulation of DRP1 and its effect on cellular and organ dynamics. DRP1 has four domains: a GTPase, middle, variable, and GED (**Fig. 3**) (Zerihun, Sukumaran, & Qvit, 2023). The further details of these domains will be discussed later.

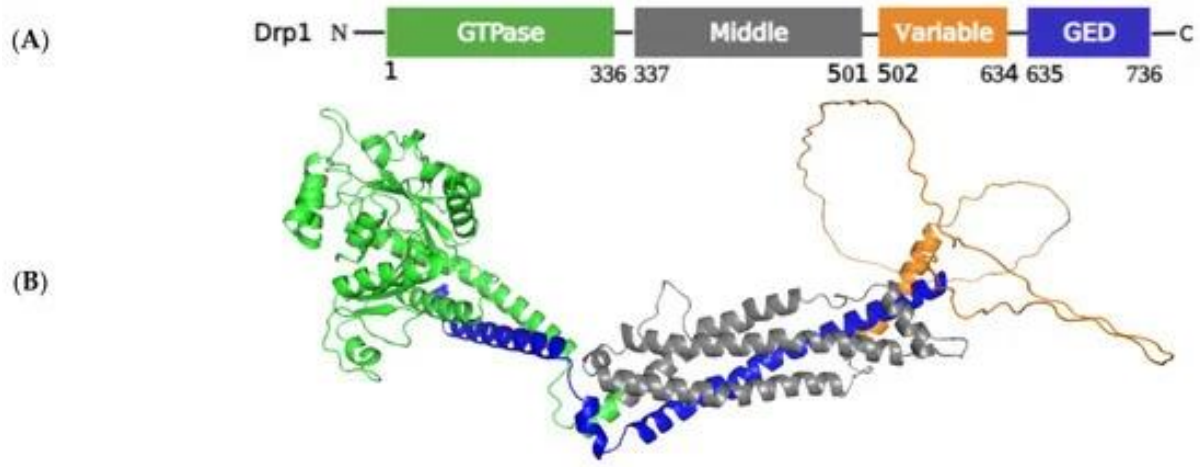

Fig. 3: ***Representative image of DRP1 structure****. DRP1 has a GTPase domain (Green) at the N-terminal and a GTPase effector domain (GED) at the C-terminal end (Blue). In between these two domains, DRP1 has a Middle domain (Grey) and a Variable domain (Orange).*

Mitochondrial fission is a multi-step process regulated by various adaptor proteins and large GTPases, and one of the critical regulators is DRP1 (C. Hu, Huang, & Li, 2017). Mitochondrial fission consists of four main stages: relocation of DRP1 to the mitochondrial outer membrane, subsequent formation of a higher-order complex, GTP hydrolysis, and disassembly (**Fig. 4**) (Zerihun et al., 2023). DRP1 attaches to receptors on the OMM and forms a functional assembly before being assembled into larger oligomers transported from the cytoplasm to sites where fission occurs (Otera & Mihara, 2011). DRP1 is recruited to the mitochondria by the endoplasmic reticulum, which aids in its transfer into the mitochondria (Ortiz-Sandoval, Hughes, Dacks, & Simmen, 2014). To eliminate dysfunctional mitochondria triggered by oxidative stress or damage (C. Hu et al., 2017), DRP1 is activated and translocated to the mitochondrial outer

membrane. Upon activation, DRP1 oligomerizes and forms higher-order structures, such as spirals or rings around the mitochondria to initiate fission. This constriction occurs at the same site where the endoplasmic reticulum interacts with mitochondria (Jonathan R Friedman et al., 2011). During fission, DRP1 interacts with other proteins in the OMM to facilitate mitochondrial division. Once DRP1 is recruited to the mitochondrial outer membrane, it binds to four receptors – mitochondrial fission factor (Mff), Mid49/51, and Fis1.

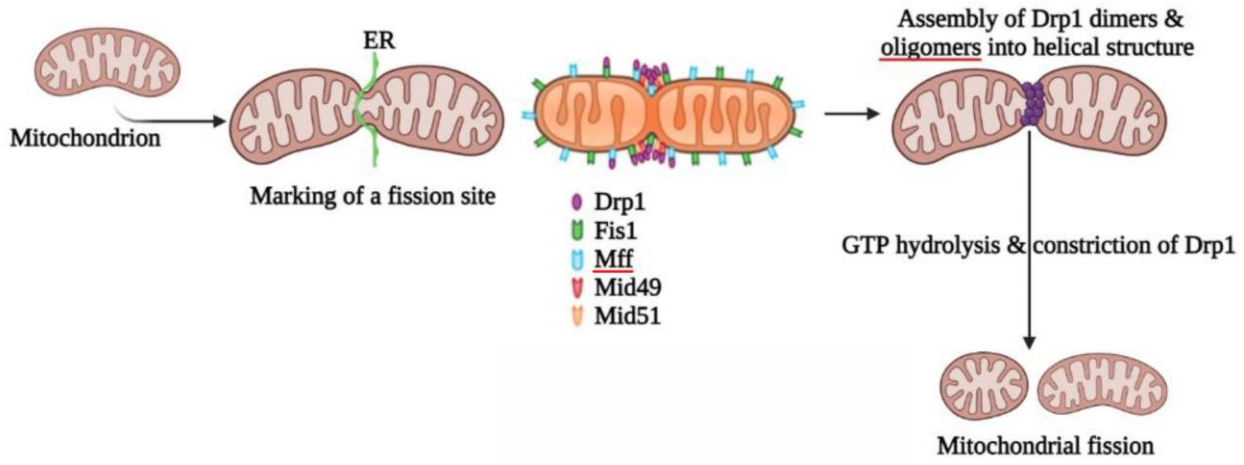

Fig. 4: ***Mechanism of DRP1 mediated mitochondrial fission****. During the process of mitochondrial division, the endoplasmic reticulum (ER) merges with mitochondria at specific sites. DRP1 is recruited to the cytosolic surface of mitochondria at these sites by Mff, Mid49, Mid51, and Fis1. DRP1 acts as a GTPase to facilitate the separation of the OMM, where DRP1 forms dimers or tetramers to generate a ring-like structure wrapping around the mitochondria, constricting it into two daughter mitochondria with the expense of GTP hydrolysis.*

Fis1 is a scaffold for OMM by creating oligomers and interacts with two tetratricopeptide repeat-like motifs on DRP1. The N-terminal section of Fis1 comprises a core domain that resembles a tetracopeptide repeat (TRP) (Scheel & Hofmann, 2005). The TPR pattern differs from conventional TRP motifs yet retains its significance in protein binding. It was initially thought that mammalian Fis1, which is highly conserved across species, operates similarly to its yeast counterpart. It was supposed to serve as a receptor for recruiting DRP1 to mitochondria, thereby promoting fission. Early studies indicated that overexpression of Fis1 led to significant mitochondrial fragmentation, while knockdown of Fis1 increased mitochondrial elongation, suggesting a pro-fission role for Fis1 (R. Yu, Lendahl, Nistér, & Zhao, 2020).

Mff was discovered in Drosophila melanogaster cells through small interfering RNA (siRNA) screen (Li Wang, Tu, & Sun, 2009). The Mff gene has at least nine isoforms (R. Yu et al., 2020).

Like Fis1, Mff comprises a C-terminal TM domain anchors to the OMM. Mff has an N-terminal domain with three short motifs (R1-R3) and a coiled-coil domain facing the cytosol. The first 50 N-terminal residues containing R1 and R2 motifs are highly involved in DRP1 recruitment to OMM- this is the minimal region required for DRP1/Mff interaction (R. Liu & Chan, 2015). Mff is essential for mitochondrial recruitment during fission, and its depletion limits mitochondrial fission and prevents DRP1 recruitment to mitochondria. In contrast, its overexpression recruits the bulk of DRP1 from the cytosol to mitochondria, promoting substantial mitochondrial fission. It is increasingly clear that Mff plays a primary role as it actively encourages mitochondrial fission in mammals (Losón, Song, Chen, & Chan, 2013).

Within humans, Mid49 and Mid51 exhibit 45 percent similarity in their amino acid sequence. They both contain an N -N-terminal TM domain that tethers them to the OMM, while Fis1 and MFF feature a C-terminal TM domain (T. Liu et al., 2013). Mid51 can attach to ADP and GDP, unlike Mid49. When Mid51 attaches to ADP, it can prompt DRP1 oligomerization, self-assembly, and GTPase activity. Additionally, Mid49 and Mid51 can potentially impact the interaction of DRP1 and Fis1 facilitating the accumulation of DRP1 on mitochondria (Losón et al., 2014). Cryo-EM analysis of DRP1 revealed four interfaces responsible for interacting with Mid49 and Mid51, providing compelling evidence for recruiting DRP1 to mitochondria. Heterologous Mid49 and Mid51 overexpression facilitates the capture of inactive DRP1 on OMM and promotes mitochondrial fusion. On the other hand, elevated endogenous levels of these proteins optimize OMM scission (Basu et al., 2017).

2.6. DRP1: Structure and function

2.6.1. GTPase Domain

The GTPase domain of DRP1 plays a role in the connection and breakdown of GTP and in creating a more complex structure on OMM. The process is mainly controlled by the 80-loop, a 16-amino acids section extending from the round GTPase domain. This loop facilitates linking between separate GTPase domains, and changes within this area prevent dimer formation (Lu et al., 2018).

2.6.2. Middle Domain

DRP1 MD (middle domain) and GED form part of the stalk. It is an intermediate region between the GTPase and V domain, and it is required for DRP1 self-assembly and the formation of higher-order structures (Chang et al., 2010). The central region plays a crucial role in enabling the self-organization of DRP1 into dimers, tetramers, and large assemblies. Analysis of dynamin and DRP1 crystal structures shows that four helices, three from the central domain and one from the GED, form a four-helix bundle that facilitates interactions between DRP1 molecules at the dimerization interface (Ford, Jenni, & Nunnari, 2011). It has been observed that genetic mutations in this specific area hinder DRP1's ability to form larger structures, leading to reduced assembly-stimulated GTPase activity (Chang et al., 2010). Significantly, a naturally occurring dominant harmful mutation (A395D) within this region has been associated with post-neonatal mortality in individuals with impaired brain development (Waterham et al., 2007).

2.6.3. GED Domain

The GED also called the C-terminal assembly domain, plays a crucial role in creating higher-order assembly and network complexes and works with the GTPase domain to enhance GTPase activity (Zhu et al., 2004). It promotes GTPase activity by folding back and binding with the N-terminal GTPase domain. Therefore, the GED domain has a low affinity for GDP and may not require typical regulatory proteins such as guanine nucleotide exchange factors or GTPase activating domains (Fukushima, Brisch, Keegan, Bleazard, & Shaw, 2001).

GED domain mutations prevent internal interaction with the GTPase domain and reduce DRP1's ability to perform GTP hydrolysis. The overexpression of GED domain mutants in mammalian cells increases the self-assembly of the protein, possibly due to the decreased binding activity with the GTPase domain, causing hindrance in mitochondrial fission (Zhu et al., 2004). A 27-year-old individual presented symptoms of static encephalopathy, a history of seizure, and nystagmus. A new genetic mutation in DRP1 Y691C within the GTPase effector domain was found in their cells. Overexpression of this mutant caused significant changes in the mitochondrial structure of muscle cells and distribution in a Drosophila model, resulting in clustered mitochondria near the perinuclear region and fewer mitochondria within muscle fiber cells (Batzir et al., 2019).

2.6.4. Variable Domain

DRP1 has multiple disordered regions, including the variable domain (VD) and the 80 loop. 80 loop is an 18-amino acid sequence that stabilizes G-domain dimerization. Isoform of DRP1 with different sequence inclusions in these areas leads to varied affinities for partner proteins and altered enzymatic stimulation (Hutson & Mears, 2024). During higher assembly formation, the DRP1 variable domain serves as a central point for guiding the arrangement of oligomerization. VD is highly flexible as it allows the formation of oligomers that can constrict and facilitate the DRP1 rings to wrap around the mitochondria. The variable domain works as a pleckstrin homology domain in the dynamin family, which is responsible for binding DRP1 to the mitochondria by interacting with cardiolipin, a specific phospholipid present in the mitochondria (Francy, Clinton, Fröhlich, Murphy, & Mears, 2017). Longer isoforms with full VD are primarily found in neuronal cells where slower rates of mitochondrial fission are observed, likely due to reduced enzymatic activity and decreased interaction with lipid and partner proteins influenced by the VD (Hutson & Mears, 2024).

2.7. DRP1 and post-translational modifications

Post-translational modifications of DRP1 involve phosphorylation, S-nitrosylation, SUMOylation, ubiquitination, acetylation, and O-GlcNAcylation. The complex nature of DRP1 phosphorylation at various locations contributes to its involvement in various mechanisms associated with multiple pathological conditions.

2.7.1. SUMOylation

The SUMOylation process, a post-translational modification similar to ubiquitination, has unique functional roles. Four mammalian isoforms are identified: SUMO1, 2, 3, and 4 (Saitoh & Hinchey, 2000). The small ubiquitin-like modifier protein (SUMO) regulates DRP1 activity through SUMOylation – a protein modification process known for either changing substrate subcellular localization or protecting them from ubiquitin-induced degradation. SUMO1 and its conjugating enzyme ubc9 are stabilizers for DRP1, thus stabilizing DRP1 at the OMM and advancing mitochondrial fission (Harder, Zunino, & McBride, 2004).

Influencing the stable attachment of DRP1 to the OMM, SUMOylation plays a crucial role in its regulation and significantly impacts its activity. This process triggers ER-mediated calcium flux, mitochondrial cristae remodeling, and cytochrome c release to trigger cell death (Prudent et al.,

2015). DRP1 forms a stable association with the mitochondrial membrane through quick recycling during the apoptosis process. SUMOylation occurs simultaneously independent of the DRP1 recruitment, which relies on BAX/BAK (Wasiak, Zunino, & McBride, 2007). Moreover, increased expression of mitochondrial SUMO E3 ligase promotes mitochondrial fission (Braschi, Zunino, & McBride, 2009), while loss of SENP3 prolongs DRP1 SUMOylation and inhibits cell apoptosis. while ectopic expression of sentrin/SUMO- specific protease-5 (SENP5) has opposing effects by facilitating deSUMOylation of DRP1 which reduces DRP1 levels. The overexpression of SENP5 reversed mitochondrial fragmentation induced SUMO1 in cultured cells, while impaired function of SENP5 leads to punctate organelles (Zunino, Schauss, Rippstein, Andrade-Navarro, & McBride, 2007).

2.7.2. O-GlcNAcylation

O-GlcNAcylation refers to adding O-linked N-acetylglucosamine groups to the cytoplasmic, nuclear, and mitochondrial proteins. In metazoans, this PTM plays a governing role. A pair of enzymes, O-GlcNAc transferase (OGT) and O-GlcNAcase (OGA) modulate the regulation of proteins by attaching and removing O-GlcNAc moieties. O-GlcNAcylation serves as a means to detect nutrient and oxidative stress (Yang & Qian, 2017). AD mice show increased activity of DRP1 O-GlcNAcylation. When N-acetyl-glucosamine activity is eliminated by blocking OGT, it decreases the O-GlcNAcylation of DRP1 activity in cells treated with Aβ. The O-GlcNAcylation of DRP1 decreases when overexpressing two defective forms of DRP1 lacking O-GlcNAcylation sites (at Thr-585 and Thr-586) within the variable domain. This overexpression subsequently decreases mitochondrial fragmentation in primary neurons treated with Aβ (S. J. Park et al., 2021).

2.7.3. S-nitrosylation

A vast majority of proteins are S-nitrosylated under physiological and pathological conditions. S-nitrosylation plays a significant role in mitochondrial fission. PDI (protein disulfide isomerase) mediated S-nitrosylation of DRP1 increases phosphorylation of DRP1 at S616, which increases the mitochondrial fission in CA1 neurons (Lee & Kim, 2018). In the S-nitrosylation process, nitric oxide (NO) reacts with thiol groups of proteins and modifies the cysteine residues of target proteins for enzymatic activity (Stamler, Lamas, & Fang, 2001). Mutant Huntington protein (mHtt) triggers the formation of SNO-DRP1. Moreover, S-nitrosylation becomes active at the

Cys644 site of the DRP1 GED domain. This activation then boosts the formation of DRP1 oligomers by increasing GTPase activity in neuronal cells, thus contributing to Huntington's disease pathology. Excessive mitochondrial fission, synaptic damage, and loss of dendritic connection were seen in HD postmortem brain samples and transgenic mice models due to elevated SNO-DRP1 levels (Haun et al., 2013).

2.7.4. Ubiquitination

In addition to the process of phosphorylation, recent studies have suggested that DRP1 activity could also be influenced by protein ubiquitination. Ubiquitination is a cellular process mechanism that regulates proteins intended for quality control. The mitochondrial E3 ubiquitin MARCH V (MITOL) was known to regulate mitochondrial dynamics and was initially proposed to promote mitochondrial fusion (Nakamura, Kimura, Tokuda, Honda, & Hirose, 2006). Karbowski et al. demonstrated MARCH V may support fission by aiding in the DRP1 subcellular transport and assembly of DRP1 to specific sites where mitochondria divide without impacting the DRP1 stability. Mutations in the RING domain of MARCH V disrupt the proper assembly of DRP1 at sites where mitochondria divide or hinder its disassembly, leading to observed mitochondrial fusion under conditions involving MARCH V RNAi-mediated knockdown conditions. (Karbowski, Neutzner, & Youle, 2007).

Elevated levels of MARCH V enhance its association with MFN2, leading to the stimulation of MFN2 and facilitating mitochondrial fusion. A study involving mutation showed that the elongation of mitochondria by MARCH-V relies on an intact RING finger, as a mutation in the Flag-RINGmut resulted in mitochondrial fragmentation. This points to the involvement of ubiquitin activity in influencing mitochondrial morphology. Additionally, MARCH-V acts as a ubiquitin ligase for DRP1 and specifically forms a complex with ubiquitinated forms of DRP1 under steady-state conditions. These discoveries suggest that increased ubiquitination of DRP1 may impede mitochondrial division, like GTPase-deficient mutants DRP1 (Nakamura et al., 2006).

2.7.5. Phosphorylation

Protein phosphorylation, facilitated by protein kinases with diverse substrate specificity, is a crucial post-translational modification utilized by cells to adjust protein function swiftly and integrate changes into cellular signaling pathways. Phosphorylation involves adding a phosphate

group to a chemical compound. Phosphorylation is a well-documented mechanism involved in the regulation of mitochondrial fission. PTMs of DRP1 have been extensively researched, and it has been found that they can either activate or inhibit the protein based on the specific modification site. Multiple phosphorylation sites such as S40, S44, S579, S585, S592, S616, S637 and S693 have been identified for DRP1. The most significant ones are S637 and S616 (Z. Qi, Huang, Xie, & Chen, 2019).

Initially, the phosphorylation at S616 by CDK1/cyclin B was reported to drive DRP1-dependent mitochondrial fission during mitosis, increasing mitochondrial fragmentation (Taguchi, Ishihara, Jofuku, Oka, & Mihara, 2007). Although this modification does not directly impact GTPase activity, it influences DRP1's interactions with other proteins, mediating the increased fission. Substantial advancements have been made in understanding the functional implications of phosphorylation on DRP1, providing compelling evidence that mitochondria dynamics are governed by phosphorylation through various signaling pathways such as CAMK1a, PKA, and CDK1/Cyclin B. Phosphorylation of S637 is believed to hinder GTPase activity by reducing the usual intramolecular interactions that promote GTP hydrolysis, unlike DRP1 phosphorylation S585 (C.-R. Chang & C. Blackstone, 2007).

DRP1 S637, which forms part of a consensus sequence that is widely conserved among metazoans. Initially, it was identified as a target for phosphorylation by protein kinase A, and its dephosphorylation is mediated by calcineurin (C. R. Chang & C. Blackstone, 2007). Subsequently, S637 was also recognized as a site for phosphorylation by Ca^{+2} calmodulin-dependent protein kinase 1α (CAMK1α). Several studies have demonstrated that modification of this site inhibits mitochondrial division through reduced GTPase activity and inhibition of DRP1 translocation to mitochondria. However, S637 phosphorylation by CAMK1α stimulates the mitochondrial translocation of DRP1 through an enhanced affinity between DRP1 and Fis1, leading to increased mitochondrial fragmentation (Han et al., 2008).

2.8. Role of DRP1 in differentiation and development

Mitochondrial dynamics play a crucial role in cell reprogramming and differentiation of iPSCs (H. W. Choi et al., 2015). Mitochondrial fission mediated by DRP1 is vital in differentiating embryonic cells in living organisms and cultured cells. Mice with complete DRP1 knockout cannot survive after 11.5 days of conception, and they show defective trophoblast giant cells

and reduced cardiomyocytes. DRP1 knockout cells displayed regular levels of intracellular ATP, resulting in cerebellar defects during postnatal development. Mice with a neural cell-specific knockout of DRP1 exhibited brain hypoplasia, while in vitro cultures of the forebrain showed decreased neurite numbers and abnormal synapse formation (Wakabayashi et al., 2009). DRP1-mediated mitochondrial fission plays a vital role in tissue development, particularly brain tissues. DRP1 heterozygote knockout ($DRP1^{-/+}$) mice show severely condensed mitochondria aggregated around the nucleus. The primary cells from these mice showed average growth rate and cellular respiration. However, severe defects were found in the Ca^{+2}-dependent apoptosis and synaptic functions, indicating the importance of DRP1 in neuronal cells (Ishihara et al., 2009). DRP1 null embryonic fibroblasts show an extensive, elongated network of mitochondria and peroxisomes. Purkinje cells from Dp1 deleted mice cerebellum show developmental defects (Wakabayashi et al., 2009). Cells with a partial reduction of DRP1 show similar characteristics as wild-type cells, including average lifespan and viability. Heterozygote DRP1 knockout mice show no defective mitochondrial, synaptic, or dendritic protein content (Manczak, Sesaki, Kageyama, & Reddy, 2012).

It signifies the importance of DRP1 in the functions of neurons and brain. Neurons are highly polarized cells, consuming ample amounts of ATP to generate synapses and axonal functioning at their terminal endpoints. DRP1-mediated mitochondrial fission is essential for these neuronal cells. A neuron-specific DRP1 variant, exon 3 containing the DRP1 variant from Dictyostelium discoideum, plays a significant part in the differentiation and development of neurons, as it only expresses in neuronal cells (Niemann, Knetsch, Scherer, Manstein, & Kull, 2001). The DRP1 depletion does not prevent the cells from differentiating from somatic to induced pluripotency stem cells (iPSCs). However, it does impact the terminal differentiation of iPSCs. The DRP1-depleted stem cells have no hindrance in proliferation or pluripotency efficiency. However, it showed a delayed response in the downregulating the pluripotency genes such as Nanog, Oct4 (Lei Wang et al., 2014).

Cell division and migration are essential cellular processes for maintaining mitochondrial dynamics during differentiation and cell maturation. For cardiac mesodermal differentiation, an extensive elongated mitochondrial network is required. DRP1 inhibition by shRNA or a specific DRP1 inhibitor, mdivi-1, turns the mitochondrial network into a highly filamentous and elongated mitochondria network, facilitating myogenic differentiation (Hoque et al., 2018).

The NO-dependent repression of DRP1 activity enhances the myogenic differentiation. NO/cGMP controls the activity of DRP1 by phosphorylating DRP1 and stopping DRP1-mediated fission activity, which forms elongated and networked mitochondria needed for myogenic differentiation (De Palma et al., 2010). Cell migration and differentiation are critical processes for neurons and many other types of cells. Mitochondria migrate toward the nucleus in the neural stem cells during the formation of brain regions. The DRP1 blockage in adult neural stem cells caused the condensation of mitochondria around the nucleus while maintaining the polarized distribution of mitochondria in the cells (H. J. Kim et al., 2015). During pluripotency, cells tend to remove degraded mitochondria through mitophagy, decreasing when cells exit the pluripotency stage and enter differentiation. A reduced expression of Parkin coincided with a decrease in DRP1 activity during differentiation, indicating that DRP1 is necessary (Pernaute et al., 2022).

2.9. Role of DRP1 in mitochondrial morphology during differentiation

There is a constant fusion and fission process in the mitochondria, which keeps its dynamic network. During differentiation, mitochondria change shape to elongated and then globular (H. W. Choi et al., 2015). The shape and distribution of mitochondria in the neural tube of chicken and mouse embryos at different stages of neurogenesis revealed that as neural progenitors transition to neurons, mitochondria are reshaping from small and round to thin and dense networks. This mitochondrial reorganization occurs across various cell types, indicating its general role in spinal cord neurogenesis. The observed small and round mitochondrial network in the neuroepithelium resembles what has been described for pluripotent cell types cultured in vitro. As the progenitor cells differentiate into neurons, mitochondrial length and network density increase, as well as indicating a shift from glycolysis toward oxidative phosphorylation supporting axonogenesis (Mils et al., 2015). DRP1 controls the retinoic acid-mediated transcriptional program of neuronal differentiation. Overexpression of DRP1 increases autophagy and apoptosis; however, DRP1 inhibition, either by silencing or overexpressing the dominant form of DRP1, causes the elongated shapes of the mitochondria during differentiation (Vantaggiato et al., 2019).

Cortical neurons and retinal ganglion cells showed tubular morphology, while cultured cortical astrocytes and non-neuronal cells in the retina displayed interconnected mitochondrial networks. An elevated level of DRP1 and Opa1 was observed in neuronal cells compared to

non-neuronal cells, partly contributing to the morphological differences. A neuron-specific splice variant (exon 3) of DRP1 was observed in cortical neurons. In cortical neurons, a knockdown or dominant-negative form of DRP1 increases the length of mitochondria, which leads to neuronal cell death (Uo et al., 2009). The role of DRP1 in myogenic differentiation discovered a potential link between mitochondrial behavior and muscle development. During myogenic differentiation, the expression of DRP1 increases and translocates to mitochondria, while inhibition of DRP1 activity leads to elongated mitochondria and increased apoptosis (B. Kim et al., 2013). During nervous system development, mitochondrial morphology changes. DRP1 protein partly controls the activity of the development of motor neurons in chick embryo formation, where an increase in the length of the mitochondria was observed (S. Y. Choi et al., 2013).

2.10. Role of DRP1 in apoptosis

During apoptosis, mitochondria are stimulated to undergo division and divide into smaller mitochondria. Overexpression of DRP1 mutant K38A blocks the fission of mitochondria by inhibiting the release of cytochrome c, indicating that DRP1 plays a direct or indirect role in apoptosis (S. Frank et al., 2001). According to Karbowski et al., DRP1 colocalizes with an apoptosis-initiating factor, Bcl-2 (Karbowski et al., 2002). During the process of apoptosis, BAX moves to the mitochondrial outer membrane and attaches to the focal points of OMM, which are the marked sites of the initiation of fission (**Fig. 5**) (Jenner et al., 2022). Another important factor for initiating apoptosis is the interaction of DRP1 and Fis1, a ligand-protein in the OMM. Inhibition of Fis1 blocks this interaction and apoptotic initiation. Fis1 blockage mainly blocks the BAX translocation, while inhibition of DRP1 blocks the release of cytochrome c (James, Parone, Mattenberger, & Martinou, 2003). Embryos lacking DRP1 fail to undergo apoptosis during neural tube formation in vivo. It is noted that these same embryonic fibroblasts usually respond to apoptotic stimuli when studied in vitro. This indicates that DRP1's apoptotic function may depend on specific physiological cues (Wakabayashi et al., 2009). Additionally, using *Drp1*$^{-/-}$ mice cells helped address several issues related to mitochondrial fission in Bax/Bak-mediated apoptosis. These indicate that while mitochondrial fission mediated by DRP1 is not vital for cytochrome c release and subsequent progression of apoptosis, it does facilitate these processes (Ishihara et al., 2009). LIM kinase 2 (LIMK2) decreases the DRP1 and DRP1 phosphorylation S616 and S637 to regulate the mitochondrial dysfunction in status

epilepticus. Overexpression of LIMK2 causes impairments in DRP1-mediated mitochondrial dynamics and leads to programmed necrotic neuronal death. LIMK2 modulates actin polymerization and cyclin D1 expression, and its overexpression potentially inhibits mitochondrial fission. LIMK2 regulates DRP1 expression and phosphorylation independently of actin polymerization, resulting in elongated mitochondria and decreased ATP production. These changes lead to necrosis rather than apoptosis. The direct mechanism by which LIMK2 regulates DRP1 is not known yet. However, it does regulate DRP1 by events related to the cell cycle (J. Kim, Ryu, Kim, & Kang, 2014).

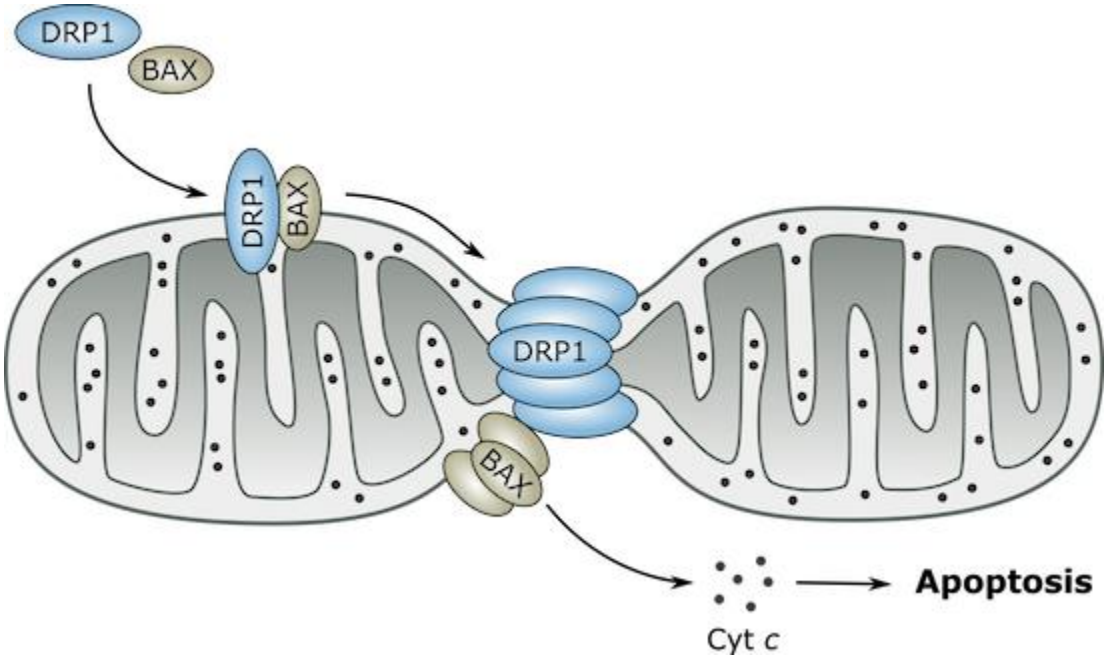

Fig. 5: ***A representative figure showing the interaction of DRP1 and BAX enhances apoptosis.*** *BAX/DRP1 make dimers to induce apoptosis, showing a noncanonical role of DRP1.*

2.11. SH-SY5Y cell line model for neuronal differentiation

In neuroscience and biology, having appropriate models plays a crucial role. Many *in vitro* models, such as rat PC12, rat B35, Neuro-2A, and neuroblastoma cell lines, provide good platforms for extensive research on neuronal cells. The results vary in different species' cell cultures but lack human components. For this purpose, we have used the SH-SY5Y human neuroblastoma cell line (Kovalevich & Langford, 2013), which is an inexpensive *in vitro* model to study neuronal behavior (Ioghen, Ceafalan, & Popescu, 2023). The SH-SY5Y cell line is a human-derived neuroblastoma cell line that has gained prominence in neuroscience research

due to its unique properties and versatile applications, especially in neuronal differentiation. Originating from a metastatic bone tumor biopsy of a four-year-old girl with neuroblastoma, the SK-N-SH cell line was established in 1970 (Biedler, Roffler-Tarlov, Schachner, & Freedman, 1978) and later subcloned to enhance its neuronal characteristics. SH-SY5Y cells exhibit several key characteristics that make them highly valuable for research. Cultures contain two types of cells, adherent and floating cells, but in most experiments, only adherent cells are used after discarding floating cells. The parental differentiated SHSY5Y cells comprised two distinct phenotypes: neuroblast-like and epithelial-like cells. The neuroblast-like cells express various catecholaminergic markers, such as tyrosine hydroxylase and dopamine-β-hydroxylase, while epithelial-like cells lack these markers (Ross, Spengler, & Biedler, 1983).

A crucial application of SH-SY5Y cells is their ability to undergo differentiation into mature neuron-like cells. This process is typically induced using a variety of chemical agents, growth factors, and environmental conditions. Differentiated SH-SY5Y cells exhibit enhanced neuronal characteristics, including extended neurites, increased expression of neuronal markers, and functional synaptic properties. Retinoic acid (RA) is one of the most widely used methods to induce differentiation in SH-SY5Y cells (Kovalevich & Langford, 2013). RA metabolite of vitamin A plays a crucial role in growth and development. When SH-SY5Y cells are exposed to RA, they exhibit morphological changes such as neurite outgrowth and increased expression of specific neuronal genes such as synapse protein Sv2 and nuclear marker NeuN. RA-treated SH-SY5Y cells also show reduced proliferation rates, which indicates their transition from a proliferative neuroblast-like state to a differentiated neuron-like state (Agholme, Lindström, Kågedal, Marcusson, & Hallbeck, 2010). Brain-derived neurotrophic factor (BDNF) is another agent commonly used to promote neuronal differentiation in SH-SY5Y cells. BDNF, a member of the neurotrophin family of growth factors, supports the survival and differentiation of neurons. Treatment with BDNF enhances the neuronal properties of SH-SY5Y cells, including neurite outgrowth and synaptic connectivity (Teppola, Sarkanen, Jalonen, & Linne, 2016). BDNF is often used with other agents like RA to achieve more robust differentiation (Encinas et al., 2000).

The synaptic transmission is adjusted by signaling through RA and its receptor (RARα) in the hippocampus and sensory cortices. RARα binds brain-derived neurotrophic factor (BDNF)

mRNA splice isoforms, activating presynaptic tropomyosin receptor kinase B receptors (TrkB) (Thapliyal, Arendt, Lau, & Chen, 2022). RA promotes the expression of neurotrophin receptors and developing neurons in human neuroblastoma cell lines by controlling the activity of TrkB, a receptor for BDNF. The addition of BDNF to RA-pre-treated SH-SY5Y neuroblastoma cells triggers the activation of TrkB through tyrosine phosphorylation and encourages neuronal differentiation. In KCNR cells that produce BDNF mRNA naturally, treatment with RA leads to the expression of TrkB and differentiation without requiring additional BDNF (Kaplan, Matsumoto, Lucarelli, & Thielet, 1993).

RA treatment activates the PI3K/AKT signaling pathway, essential for neuroblastoma cell differentiation. Cells treated with the PI3K-specific inhibitor LY294002 result in impaired differentiation induced by RA, indicating a role in neural cell differentiation and supporting cell survival (López-Carballo, Moreno, Masiá, Pérez, & Barettino, 2002). Multiple pathways regulating neuronal differentiation activate and promote the expression of neuronal genes. Several MAP kinases, such as ERK1/2, JNK1, and p38α/β/γ, activate during these pathways (Singh et al., 2003). Moreover, JNK1 plays a vital role in RA-induced neurite outgrowth. RA treatment induces JNK1 activity within ten minutes and after a 24-hour period, which coincides with substantial neurite outgrowth (Y.-M. Yu, Han, & Lee, 2003). RA-induced neuritogenesis using SH-SY5Y human neuroblastoma cell line demonstrates the ERK1/2 phosphorylation persists for up to 96 hours, with MEK inhibition reducing this effect significantly (Miloso et al., 2004).

2.12. Neurodegeneration and Protein Aggregation: A Brief Overview

Etymologically, the term is derived from the prefix “neuro-,” which refers to nerve cells (i.e., neurons), and “degeneration,” which signifies a process of structural or functional deterioration in tissue or organs. Therefore, neurodegeneration strictly relates to any pathological condition primarily impacting neurons. In practice, neurodegenerative conditions encompass a diverse range of neurological disorders with varied clinical and pathological manifestations affecting specific subsets of neurons within distinct functional anatomical systems; they develop for unknown reasons and advance persistently. On the other hand, neoplasm, edema, hemorrhage, and nervous system trauma- conditions that are not primarily neuronal diseases – are not classified as neurodegenerative disorders (Przedborski, Vila, & Jackson-Lewis, 2003).

Many neurodegenerative disorders share common mechanisms that contribute to their development and progression. These include abnormalities in protein dynamics, oxidative stress leading to the formation of reactive oxygen species, impaired bioenergetics, and mitochondrial function, neuronal Golgi apparatus fragmentation, disruption of cellular and axonal transport, dysfunction of neurotrophins, and neuroinflammatory processes. These interrelated mechanisms create complex cycles resulting in cell dysfunction and death (Jellinger, 2009).

Aberrant interactions among proteins lead to the abnormal accumulation of misfolded proteins inside and outside cells, forming insoluble fibrils. These irregular protein deposits are characteristics of various neurodegenerative diseases. Several types of neurons are affected based on the specific protein involved, causing diverse clinical symptoms for each disease. However, some disorders can affect the same group of neurons. Similar clinical manifestations may result from genetic abnormalities due to complex interactions between genes and environmental factors. This triggers abnormal protein interactions or lesions, leading to dysfunction and death of nerve and glial cells, ultimately disrupting neuronal networks (**Fig. 6**) (H. Chen & Chan, 2009).

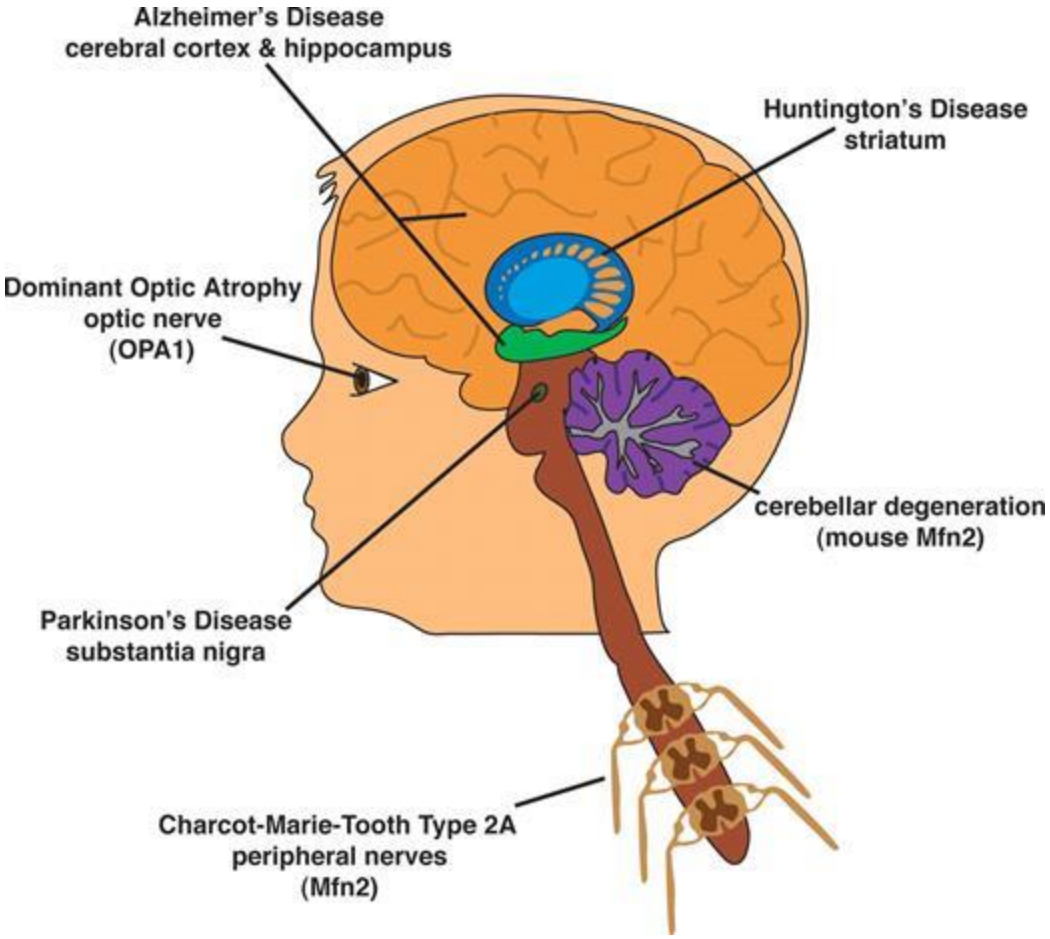

Fig. 6: ***Representative image indicating some neurodegenerative disorders along with areas affected.*** *Neurodegenerative diseases are severe conditions associated with defects in mitochondrial dynamics, which can lead to a wide range of implications for the neuronal system. The primary affected regions for each disease are indicated, but it is important to note that there is evidence suggesting more mechanisms are involved beyond these initial regions.*

2.12.1 DRP1 and Huntington's Disease

Huntington's disease is a lethal genetic disorder that causes involuntary movements, cognitive deterioration, and early mortality (Vonsattel & DiFiglia, 1998). It is characterized by the progressive decline of medium spiny neurons, mainly in the striatum and cerebral cortex, and the buildup of misfolded proteins within the nucleus. Huntington's disease is an inherited neurological condition arising from mutations leading to increased CAG repeat in the Huntington protein's polyglutamine (polyQ) region (Htt). The leading cause of Huntington's disease is a mutation in the huntingtin gene that increases the number of polyglutamine repeats in the Htt protein (Ghosh & Tabrizi, 2018). Htt protein, with a molecular weight of 350 kDa, is present in the central and peripheral nervous systems. Additionally, lesser amounts of Htt have been

observed in various subcellular organelles such as the nucleus, plasma membrane, ER, and mitochondria. Huntingtin protein regulates vesicular transport and synaptic transmission, but the mutated form, mHtt, causes neurotoxic effects, and an elevated expression results in immune response-mediated neurodegeneration (X.-J. Li & Li, 2011).

The repetition of polyglutamine leads to the misfolding of proteins and abnormal interactions between proteins. An essential aspect of Huntington's disease pathology is mitochondrial dysfunction caused by excessive division. Increased expression of DRP1 has been observed in the HD patient's striatum and cortex, generating mitochondrial dysfunction. The abnormal polyQ binds to DRP1's GTPase domain with greater affinity than normal polyQ in mice and human Huntington's disease patients' brains. Mutant Huntington (mHtt) abnormally interacts with DRP1 to OMM and then promotes GTPase activity, leading to excessive mitochondrial fragmentation. In HD neurons, excessive fragmentation disrupts the mitochondrial transport. Mitochondrial fragmentation increases by the interaction between DRP1 and mHtt. and the cells become more sensitive towards apoptosis in rat neurons and fibroblasts of HD patients.

HD manifests as a gradual decline in the ability to regulate movement, cognition, and emotional expression, along with other symptoms. The striatum and the cerebral cortex are the main regions affected by the degeneration. The peripheral blood cells of HD individuals have been observed with mitochondrial fragmentation. These patients show decreased levels of MFNs and Opa1 and elevated levels of DRP1 (Zhao, Sun, & Qi, 2018).

Mutant Htt also contributes to the increased production of NO. DRP1 s-nitrosylation results when NO attaches DRP1, causing increased mitochondrial fission and neuronal damage. Interestingly, this DNA-DRP1 has also been noticed in AD. Additionally, this research indicates that mutant huntingtin undergoes S-nitrosylation, potentially leading to transnitrosylation or transmission of NO onto DRP1 and subsequent S-nitrosylation of DRP1. The finding further suggests that s-nitrosylation in DRP1 might enhance DRP1 and mutant Htt interaction (Song et al., 2011).

Cherubini and his team recently found that in the striatum of HD mutant mice, the higher DRP1 activity starts increased mitochondrial fragmentation. This is also caused by disruption of the ER-mitochondrial association. Additionally, calcium homeostasis intracellular loss and an

increase in superoxide production in the mitochondria highlight the significance of DRP1 in HD pathogenesis (Cherubini, Lopez-Molina, & Gines, 2020).

Mutant Htt damages the mitochondrial membrane and causes calcium imbalance. Elevated cytoplasmic calcium levels may activate calcium-dependent protein phosphatase calcineurin through DRP1 dephosphorylation, leading to its association with mitochondria (Costa et al., 2010). Mitogen-activated protein kinase 1 can bind to DRP1 and phosphorylate it as S616, resulting in excessive activation of DRP1 in HD knock-in mouse-derived striatal cells (Z. Qi et al., 2019).

2.13. Potential Therapeutic Targets: Focusing on DRP1 inhibition

Neurodevelopmental delay and cognitive delay, the primary indicators of Down's syndrome (DS), are majorly due to mitochondrial dysfunctions. The neural progenitor cells from the DS mouse model revealed that cells had less functional mitochondria and compromised cell proliferation, indicating a promising connection between impaired mitochondria and neurogenesis disruptions. These cells showed increased mitochondrial fission and decreased fusion. When treated with mdivi-1, cells restored regular mitochondrial organization, cell proliferation, neuronal differentiation, and energy production (Valenti et al., 2017). The regulation of mitochondria involves maintaining their structure and function within cells. Research suggests that exposure to synthetic xenoestrogen bisphenol A (BPA) disrupts this balance, increasing oxidative stress and cellular damage in hippocampal neural stem cells. BPA also affects the proliferation and differentiation of these cells, but these effects can be mitigated by inhibiting Drp-1. This research highlights Drp-1 as a potential target for addressing BPA-induced disruptions in mitochondrial dynamics and neurodegeneration in the hippocampus (Agarwal et al., 2016). Paraquat (PQ), a widely used herbicide to control the effects of weed, was found to cause Parkinson's disease by increasing ROS production, decreasing mitochondrial membrane potential, and activating mitophagy pathways in neuronal cells. High levels of PQ caused excessive mitophagy and mitochondrial fission, which were ameliorated by the inhibition of DRP1 by mdivi-1 (N. Chen et al., 2021). Another study on the impact of paraquat on neurogenesis in primary murine neuronal progenitor cells (NPCs) shows that the cells treated with paraquat showed abnormal mitochondrial fragmentation induced by oxidative stress, increased expression of mitochondrial fission proteins, and decreased expression

of the fusion proteins. Using mdivi-1 reversed the adverse effects of this chemical on neurogenesis, neuron differentiation, and mNPC migration. (B. Zhang et al., 2023) DRP1 plays a crucial part in ischemic brain injury caused by glutamate toxicity or oxygen-glucose deprivation, which leads to neuronal cell death. In neuronal HT-22 cells, DRP1 siRNA and small molecule inhibitors effectively corrected mitochondrial fission, mitochondrial membrane potential (MMP) loss, and cell death induced by glutamate toxicity (Grohm et al., 2012). In Alzheimer's disease, inhibiting DRP1 reduces mitochondrial fragmentation, MMP, generation of ROS, and synaptic defects in neurons exposed to amyloid-β (Aβ) (Baek et al., 2017).

The compound mdivi-1 has been identified as an inhibitor of protein DRP1, leading to reduced levels of mitochondrial ROS and inhibition of LPS-induced cellular inflammation. However, a recent study suggests that the neuroprotective effects of mdivi-1 are primarily due to its regulation of mitochondrial function and intracellular calcium signaling rather than its interaction with DRP1 (Ruiz, Alberdi, & Matute, 2018). Additionally, it has been suggested that mdivi-1 may inhibit impairment in the mitophagy pathway in a model of traumatic brain injury (Wu et al., 2018).

Mdivi-1 rescues the characteristics of mitochondrial fragmentation by inhibiting GTPase activity, inhibiting mitochondrial fission. Additionally, a peptide-based DRP1 inhibitor known as P110 was shown to reduce excessive mitochondrial fission and ROS production in a PD model of primary dopaminergic neuronal cells by blocking DRP1 GTPase activity and DRP1 and Fis1 interaction (X. Qi, Qvit, Su, & Mochly-Rosen, 2013). Guo and team documented the impact of the P110 peptide inhibitor on mitochondrial fission in various models of HD. The results show that P110 prevented excessive mitochondrial fragmentation induced by mHtt, enhanced mitochondrial function, and boosted cell viability in HD fibroblast and mouse models (Guo et al., 2013).

Upon treatment with P110, a DRP1 GTPase activity selective inhibitor, mitochondrial fission was suppressed in response to various mitochondrial stressors, including MPP, CCCP, H2O2, and rotenone. P110 explicitly hinders the formation of tetramers required for fission. Additionally, it enhanced mitochondrial membrane potential and cell viability, reduced ROS levels, and preserved mitochondrial integrity in the presence of mitochondrial toxins. Furthermore, it decreased neuron cell death and improved neurite degeneration in Parkinsonism dopaminergic

cells experiencing neurite loss. It is well-recognized that increased DRP1 activity increases cell death and impacts mitophagy and neuronal survival (X. Qi et al., 2013).

Aims and Objectives

- This study investigates the role of Dynamin-related protein 1 (DRP1) on neuronal development and mitochondrial remodeling during differentiation.
- This study uses SH-SY5Y human neuroblastoma cells to analyze the effect of DRP1 knockdown on neuronal differentiation and morphology.
- This study explores the signaling pathways activated during neuronal differentiation and changes in other mitochondrial proteins related to the fusion/fission cycle DRP1 is stably depleted.
- This research will employ various methods, including High-Content analysis, transmission electron microscopy, RT-qPCR, and RNA sequencing, to assess the changes in differentiated and undifferentiated neuroblastoma cells.
- By addressing these objectives, the research hopes to lay the groundwork for future studies on mitochondrial dynamics, cellular ATP production, and neuronal death related to DRP1. Therefore, DRP1 could provide future insight into understanding the therapeutics for treating neurodegenerative disorders.

3. Materials and Methods

3.1. Cell culture

SH-SY5Y human neuroblastoma cells (European Tissue Culture), modified for DNM1L knockdown and control (unmodified), were cultured in high-glucose DMEM supplemented with 10 % fetal bovine serum (FBS), 2 mM L-glutamine, and 1x (V/V) antibiotic-antimycotic solution (Gibco), at 37 ºC in a 5% CO_2 incubator. HEK293T cells were grown in DMEM with conditions and supplements similar to SH-SY5Y cells.

3.2. *hDNM1L*/hDRP1 knockdown

We used a lentiviral technique to reduce the expression of h*DNM1L*/hDRP1 as described by (Abdennour Douida et al., 2020). HEK293T cells were seeded in a 24-well plate one day before the transfection. The cells were transfected with pGIPZ-GFP plasmids containing the target sequences and control plasmids (obtained from the shRNA facility of Albert Einstein College of Medicine, Bronx, NY, USA) and provided by Dr. Marion Schmidt. All the plasmid information is provided in Table 1. The packaging and enveloping vectors (HDM-Hgpm2, RC-CMV/Rev, HDM-tat1b, and HDM-VSV-G) were courtesy of Dr. Orsi Giricz (Albert Einstein College of Medicine, Bronx, NY, USA). Transfection was conducted using Lipofectamine 3000 (cat. L3000001, ThermoFisher Sci.) according to the manufacturer's instructions. Plasmids containing the target sequence were expressed in four replicates (wells). 25 ng/µl of each of HDM-MIX, HDM-Hgpm2, RC-CMV/Rev, HDM-tat1b and 50 ng/µl of HDM-VSV-G were used. However, 100 ng/µl of expression of plasmids were used. A 1:1 ratio of HDM-MIX and expression plasmid was used for co-transfection. Fluorescent microscopy confirmed the GFP expression in transfected cells after 24 and 48 hrs. Culture media containing the viruses were collected and filtered through 0.45 µm pore filters after 48 and 96 hrs of transfection. The collected media was used for transduction immediately.

The transduction of SH-SY5Y neuroblastoma cells was done using the following procedure: The cells were exposed to the virus in antibiotic-free media supplemented with 8 µg/ml polybrene and monitored under a fluorescent microscope daily to assess GFP expression. Selection with 1.25 µg/ml puromycin commenced 72 hrs after viral transduction. Subsequently, the puromycin-selected and amplified cells underwent additional real-time PCR and western blotting analysis to confirm h*DNM1L*/hDRP1 depletion.

Table 1. shRNA clone list used in this study

Gene ID	Gene symbol	Species	Vector	Marker	Sense strand sequence	Start	End	Target
10059	DNM1L	Human	pGIPZ	GFP	GTAAATTTCTTCACACCAA	436	454	CDS
None	GIPZ empty vector		pGIPZ	GFP	Empty pGIPZ vector (no shRNA)	-	-	-
None	GIPZ non-targeting		pGIPZ	GFP	Non-silencing shRNA sequence CTCGCTTGGGCGAGAGTAA	-	-	-

3.3. Titration of antibiotic selection

The concentration of the selected antibiotic was adjusted to identify the most effective dosage for selecting transduced target cells to establish a stable cell line effectively. SH-SY5Y cells were cultured in a 6-well plate until they reached 90% confluency. Various concentrations of puromycin (cat. 12122530, Gibco) ranging from 0 to 5 µg/ml were added to the complete medium. The cells were then incubated for 10 days with the replacement of the selection media every other day and observed daily under a light microscope. 1.25 µg/ml concentration initiated significant cell death within 7 days, leading to complete cell death by day 10. This specific concentration was chosen for subsequent selection and maintenance as it effectively sustained a stable cell line under selective antibiotic pressure.

3.4. Quick change mutagenesis

The mCherry-DRP1 S39A mutant was created using the manufacturer's quick-change site-directed mutagenesis protocol (cat. 200523, Agilent Technologies). The mCherry-DRP1 WT plasmid utilized in this research was a generous gift from Gia Voeltz (Addgene plasmid # 49152; http://n2t.net/addgene:49152; RRID: Addgene_49152) (J. R. Friedman et al., 2011). The following primers were used: 5' GCTTTCTAGCACTGAGGCCTTTCCGCTGCTCTGC 3' and

5’ GCAGAGCAGCGGAAAGGCCTCAGTGCTAGAAAGC 3’. The Center for Clinical Genomics and Personalized Medicine, a Core Facility of the University of Debrecen for sequencing (Debrecen, Hungary), confirmed this mutation. The mCherry control vector was a gift from Dr. György Vámosi (Department of Biophysics and Cell Biology, Faculty of Medicine, University of Debrecen, Hungary).

3.5. Transfection and generation of stable cell lines

Cells were transfected with the mCherry control, mCherry-DRP1 WT, and mCherry-DRP1 S39A plasmids using Lipofectamine 3000 (cat. L3000001, ThermoFishers Sci.) as per the manufacturer’s guidelines. Transfection efficiency was assessed by fluorescent microscopy to observe mCherry expression. After 72 hrs of transfection, cells underwent geneticin antibiotic selection at a concentration of 800 µg/ml (cat. 11811023, ThermoFisher Sci.) to establish stable cells expressing the recombinant proteins. The titration of antibiotics and cell scale-up followed previously documented methods (Abdennour Douida et al., 2020).

3.6. Neuronal Differentiation

The SH-SY5Y cells underwent differentiation following the method (Forster et al., 2016) described, with a slight modification. During phase 1 (days 0-3), the culture medium consisted of DMEM with high glucose (25 mM), 4 mM L-glutamine, and 1% penicillin/streptomycin (P/S) but without sodium pyruvate. Additionally, the media was supplemented with 10 µM RA and 3% heat-inactivated FBS. For phase 2 differentiation (days 3-6), Neurobasal-A medium without phenol red (cat. 21103049, ThermoFisher Sci.) supplemented with BDNF (cat. 450-02, Peprotech) at a final concentration of 50 ng/ml along with 1% N2 supplement 100x (cat. 17502048, ThermoFisher Sci) and 1% P/S was used. Cells were sampled or examined on Day 0 (before differentiation), after completing Phase 1 (Day 3), and Phase 2 (Day 6) of differentiation.

3.7. Live cell imaging

To stain the cells with neuron-specific ß-tubulin III, 5000 cells per well were seeded in a 96-well plate (Corning, Merck) coated with 5 ug/cm^2 laminin at 37 ºC for two hours before seeding cells. The control and shDrp1 cells underwent differentiation using the neuronal differentiation protocol (Section 3.6). On Day 6, cells were treated with 1 µM Tubulin Tracker Deep Red (cat. T34077, ThermoFisher Sci.) to observe neurite outgrowth and with 10 µM Hoechst 333642 for

nuclei staining for 30 minutes at 37 ºC and 5% CO_2. After staining, the cells were washed twice with Hanks' Balanced Salt Solution (HBBS), which contains calcium and magnesium (cat. 14025092, ThermoFisher Sci). Live cell images were captured at 37 ºC with a 5% CO_2 Opera Phoenix High Content Screening system (Perkin Elmer).

3.8. Neurite Analysis

Automated confocal microscopy was performed on an Opera Phenix High Content Analysis system. Image-acquisition settings were 40x water objective (NA = 1.1), and appropriate lasers and filters for Hoechst, eGFP, and Tubulin Tracker Deep Red were used sequentially to exclude spectra overlap. Neurites were detected with a 16-bit camera under nonsaturating conditions. Quantitative image analysis was performed with the built-in software (Harmony 4.9, PerkinElmer). Cell segmentation was based on Hoechst and eGFP staining to detect the nuclei and cytoplasm, respectively. The neurite analysis utilized the "CSIRO neurite Analysis 2" method of the Harmony 4.9 software as described by (D. Wang et al., 2010). The true nuclei were defined based on the Hoechst channel, while neurites were detected using the Tubulin Tracker Deep Red signal with the "Find-Neurites" building block. The length, width, and area units were defined as µm, µm, and μm^2, respectively. Other parameters were adopted from HCA built-in software functions and presented as arbitrary units; results are presented as mean ± SD normalized to the cell numbers based on true nuclei.

3.9. High Content Analysis parameters for neurite outgrowth

The parameters for analyzing neurite outgrowth were selected based on the "CSIRO Neurite Analysis 2" built-in method and from Wang et al., as summarized in Table 2.

Table 2.: List of defined parameters for neurite outgrowth analysis

Terms	**Definitions**
Maximum neurite length (µm)	The length of the longest path from a neuron body to an extreme segment.
Total neurite length (µm)	The sum of the length of each neurite segment for the cell.
Number of roots	The number of points where neurite structure touches a neuron body.

Number of nodes type 1	The number of branching points type 1 of each neurite tree.
Number of nodes type 2	The number of branching points type 2 of each neurite tree.
Number of segments	A segment is a linear structure between branching points or a neuron body.
Number of extremities	The number of terminating neurite segments.
Number of extremities vs cell number	number of extremities/number of objects

3.10. RNA Extraction

According to the manufacturer's instructions, total RNA was isolated using a TRI reagent (Molecular Research Center, lnc). Before reverse transcription with random primers, samples were treated with DNase I in a DNA digestion buffer for 15 minutes. The cDNA synthesis was carried out by reverse transcribing 1 µg of total RNA using a High-capacity cDNA Reverse Transcription Kit (cat. 4368814, Applied Biosystems). A quality check of cDNA was conducted by loading a 1 µl sample onto a 1% agarose gel.

3.11. Quantitative Real-Time PCR

Real-time PCR was carried out using a Lightcycler 480 Thermocycler (Roche) and Xceed qPCR Probe 2x Mix Hi-ROX (Institute of Applied Biotechnologies, IAB) per the manufacturer's instructions. The cycling conditions consisted of initial denaturation at 95 ºC for 30 seconds in one cycle, followed by PCR at 95 ºC for 5 seconds and 60 ºC for 30 seconds in 40 cycles. Subsequently, melt curve analysis was performed at 95 ºC for 0 seconds, 65 ºC for 15 seconds, 95 ºC for 0 seconds, and cooling at 50 ºC for 30 seconds in one cycle. CT values (threshold values) were normalized to GAPDH and/or PPIA, with each biological replicate including at least three technical replicates per gene in every sample. Gene expression fold change relative to undifferentiated cells was determined using the ΔΔCT method (Livak & Schmittgen, 2001). Table 3 enlists the primers used in this study.

Table 3. List of primers used in this study

Gene Name	Forward Sequence	Reverse Sequence	Ref.

hGAPDH	GAGTCAACGGATTTGGTCGT	GATCTCGCTCCTGGAAGATG	(Forster et al., 2016)
hDDC	GCAAGTGAATTCCGAAGGAG	CCCCAGGCATGATTATCTTC	(Forster et al., 2016)
hACHE	CCTCCTTGGACGTGTACGAT	AAACAGCGTCACTGATGTCG	(Forster et al., 2016)
hNES	AACAGCGACGGAGGTCTCTA	TTCTCTTGTCCCGCAGACTT	(Forster et al., 2016)
hPAX6	TGTCCAACGGATGTGTGAGT	TTTCCCAAGCAAAGATGGAC	(Forster et al., 2016)
hSNAP25	CTGCTCGTGTAGTGGACGAA	CGATCTGGCGATTCTGTGTA	(Forster et al., 2016)
hSOX2	AACCCCAAGATGCACAACTC	CGGGGCCGGTATTTATAATC	(Forster et al., 2016)
hSYN1	AATACTGGCTCTGCGATGCT	TGACCACGAGCTCTACGATG	(Forster et al., 2016)
hTUBB3	CATCCAGAGCAAGAACAGCA	CTCGGTGAACTCCATCTCGT	(Forster et al., 2016)
hPPIA	TTCATCTGCACTGCCAAGAC	TCGAGTTGTCCACAGTCAGC	(Forster et al., 2016)
hβ-Actin	GACCCAGATCATGTTTGAGACC	CATCACGATGCCAGTGGTAC	(Nagy et al., 2013)
hDUSP2	GGCCTTTGACTTCGTTAAGC	CCACCTCAGTGACACAGCAC	This study
hDNM1L Primer #1	CGCTGTCACTGCTGCTAATA	GACCATCTGGATCTACCTCTCT	This study
hDNM1L Primer #2	GGTCCTCGTCCTGCTTTATTT	GGGCTCTTCTAGACGTTTGATT	This study

3.12. Western Blotting

Cells were initially washed with 1x phosphate buffer saline (PBS) and then lysed in RIPA buffer containing 50 mM Tris-HCL Ph 7.4, 150 mM NaCl, 0.5 % Na-deoxycholate, 2 mM EDTA, 1% NP-40, and 50 mM NaF. The lysis buffer was supplemented with a 1 mM benzamidine, 1 mM PMSF, and a cOmplete Mini-EDTA-free protease inhibitor cocktail. Subsequently, the cells were centrifuged at 12,000 RPM at 4 ºC for 15 minutes to collect the supernatant for protein concentration estimation using a BSA protein assay. Following this step, wells containing 20 µg of protein were prepared and resolved on SDS-PAGE. The resolved proteins were then transferred to the nitrocellulose membrane (GE Healthcare Life Sciences) using the wet transfer method. Samples that received primary antibodies underwent overnight incubation at 4 ºC and afterward were incubated with secondary antibodies for two hours at room temperature. The blots were developed using an enhanced chemiluminescence western blotting detection system from Santa Cruz Biotechnologies. A list of antibodies and recommended dilution can be found in Table 4.

Table 4. List of antibodies used in this study

Antibody	Source	Catalog Number	Dilution
DRP1	BD Biosciences	611112	1:1000
MFN1	Abnova	HOOO55669 M04	1:1000
MFN2	Sigma Aldrich	WH0009927M3	1:1000
Opa1	Novus Biologicals	NB110-55290	1:1000
Akt	Cell Signaling	4691S	1:1000
P-Akt	Cell Signaling	4060S	1:500
SAPK/JNK	Cell Signaling	9252S	1:1000
P-SAPK/JNK	Cell Signaling	9251S	1:500
P38 MAPK	Cell Signaling	9212S	1:1000
P- P38 MAPK	Cell Signaling	9211S	1:500
ERK1/2	Cell Signaling	9102S	1:1000
P-ERK1/2	Cell Signaling	9101S	1:500
MEK	Cell Signaling	9122	1:1000
P-MEK	Cell Signaling	9121	1:500

Tuj1	Biolegend	801202	1:1000
Anti-HA (c29F4)	Cell signaling	3724s	1:1000
DRP1 p-S616	Cell signaling	3455	1:500
DRP1 p-S637	Cell signaling	6319	1:500
β-actin (C4)	Santa Cruz Biotechnology	SC-47778	1:3000
β-actin (C4) HRP	Santa Cruz Biotechnology	SC-47778 HRP	1:2000
TOMM20	Abcam	5683	1:500

3.13. Mitochondrial Staining for High Content Screening Live Cell Confocal Imaging

To label the mitochondria, laminin was applied to 96 well-plate at a concentration of 5 µg/cm^2 and incubated at 37 ºC for two hours before seeding 5000 cells in each well. The control and shDrp1 neuroblastoma cells underwent neuronal differentiation using the designated protocol. On Day 6 of the differentiation process, the cells were washed with 1x PBS and then stained with a solution containing 100 nM Mitotracker Red CMX ROS and 10 µM Hoechst 333242 in serum-free media for 20 minutes at an optimal temperature of 37 ºC, inside a 5% CO_2 incubator. Subsequently, fresh complete DMEM was added as replacement media prior to conducting live cell imaging using an Opera Phoenix High-Content Screening system by Perkin Elmer operating under consistent conditions of 37 ºC and 5% CO_2. The image-acquisition procedure entailed employing specific settings: usage of water objective lens rated at 63x magnification power with NA = 1.15; appropriate lasers along with filters were used for Hoechst staining, eGFP, and a detection signal from Mitotracker Red conducted sequentially to exclude any potential interference arising due to shared spectra overlaps. Image acquisition occurred via the employment of non-saturating conditions-driven operation facilitated using a 16-bit camera setup.

mCherry Control, mCherry-DRP1 WT, and mCherry-DRP1 S39A cells were added to cell carrier 96 ultra microplates at a density of 1.5 x 10^4 cell/well in DMEM high glucose medium until reaching 70% confluency. The cells were then incubated at 37 ºC in a 5% CO_2 environment with the addition of 50 nM Mitotacker Green (cat. 1829928, Thermofishers Sci) and 10 µM Hoechst 33342 in serum-free media for half an hour. Subsequently, the cells underwent two washes using

flourobrit media before live cell imaging was conducted using an Opera Phenix HCA System with adjustments made to maintain a temperature of 37 ºC and a CO_2 level of 5%.

3.14. Mitochondrial Morphology Analysis

Opera Phenix HCA system was used for live cell imaging. The system configuration included a water objective (63x, NA=1.15), and filters were adjusted for mCherry, Hoechst 33342, and Mitotacker Green for mCherry, mCherry DRP1, and mCherry DRP1 mutant S39A cell to prevent spectral overlap. However, for control and shDrp1 cells, eGFP, Hoechst 33342, and Mitotracker Red channels were selected. A 16-bit camera under nonsaturating conditions was used for imaging detection after determining the most suitable z-frame position. Image analysis used Harmony 4.9 software with different fluorescence staining for cell segmentation; Depending on the cell line, eGFP or mCherry identified the cytoplasm, Hoechst determined nuclei and Mitotracker green or Mitotracker Red delineated mitochondrial compartments and defined cytoplasm boundaries for each cell. Classification of mitochondria involved identification from deconvolved and preprocessed images using the find spots algorithm in the PhenoLogic machine learning system due to their varied shapes categorized into fragmented, long tubular, short tubular, compact tubular, and hyperfused forms.

3.15. Seahorse Assay

Oxygen consumption rate was assessed in undifferentiated cells at Day 0 and during phases 1 (Day 3) and 2 (Day 6), comparing the control and shDrp1 cells. For mCherry control, mCherry DRP1, and mCherry DRP1 S39A cells, the OCR was measured after 24 hours of cell seeding. Cells were plated in XF96 cell culture microplates with appropriate background correction wells, then incubated overnight at 37 ºC in a 5% CO_2 incubator. The following day, the media was changed to phase 1 media for cells undergoing phase 1 differentiation. On day 3, the media was replaced with phase 2 media for those undergoing further differentiation. Concurrently, the sensor cartridge was prepared a day before the assay by adding Seahorse Bioscience XF96 calibrant solution to each Seahorse Bioscience utility plate well in a non-CO2 incubator overnight. Measurement was conducted using the Seahorse XF96 Analyzer.

For XF cell Mito stress analysis on measurement day, the media was replaced with assay media supplemented with L-glutamine and glucose before an hour of incubation without CO_2. Oxygen

consumption rate measurements occurred every six minutes after twenty minutes of equilibration over five cycles: one minute of mixing followed by five minutes of measurement time. Mitochondrial inhibitors Oligomycin, FCCP, and Antimycin A/Rotenone were introduced sequentially with a final concentration of 1 µM, 1 µM, and 1 µM. The OCR values underwent normalization based on total protein concentration determined through quick Bradford protein assays using software such as Wave Agilent Seahorse. Statistical analysis relied upon GraphPad Prism.

3.16. Sulphorhodamine B assay

The cell viability assay using the sulphorhodamine B method was assessed after 24 hours of cell seeding in mCherry, mCherry DRP1, and mCherry DRP1 S39A cells. For control and shDrp1, the cells were further treated with RA and mitochondrial inhibitors such as Oligomycin, Antimycin A, and Rotenone in control and shDrp1 cells. Suphorhodamine B assay evaluates the cell viability by measuring the cellular protein content, and the calculation for cell viability was performed according to the formula % cell viability = Absorbance sample/ Absorbance negative control or untreated sample x 100, as described by (Vichai & Kirtikara, 2006).

3.17. Propidium Iodide Staining to Assess Cell Viability

Cell viability was evaluated for undifferentiated, Phase 1 and 2 differentiated control and shDrp1 cells by using propidium iodide (PI) at a concentration of 500 ng/ml, along with counterstaining with Hoechst at a concentration of 10 µM. In short, the respective differentiation media was removed, and complete DMEM containing PI at 500 ng/ml and Hoechst at 10 uM was added to the cells. The cells were then incubated for 15 minutes at 37 ºC in a CO_2 incubator with a level of 5%. Live cell imaging was conducted utilizing an Opera Phenix High Content Screening confocal microscopy system from PerkinElmer set to operate at an ambient temperature of 37 ºC and 5% CO_2. Image acquisition settings included using a 10x objective (NA=0.3), appropriate lasers and filters for Hoechst, and Alexa 568 specifically used for PI detection in sequential mode to eliminate any spectral overlap. Detection took place using a 16-bit camera under non-saturating conditions. The analysis stage involved utilization of the “Live/Dead cells” built-in method found within Harmony 4.9 software developed by Perkin Elmer that allows output data based on criteria such as true nuclei defined via the Hoechst channel, selection identification via Alexa flour 568 channel labeling it positive if stained while providing results when combined

according to this formula: (cells stained positive)= Alexa flour 568 /true nuclei) x 100 which calculated percentage representing dead cell count.

3.18. Immunofluorescence Staining

1.5 x 10^4 control and shDrp1 cells were plated in a 12-well plate and subjected to differentiation as outlined in the neuronal differentiation section of the material and methods. On days 3 and 6, both differentiated control and shDrp1 cells underwent standard fixation, permeabilization, blocking, and stained with Tuj1 antibody for neuron-specific Tubulin beta-III before being mounted on slides using Moviol 4-88: Dabco 33-LV (1:50) for imaging with a Leica SP8 confocal laser scanning microscope.

The 12-well plate was coated with 1% gelatin four hrs before cell seeding. After 24 hrs the cells were transfected with DRP1-mCherry and DRP1-mCherry mutant (S39A) plasmids using lipofectamine 3000 (cat. L3000001, Thermofishers Sci.) and incubated for 72 hrs. The cells were washed with 1X PBS three times, fixed with 3.7% paraformaldehyde (PFA), and permeabilized with 1X triton X-100 for 15 minutes each. After washing three times with 1X PBS, cells were stained with TOMM20 antibody (cat. Ab5683, Abcam) for one and half hours at room temperature and then with secondary antibody Alexa 488 (cat. A11001, Thermofisher Sci.) for one hour. The coverslips were mounted on the slides and subjected to oil-immersion 40x objective of SP8 Leica Laser Confocal microscope.

Approximately 7000 control and shDrp1 cells were seeded onto laminin-coated Perkin Elmer microplates for transient transfection experiments. The following day, transient transfection was carried out with pHM6-Q23 expressing wild-type N-terminal Huntington fragment and pHM6-Q74 expressing mutant N-htt Huntington fragment using lipofectamine 3000 as per the protocol by (Aladdin et al., 2020). After a 72-hour incubation period, cells were fixed, permeabilized, and processed for antibody staining before analysis using an Opera Phenix High Content Screening System from Perkin Elmer.

Image acquisition settings included a water objective with appropriate lasers for Hoechst, eGFP, and Alexa 568 channels under nonsaturating conditions. Images were further analyzed in Harmony software provided by PerkinElmer for nuclear segmentation on Hoechst channel is extended borders of eGFP object followed by insoluble Huntington protein fragments segmented upon Alexa 568 channel using an embedded spot analysis module of Harmony 4.9 software. The results are reported as mean ± SD.

3.19. Transmission Electron Microscopy (TEM)

The Aclar thermoplastic film (EMS-Electron Microscopy Sciences) was used to grow control and shDrp1 monolayers. Cell pellets were fixed for one hour at room temperature in 3% glutaraldehyde dissolved in 0.1 M cacodylate buffer (Ph: 7.4) containing 5% sucrose. After washing the cells multiple times in cacodylate buffer with a pH of 7.4, the samples were subsequently fixed in 2% osmium tetroxide dissolved in 0.1 M cacodylate buffer (Ph: 7.4) for an hour at room temperature. After further washing in cacodylate buffer (pH: 7.4), the cells underwent dehydration and embedding, not Durcupan ACM resin. Ultrathin slices were prepared and gathered on single-slot grids coated with Formvar, then stained with uranyl acetate and lead citrate. The sections were examined using a JEOL 1010 transmission electron microscope and captured at a magnification ranging from 5000-30000x with an Olympus Veleta CCD camera. Cell and mitochondria outlines were manually delineated. Only mitochondria with observable and intact internal membranes were included for subsequent analysis. Amira 3D (version 2022; ThermoFisher Scientific) imaging software was utilized to assess the numerical characteristics of the outlined structures, including the visible area (μm^2) of the cell in a specific image, as well as the total (summed) and average area (μm^2) and inside length (μm) of mitochondria within the observable part of the cell.

3.20. Human phospho-Kinase Array

Relative protein expression was obtained by analysis of 43 specific phosphorylation sites using the proteome profiler human phospho kinase assay (cat. ary003b R & D systems) according to the manufacturer's protocol. Briefly, the cells were either treated with DMSO or 10 μM RA for three days and on the day of assay, the cells were washed with 1x PBS and solubilized with lysis buffer for 30 minutes on a shaker at 4 ºC. After blocking, membranes with capture antibodies were incubated with samples overnight at 4 ºC. After that, the biotinylated antibodies were added for 2 hours at room temperature. The membranes were exposed to streptavidin HRP/ chemiluminescence substrate, and images were taken using a ChemiDoc imager at different exposure times.

3.21. RNA-Seq method

A high-throughput mRNA sequencing analysis was conducted using an Illumina sequencing platform to acquire comprehensive transcriptomic data. Total RNA was isolated from T-75 flasks

containing control and shDrp1 cells at 90 % confluency following the protocol provided by Zymo Research. The quality of total RNA samples from both control and shDrp1 cells was assessed using the Eukaryotic Total RNA Nano Kit on Agilent Bioanalyzer according to the manufacturer's instructions. Samples with an RIN value exceeding 7 were deemed suitable for the library preparation. The generation of RNA-Seq libraries from total RNA involved utilizing an Ultra II RNA samples prep kit by the manufacturer's guidelines. In brief, poly-A RNAs were captured using Oligo-Dt conjugated magnetic beads, followed by elution and fragmentation of mRNAs at 94 ºC. Subsequently, first-strand cDNA synthesis occurred through random priming reverse transcription; this was succeeded by double-stranded cDNA production after seconds-strand synthesis. Further steps included end repair, A-tailing, adapter ligation, and amplification via enrichment PCR of adapter-ligated fragments before finally generating sequencing libraries. Sequencing runs took place on an Illumina NextSeq 500 instrument employing single-end 75 cycles sequencing.

3.22. RNA-Seq data analysis

Raw sequencing data in fastq format were aligned to the human reference genome GRCh38 using the HISAT2 algorithm, leading to the generation of BAM files. Subsequent analysis was conducted utilizing Strand NGS software (www.strand-ngs.com). The BAM files were imported into DESeq for normalization, and differential gene expression was determined via moderated T-test with Benjamini-Hochberg FDR for multiple testing corrections. A significance level of $p < 0.05$ was applied to identify significant changes. Gene ontology analysis of differentially expressed genes was performed using CytoScape 3.4.0 with ClueGo application.

3.23. In silico molecular modeling

Protein data for molecular modeling was sourced from UniProt (000429; DNM1L_HUMAN), and post-translational modifications were obtained from the PhosphoSitePlus database. (Hornbeck et al., 2015). Furthermore, ligand-bound structures of human DRP1 protein (PDBID: 3W6N) (Kishida & Sugio, 2014) and (PDBID: 4H1V) (Wenger et al., 2013) as well as the structure of the oligomeric protein (PDBID: 4BEJ) (Fröhlich et al., 2013) were downloaded from the RCSB protein Data Bank (Berman et al., 2000). The NetPhos-3.1 online tool was utilized to predict phosphorylation sites based on the protein sequence with scores ranging between 0-1,

indicating phosphorylation probability; sites with <0.5 scores are not considered phosphorylated areas per Bolm (Blom, Sicheritz-Pontén, Gupta, Gammeltoft, & Brunak, 2004).

3.24. BCI treatment

BCI (cat. SML1817, Sigma) was dissolved in DMSO to prepare a stock solution. The stock solution was aliquoted and stored at -20 ºC until further use. Cells were seeded in a 6-well plate at a density of $2x10^5$ cells per well and allowed to grow for 24 hours. After 24 hours, the medium was replaced with fresh medium containing the 10 μM RA or DMSO and incubated for 48 hours. After 48 hours before treatment, the stock solution was diluted to achieve the final concentration of 0.25 μM, 0.5 μM, and 1 μM of BCI. The cells were treated with BCI at the specified concentration, and the control groups were treated with an equivalent volume of DMSO for 24 hours.

3.25. Statistical analysis

Data from 3 or more than 3 (≥) independent experiments were presented as mean values ±SD. Statistical analysis was done using an unpaired t-test, Mann-Whitney test, One-Way ANOVA, or Two-Way ANOVA followed by Sidak or Tukey's multiple comparisons t-test after passing the normality test of the Shapiro-Wilk test. The samples with negative normality tests were analyzed using a non-parametric analysis of Kruskal-Wallis's test following the DUNN's multiple comparison t-test. GraphPad Prism v9.5.1 software was used where statistical significance was defined as * $p<0.05$, ** $p<0.01$, *** $p<0.001$ and **** $p<0.0001$.

4. Results

4.1. DRP1 knockdown generates long filamentous mitochondrial ultrastructure and induces changes in global transcriptomics of SH-SY5Y cells

The protocol described previously (Abdennour Douida et al., 2020) was used to generate a depleted DRP1/DNML1 cell line using SH-SY5Y human neuroblastoma cells. qRT-PCR and western blotting were used to confirm the efficiency of knockdown (**Fig. 7A-B**). Two primer pairs (mentioned in the Table. 1) were used to verify the efficient relative change in the gene expression of DNM1L (DRP1 gene name). The cells stably expressing pGIPZ-GFP and those stably depleted of DRP1 will be referred to hereinafter as control and shDrp1, respectively.

DRP1 plays a key role in controlling mitochondrial fission. Additionally, impaired mitochondrial fission halts the cell cycle at the G2/M transition. The absence of DRP1 leads the mitochondrial dynamics toward fusion, resulting in an elongated and hyperfused network of mitochondria (Kitamura et al., 2017). We performed transmission electron microscopy (TEM) to assess the characteristics and physiological effects of DRP1 depletion on mitochondrial ultrastructure of both control and shDrp1 cells (**Fig. 7C**). The shDrp1 cells showed a high number of long, hyperfused and compact mitochondrial shapes as compared to control cells in TEM images (**Fig. 7C**). Using the Amira 3D software, we determined the mitochondrial inside length, area, and the formation of clusters of mitochondria. shDrp1 cells showed a significant enhancement in the average inside length of mitochondria (**Fig. 7D**), area (**Fig. 7E**), and total (SUM) mitochondrial area (**Fig. 7F**) compared to the control group. Figure. 7C shows that in DRP1 depleted cells, the mitochondria come in close proximity to each other and form clustering around the nucleus. The average distance of each mitochondrion to its closest mitochondria was measured to quantify this clustering. The results proved that the average distance between two mitochondria was shorter in shDrp1 cells compared to control cells (**Fig. 7G**). However, we could not detect any difference in the total inside length of mitochondria in shDrp1 cells (**Fig. 7H**).

A.

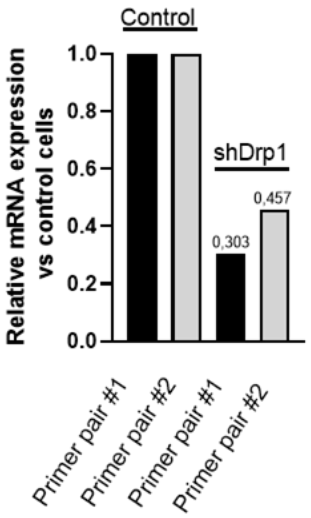
Control
shDrp1
Relative mRNA expression vs control cells
1.0
0.8
0.6
0.4
0.2
0.0
0,303
0,457
Primer pair #1
Primer pair #2
Primer pair #1
Primer pair #2

B.

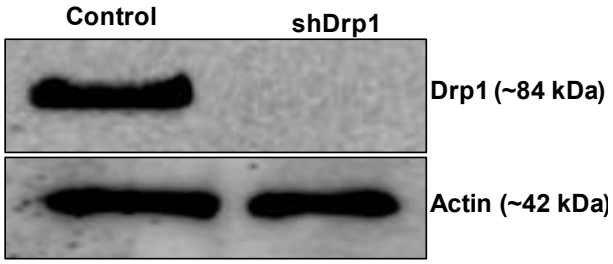
Control
shDrp1
Drp1 (~84 kDa)
Actin (~42 kDa)

C.

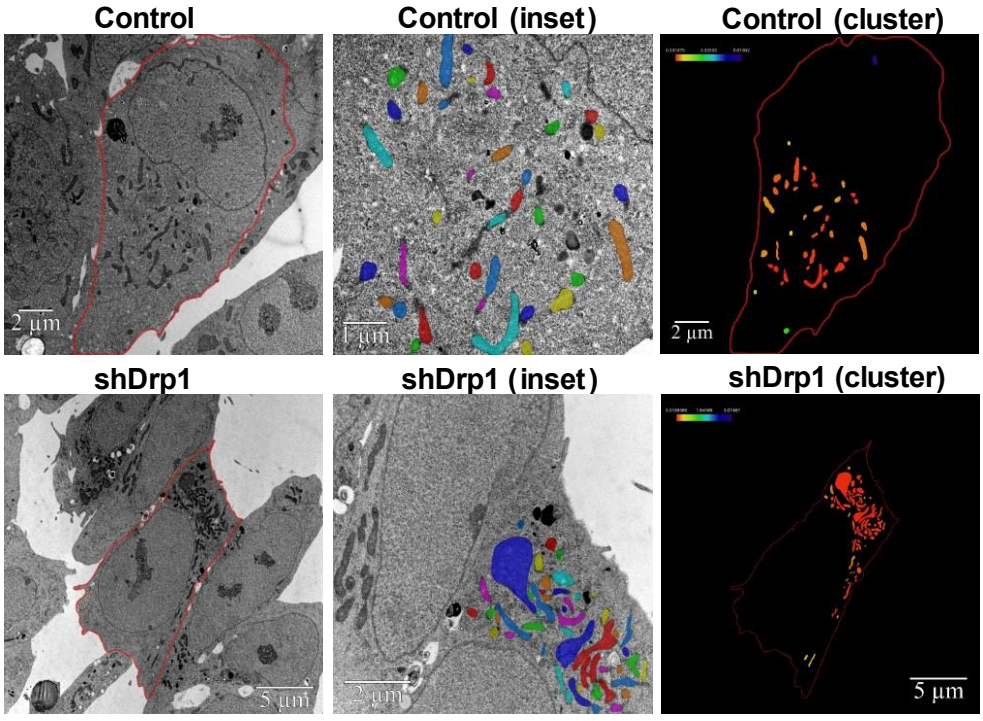
Control
Control (inset)
Control (cluster)
2 µm
1 µm
2 µm
shDrp1
shDrp1 (inset)
shDrp1 (cluster)
5 µm
2 µm
5 µm

D.

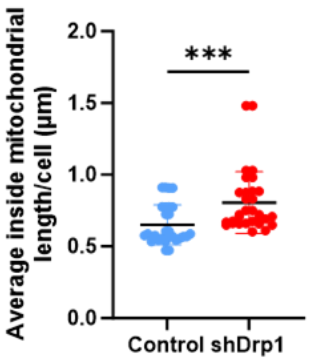
Average inside mitochondrial length/cell (µm)
2.0
1.5
1.0
0.5
0.0
***
Control shDrp1

E.

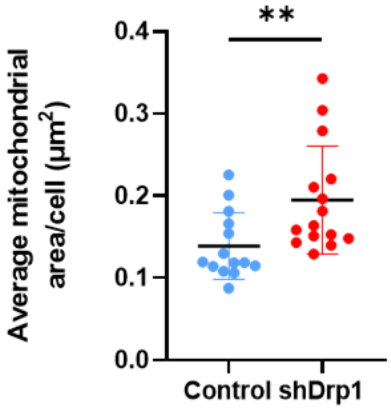
Average mitochondrial area/cell (µm²)
0.4
0.3
0.2
0.1
0.0
**
Control shDrp1

F.

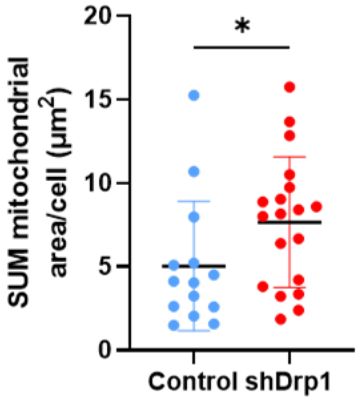
SUM mitochondrial area/cell (µm²)
20
15
10
5
0
*
Control shDrp1

G.

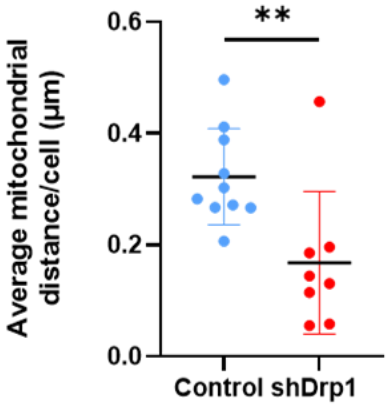
Average mitochondrial distance/cell (µm)
0.6
0.4
0.2
0.0
**
Control shDrp1

H.

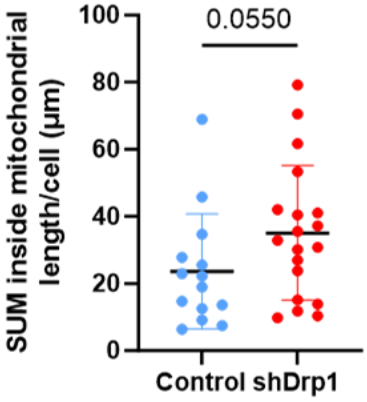
SUM inside mitochondrial length/cell (µm)
100
80
60
40
20
0
0.0550
Control shDrp1

Fig. 7: ***DRP1 depleted cell line generation using the SH-SY5Y human neuroblastoma cells line by lentiviral technique****. The protocol of the knockdown of DNM1L is mentioned in section 3.2 of materials and methods. (A) The qPCR analysis of successful DRP1/DMN1L depletion in shDrp1 cells. Table 1 shows the sequences of shRNA used for silencing DRP1. (B) Total cell lysate from shDrp1 and control cells were lyzed with RIPA buffer, and 20 ug of protein was loaded into each well, separated using SDS-PAGE, and analyzed by western blot for DRP1 protein levels. Actin was used as the loading control. The images were taken with ChemiDoc imaging machine. (C) Representative images of mitochondria of control (upper panel) and shDrp1 (lower panel) by transmission electron microscopy. The inset shows the mixed population of mitochondria in control cells, while DRP1 silenced cells show elongated and fused mitochondria—quantitative analysis of mitochondrial length, width, and distance ratio. An Amira 3D software 2022 version (ThermoFisher Scientific) assessed the numerical parameters of segmented structures. Mitochondrial clustering was evaluated by determining the closest neighbor of each mitochondrion, with mitochondria color-coded according to their proximity to their nearest neighbor. Quantitative analysis included the average inside mitochondrial length (μm) (D), the average mitochondrial area (μm^2) (E), the sum mitochondrial area (μm^2) (F), and the average distance between mitochondria (μm)* (G)*, the sum inside mitochondrial length (μm) (H). Data are presented as the mean ± SD. Statistical analysis was performed using the Mann-Whitney test, with p values <0.05 considered statistically significant (* indicates p< 0.05, ** indicates p< 0.01, and *** indicates p< 0.001).*

We performed RNA Seq on both control and shDrp1 cells and analyzed GO term enrichment analysis on significantly up and downregulated genes to determine the significant biological relevance of DEGs. The network enriched and bar graph GO terms analysis showed the genes associated with the regulation of neurogenesis, neuron projection development, synapse assembly, and axon development were significantly increased in shDrp1 cells compared to the control (**Fig. 8A-B**). The stably depleted DRP1 cells showed significantly downregulated GO terms of heart and circulatory system development processes, cellular response to chemical and growth stimuli, and regulation of signaling and MAPK cascade in the network enriched and bar graphs GO terms (**Fig. 8C-D**).

A.

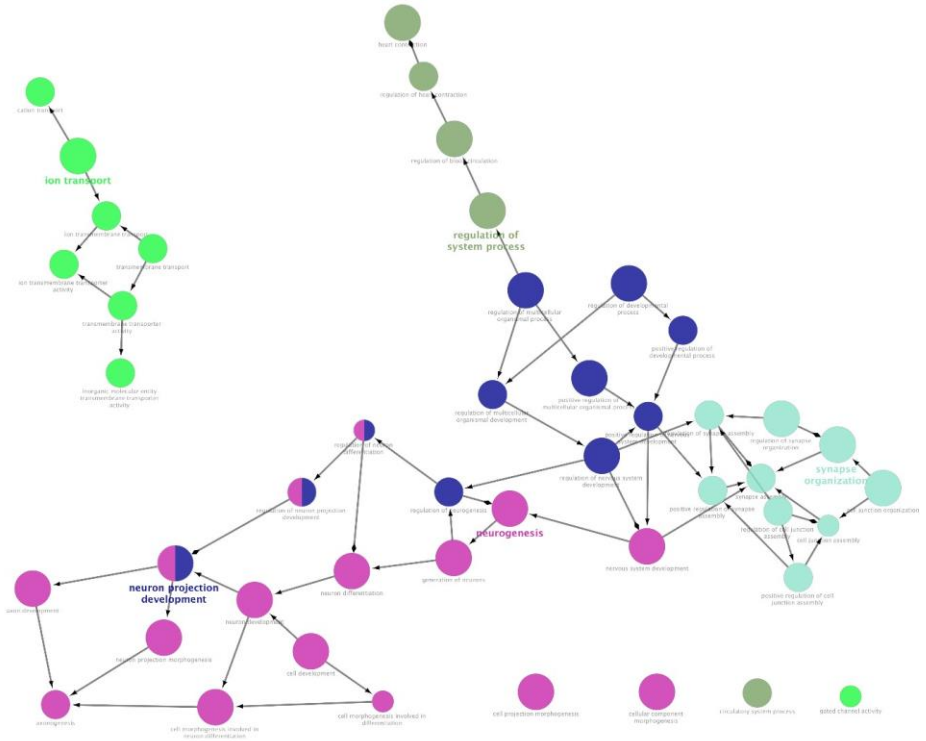
ion transport
regulation of system process
neurogenesis
neuron projection development
synapse organization

B.

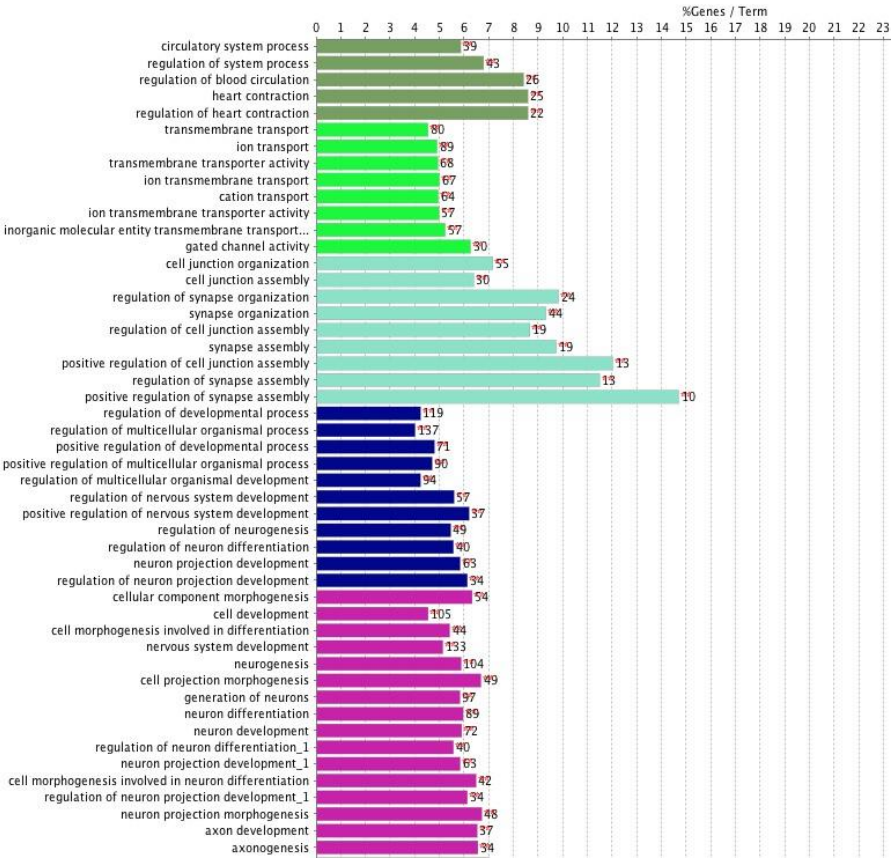
%Genes / Term
0 1 2 3 4 5 6 7 8 9 10 11 12 13 14 15 16 17 18 19 20 21 22 23
circulatory system process 39
regulation of system process 43
regulation of blood circulation 26
heart contraction 25
regulation of heart contraction 22
transmembrane transport 80
ion transport 89
transmembrane transporter activity 68
ion transmembrane transport 67
cation transport 64
ion transmembrane transporter activity 57
inorganic molecular entity transmembrane transport... 57
gated channel activity 30
cell junction organization 55
cell junction assembly 30
regulation of synapse organization 24
synapse organization 44
regulation of cell junction assembly 19
synapse assembly 19
positive regulation of cell junction assembly 13
regulation of synapse assembly 13
positive regulation of synapse assembly 10
regulation of developmental process 119
regulation of multicellular organismal process 137
positive regulation of developmental process 71
positive regulation of multicellular organismal process 90
regulation of multicellular organismal development 94
regulation of nervous system development 57
positive regulation of nervous system development 37
regulation of neurogenesis 49
regulation of neuron differentiation 40
neuron projection development 63
regulation of neuron projection development 34
cellular component morphogenesis 54
cell development 105
cell morphogenesis involved in differentiation 44
nervous system development 133
neurogenesis 104
cell projection morphogenesis 49
generation of neurons 97
neuron differentiation 89
neuron development 72
regulation of neuron differentiation_1 40
neuron projection development_1 63
cell morphogenesis involved in neuron differentiation 42
regulation of neuron projection development_1 34
neuron projection morphogenesis 48
axon development 37
axonogenesis 34

C.

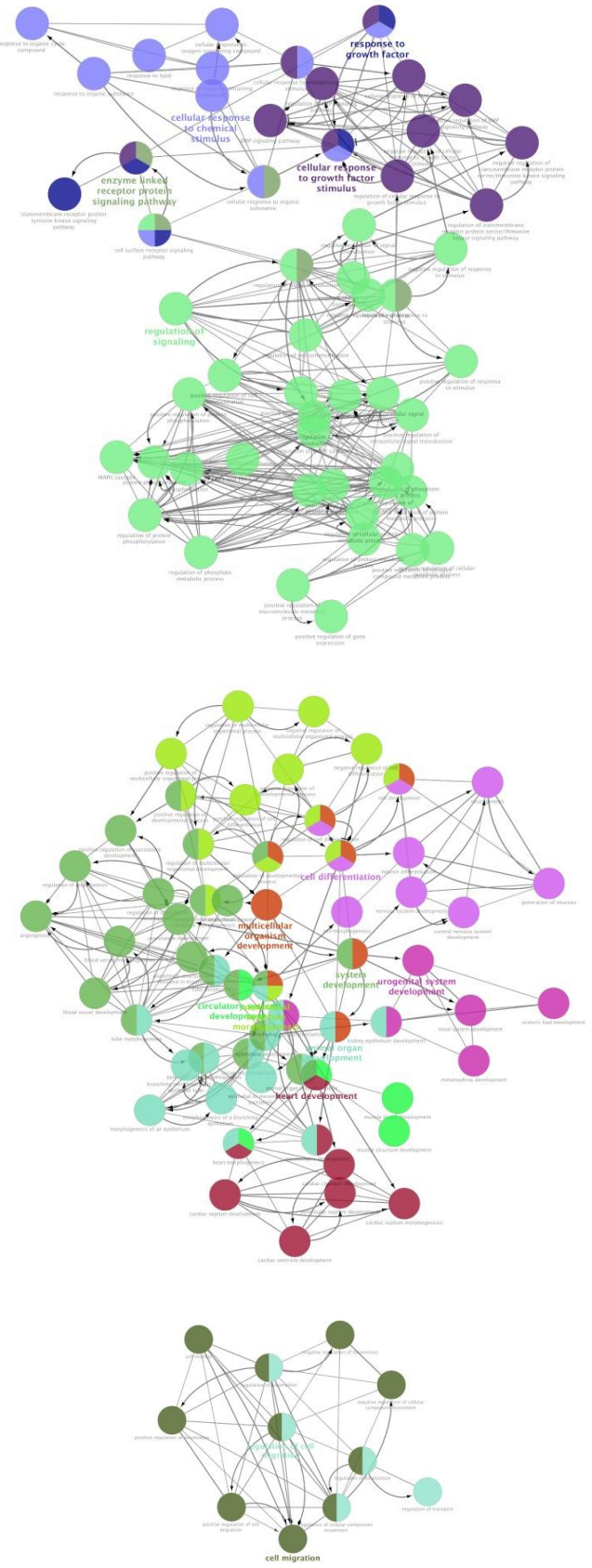
response to growth factor
cellular response to chemical stimulus
cellular response to growth factor stimulus
enzyme linked receptor protein signaling pathway
regulation of signaling
cell differentiation
multicellular organism development
system development
urogenital system development
heart development
cell migration

D.

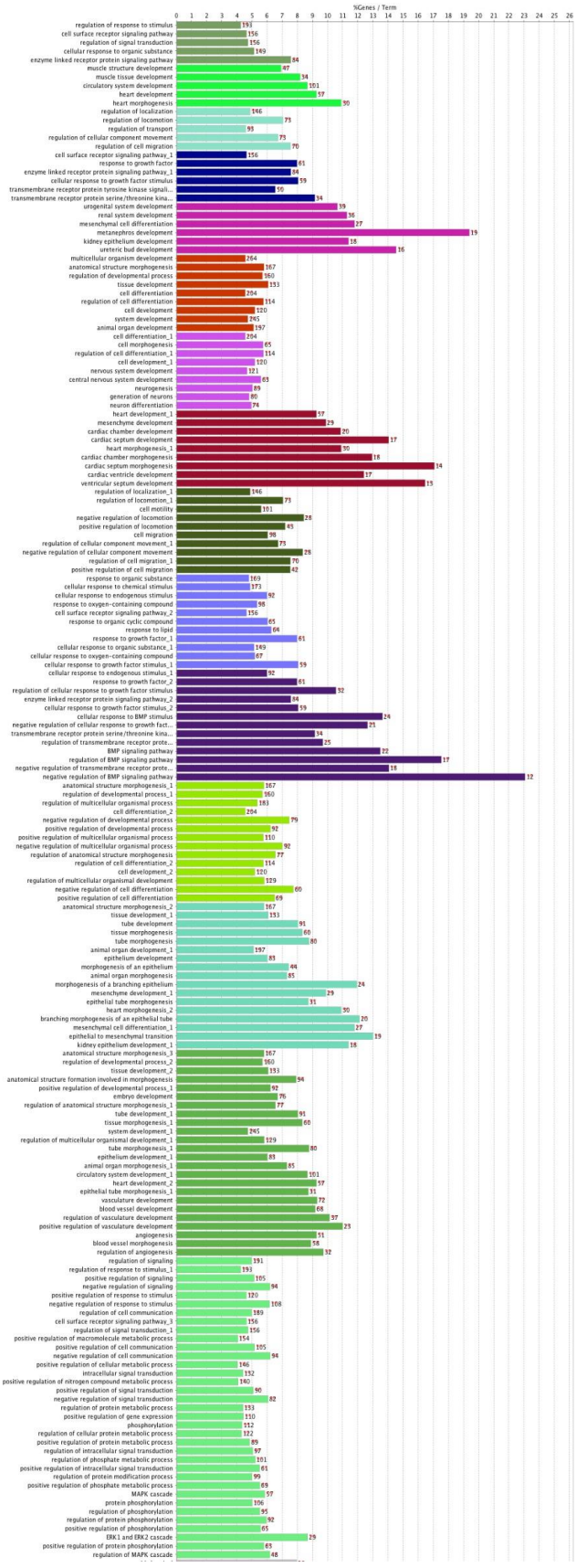
%Genes / Term
0 1 2 3 4 5 6 7 8 9 10 11 12 13 14 15 16 17 18 19 20 21 22 23 24 25 26
regulation of response to stimulus 193
cell surface receptor signaling pathway 156
regulation of signal transduction 156
cellular response to organic substance 149
enzyme linked receptor protein signaling pathway 84
muscle structure development 47
muscle tissue development 34
circulatory system development 101
heart development 57
heart morphogenesis 30
regulation of localization 146
regulation of locomotion 73
regulation of transport 93
regulation of cellular component movement 75
regulation of cell migration 70
cell surface receptor signaling pathway_1 156
response to growth factor 61
enzyme linked receptor protein signaling pathway_1 84
cellular response to growth factor stimulus 59
transmembrane receptor protein tyrosine kinase signali... 10
transmembrane receptor protein serine/threonine kina... 34
urogenital system development 39
renal system development 36
mesenchymal cell differentiation 27
metanephros development 19
kidney epithelium development 18
ureteric bud development 16
multicellular organism development 264
anatomical structure morphogenesis 167
regulation of developmental process 160
tissue development 133
cell differentiation 204
regulation of cell differentiation 114
cell development 120
system development 245
animal organ development 197
cell differentiation_1 204
cell morphogenesis 65
regulation of cell differentiation_1 114
cell development_1 120
nervous system development 121
central nervous system development 63
neurogenesis 89
generation of neurons 80
neuron differentiation 74
heart development_1 57
mesenchyme development 29
cardiac chamber development 20
cardiac septum development 17
heart morphogenesis_1 30
cardiac chamber morphogenesis 18
cardiac septum morphogenesis 14
cardiac ventricle development 17
ventricular septum development 13
regulation of localization_1 146
regulation of locomotion_1 73
cell motility 101
negative regulation of locomotion 28
positive regulation of locomotion 45
cell migration 98
regulation of cellular component movement_1 75
negative regulation of cellular component movement 28
regulation of cell migration_1 70
positive regulation of cell migration 42
response to organic substance 169
cellular response to chemical stimulus 173
cellular response to endogenous stimulus 92
response to oxygen-containing compound 98
cell surface receptor signaling pathway_2 156
response to organic cyclic compound 65
response to lipid 64
response to growth factor_1 61
cellular response to organic substance_1 149
cellular response to oxygen-containing compound 67
cellular response to growth factor stimulus_1 59
cellular response to endogenous stimulus_1 92
response to growth factor_2 61
regulation of cellular response to growth factor stimulus 92
enzyme linked receptor protein signaling pathway_2 84
cellular response to growth factor stimulus_2 59
cellular response to BMP stimulus 24
negative regulation of cellular response to growth fact... 21
transmembrane receptor protein serine/threonine kina... 34
regulation of transmembrane receptor prote... 25
BMP signaling pathway 22
regulation of BMP signaling pathway 17
negative regulation of transmembrane receptor prote... 18
negative regulation of BMP signaling pathway 12
anatomical structure morphogenesis_1 167
regulation of developmental process_1 160
regulation of multicellular organismal process 183
cell differentiation_2 204
negative regulation of developmental process 79
positive regulation of developmental process 92
positive regulation of multicellular organismal process 110
negative regulation of multicellular organismal process 92
regulation of anatomical structure morphogenesis 77
regulation of cell differentiation_2 114
cell development_2 120
regulation of multicellular organismal development 129
negative regulation of cell differentiation 60
positive regulation of cell differentiation 69
anatomical structure morphogenesis_2 167
tissue development_1 133
tube development 91
tissue morphogenesis 60
tube morphogenesis 80
animal organ development_1 197
epithelium development 83
morphogenesis of an epithelium 44
animal organ morphogenesis 85
morphogenesis of a branching epithelium 24
mesenchyme development_1 29
epithelial tube morphogenesis 31
heart morphogenesis_2 30
branching morphogenesis of an epithelial tube 20
mesenchymal cell differentiation_1 27
epithelial to mesenchymal transition 19
kidney epithelium development_1 16
anatomical structure morphogenesis_3 167
regulation of developmental process_2 160
tissue development_2 133
anatomical structure formation involved in morphogenesis 94
positive regulation of developmental process_1 92
embryo development 76
regulation of anatomical structure morphogenesis_1 77
tube development_1 91
tissue morphogenesis_1 60
system development_1 245
regulation of multicellular organismal development_1 129
tube morphogenesis_1 80
epithelium development_1 83
animal organ morphogenesis_1 85
circulatory system development_1 101
heart development_2 57
epithelial tube morphogenesis_1 31
vasculature development 72
blood vessel development 68
regulation of vasculature development 37
positive regulation of vasculature development 25
angiogenesis 51
blood vessel morphogenesis 58
regulation of angiogenesis 32
regulation of signaling 191
regulation of response to stimulus_1 193
positive regulation of signaling 105
negative regulation of signaling 94
positive regulation of response to stimulus 120
negative regulation of response to stimulus 108
regulation of cell communication 189
cell surface receptor signaling pathway_3 156
regulation of signal transduction_1 156
positive regulation of macromolecule metabolic process 154
positive regulation of cell communication 105
negative regulation of cell communication 94
positive regulation of cellular metabolic process 146
intracellular signal transduction 132
positive regulation of nitrogen compound metabolic process 140
positive regulation of signal transduction 90
negative regulation of signal transduction 82
regulation of protein metabolic process 133
positive regulation of gene expression 110
phosphorylation 152
regulation of cellular protein metabolic process 122
positive regulation of protein metabolic process 89
regulation of intracellular signal transduction 97
regulation of phosphate metabolic process 101
positive regulation of intracellular signal transduction 61
regulation of protein modification process 99
positive regulation of phosphate metabolic process 69
MAPK cascade 57
protein phosphorylation 106
regulation of phosphorylation 95
regulation of protein phosphorylation 92
positive regulation of phosphorylation 65
ERK1 and ERK2 cascade 29
positive regulation of protein phosphorylation 65
regulation of MAPK cascade 48

Fig. 8: ***Separate GO term analysis of upregulated and downregulated genes in shDrp1 and control cells.*** *The network enrichment analysis of upregulated and downregulated GO terms in shDrp1 cells compared to control cells. The arrows between the nodes show the connection between the GO terms (A) and (C). A separate overview of upregulated and downregulated GO terms (biological processes) is shown in shDrp1 cells in relation to control cells. (B) and (D) Bar showing the number of affiliated genes with each GO term. The % genes/term indicates the number of genes associated with each term. The application CytoScape 3.4.0 with ClueGo was used for differential gene expression ontology analysis. Bonferroni step-down correction after hypergeometric test was used to analyze the overrepresented GO terms.*

We performed mRNA sequencing and analyzed the GO terms to determine the effect of DRP1 depletion on cellular homeostasis. A comparison of transcriptomics of shDrp1 and control cells revealed the DNML1 gene was substantially decreased in shDrp1 cells (**Fig. 9A**). The DRP1 deficient cells revealed changes in gene expression. Our differentially expressed genes (DEGs) data showed that 782 and 972 genes were significantly down- and upregulated, respectively (**Fig. 9B**). Heatmaps depict the expression pattern of genes associated with neurogenesis, such as regulation of neuron differentiation, generation of neurons, neuron differentiation, and neuron development (**Fig. 9C**), axon development (**Fig. 9D**), and regulation of synapse organization (**Fig. 9E**) and synapse assembly (**Fig. 9F**) linked to DRP1 knockdown. The top ten notably upregulated genes in shDrp1 cells are involved in regulating cell growth and cellular energy (DDIT4-DNA damage-inducible transcript 4 protein), neuronal differentiation (NEUROG2-neurogenin 2), navigation and projection of axons during neuronal development (ROBO2-Roundabout homolog 2), transcriptional regulation in neurogenesis (INSM1-Insulinoma-associated protein 1 and HES7-Transcription factor HES-7), promoting an increase both neurite number and in neurite length (FLRT1-leucine-rich repeat transmembrane protein), scaffolding and trafficking multiprotein signaling complexes in neurons (GRIP1-Glutamate receptor-interacting protein 1), neuronal differentiation and plasticity (GPM6A- Neuronal membrane glycoprotein M6-a), the biosynthesis of catecholamines, dopamine, noradrenaline, and adrenaline (TH-Tyrosine 3-monoxygenase), and axon guidance and neurite outgrowth (EPHA8-Ephrin type-A receptor 8) (**Fig. 9G**).

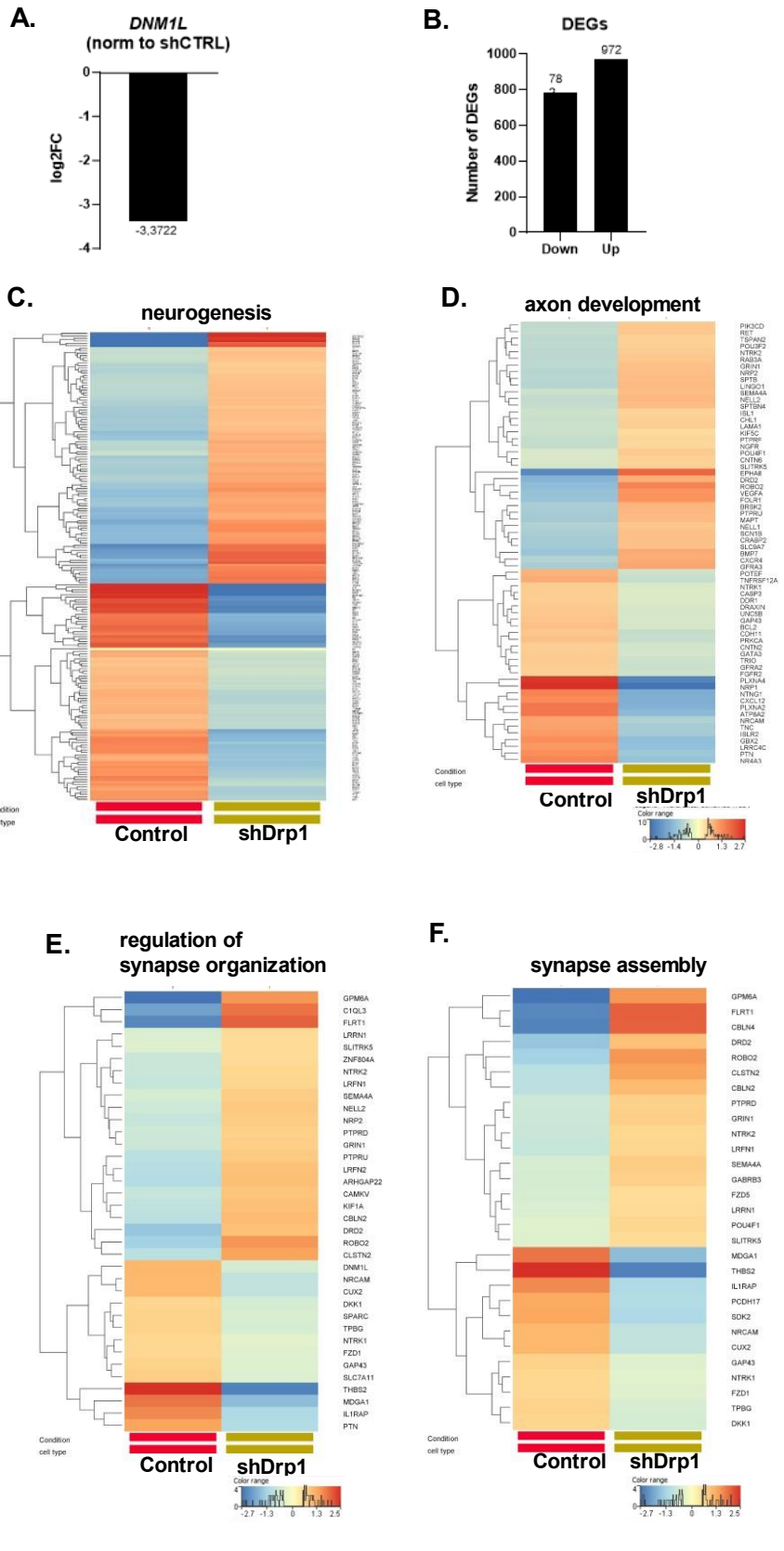
A.
DNM1L
(norm to shCTRL)
log2FC
0
-1
-2
-3
-4
-3,3722
B.
DEGs
Number of DEGs
1000
800
600
400
200
0
78
972
Down
Up
C.
neurogenesis
Condition
cell type
Control
shDrp1
D.
axon development
Condition
cell type
Control
shDrp1
Color range
E.
regulation of
synapse organization
GPM6A
C1QL3
FLRT1
LRRN1
SLITRK5
ZNF804A
NTRK2
LRFN1
SEMA4A
NELL2
NRP2
PTPRD
GRIN1
PTPRU
LRFN2
ARHGAP22
CAMKV
KIF1A
CBLN2
DRD2
ROBO2
CLSTN2
DNM1L
NRCAM
CUX2
DKK1
SPARC
TPBG
NTRK1
FZD1
GAP43
SLC7A11
THBS2
MDGA1
IL1RAP
PTN
Condition
cell type
Control
shDrp1
Color range
F.
synapse assembly
GPM6A
FLRT1
CBLN4
DRD2
ROBO2
CLSTN2
CBLN2
PTPRD
GRIN1
NTRK2
LRFN1
SEMA4A
GABRB3
FZD5
LRRN1
POU4F1
SLITRK5
MDGA1
THBS2
IL1RAP
PCDH17
SDK2
NRCAM
CUX2
GAP43
NTRK1
FZD1
TPBG
DKK1
Condition
cell type
Control
shDrp1
Color range

G.

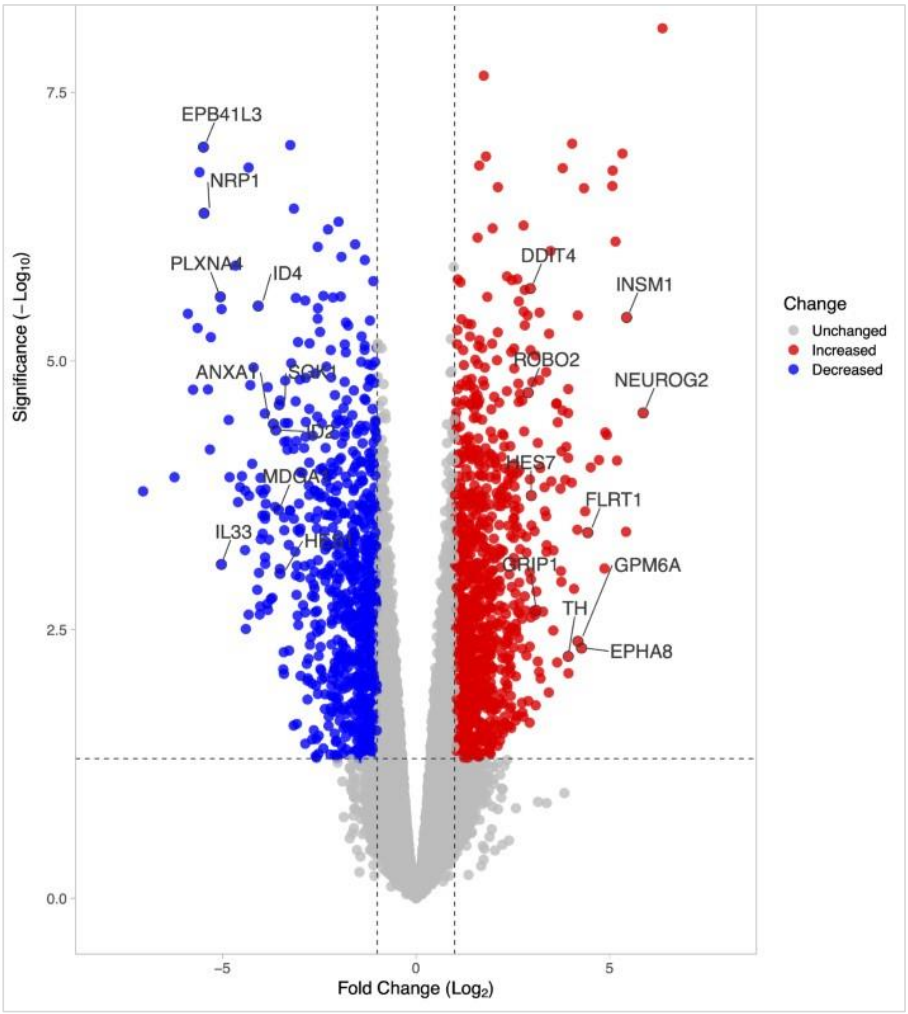

Fig. 9: ***Transcriptomic data represents that DRP1 depletion modulates gene expression.*** *(A) Verification of DRP1/DNM1L mRNA knockdown by three independent experiments of RNA-Seq analysis in SH-SY5Y cells. (B) The differentially downregulated genes (DEGs) in shDrp1 and control cells cover 972 upregulated and 782 downregulated genes (Bejamini-Hochberg FDR corrected p-value < 0.05). GO Analysis of genes that were expressed differentially between shDrp1, and control cells indicated several significantly enriched pathways related to the nervous system (Bonferroni step-down corrected p<0.05). Heatmaps were employed to illustrate the expression pattern of genes linked to neurogenesis (C), axon development (D), regulation of synapse organization (E), and synapse assembly (F). The visualization tools StranNDS software and volcano NoseR2 were used to create heatmaps and a volcano plot, respectively. https://huygens.science.uva.nl/VolcaNoseR2/ (G). Furthermore, the ten most prominently upregulated and downregulated genes in shDrp1 cells are presented.*

In downregulated genes, the top ten genes are related to the cardiovascular system (NRP1-Neuropilin-1), apoptosis and angiogenesis (ID2-DNA-binding protein inhibitor ID-2, ID-4-DNA-binding protein inhibitor ID-4), cytoskeleton remodeling (PLXA4-Plexin A4), immune response (ANXA1-Annexin A1, IL33-Interleukin 33), responses to environmental stress (SOK1-Serine/threonine-protein kinase 25) and DNA damage (HES1-Transcription factor HES1), and the formation or maintenance of inhibitory synapses (MDGA1 MAM domain-containing glycosylphosphatidylinositol anchor protein 1) (**Fig 9G**). These results indicate that DRP1 regulates vital cellular functions by controlling transcriptional processes.

4.2. RA-BDNF-induced neuronal differentiation improves in DRP1 depleted cells *in vitro*

As our transcriptomic data indicated, GO terms related to neuronal differentiation, synapse formation, and axon formation, we differentiated shDrp1 and control cells using an established protocol by Foster et al. (Forster et al., 2016). Adding BDNF to the RA-differentiated cells shows a notable rise in neurite density and an increase in densely connected synaptic networks. RA+BDNF treatment increases the expression pattern of cholinergic markers (de Medeiros et al., 2019). The differentiated cells were monitored after phase 1 (Day 3) and phase 2 (Day 6) by bright field and fluorescence microscopy (**Fig. 10A-B**). Neuronal differentiation was confirmed by the neuron-specific β-III tubulin (Tuj1) staining on fixed cells (**Fig. 10C**) and tubulin tracker staining on live cells (**Fig. 10D**). Undifferentiated cells showed a characteristic clumping structure (**Fig. 10D**) (Forster et al., 2016). The differentiated cells showed neurofilament outgrowth and interconnected neuronal networks. The imaging results demonstrate that the shDrp1 cells showed longer neurite outgrowth and enhanced neuronal networks than the control cells (**Fig. 10D, insets**).

To further analyze the expression of neuronal marker genes during differentiation, we performed qRT-PCR comparing all four groups that are undifferentiated and differentiated control and shDrp1 cells. Here, we analyzed SYN1 (Syanpsin1), and SNAP25 (Synaptosomal-associated protein 25), the Gene for encoding nestin protein (NES) (Yaworsky & Kappen, 1999), TUBβ3 (Tubulin beta-III), DDC (dopa decarboxylase), and Transcription factor SOX-2 (SOX2). SYN1 and SNAP25 are synaptic marker genes. NES is crucial for the development of the central nervous system. DDC is a serotonergic marker, TUBβ3 is an axonal neuronal marker gene, while SOX2 is a pluripotency marker gene. SYN1 and SNAP25 showed a trend (not significant)

expression in differentiated control cells compared to undifferentiated cells. (**Fig. 10E-F**). However, the expression level of NES showed no significant difference between differentiated and undifferentiated control cells. The same results were found by (Forster et al., 2016) (**Fig. 10H**). SOX2 and DDC showed significant downregulation in differentiated control and shDrp1 cells, indicating initiation of differentiation (**Fig. 10I-J**). On the other hand, differentiated shDrp1 compared to undifferentiated cells showed a significant increase in various genes such as SYN1, and SNAP25 (**Fig. 10E-F**). While comparing the differentiated shDrp1 cells to the differentiated control cells, SYN1, SNAP25, TUBβ3 and NES were significantly upregulated. (**Fig. 10E-H**).

A.

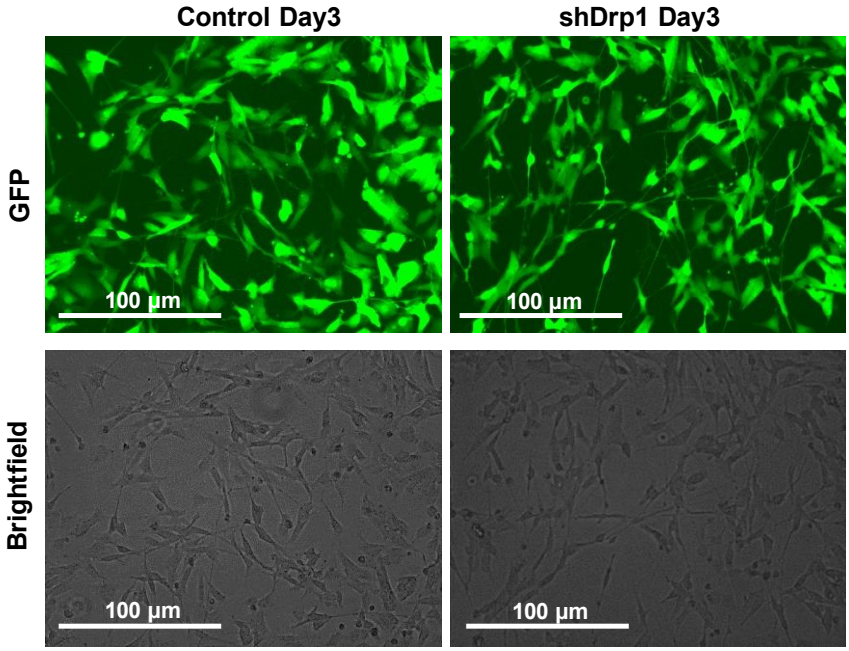
Control Day3
shDrp1 Day3
GFP
Brightfield
100 µm
100 µm
100 µm
100 µm

B.

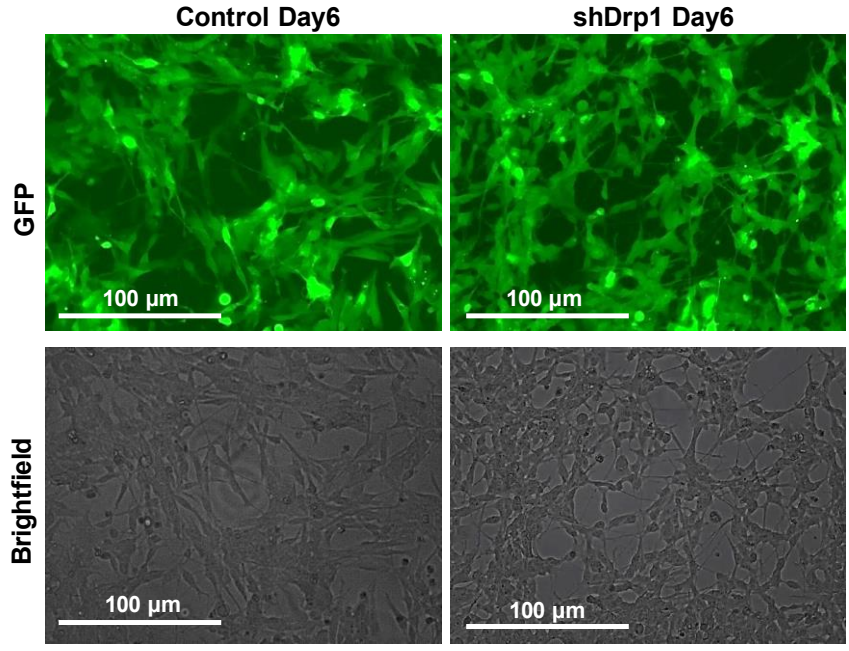
Control Day6
shDrp1 Day6
GFP
Brightfield
100 µm
100 µm
100 µm
100 µm

C.

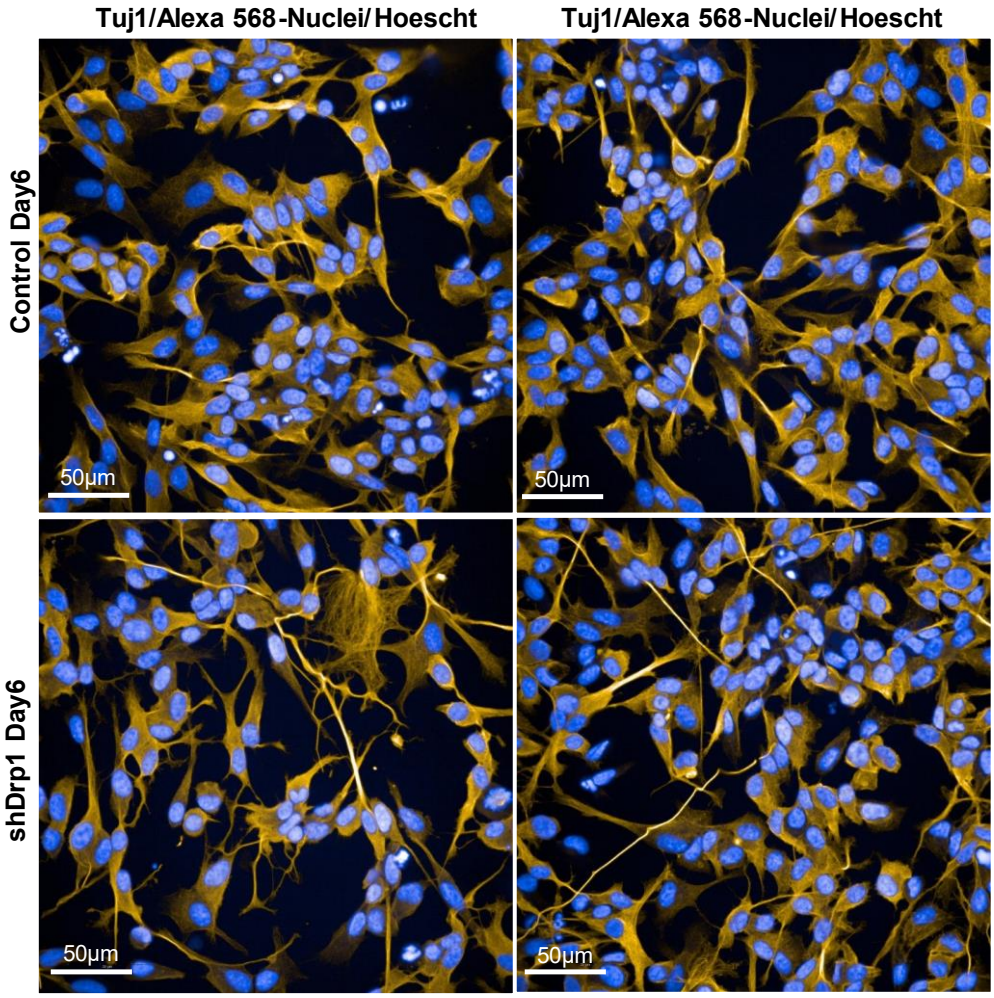
Tuj1/Alexa 568-Nuclei/Hoescht
Tuj1/Alexa 568-Nuclei/Hoescht
Control Day6
shDrp1 Day6
50µm
50µm
50µm
50µm

D.

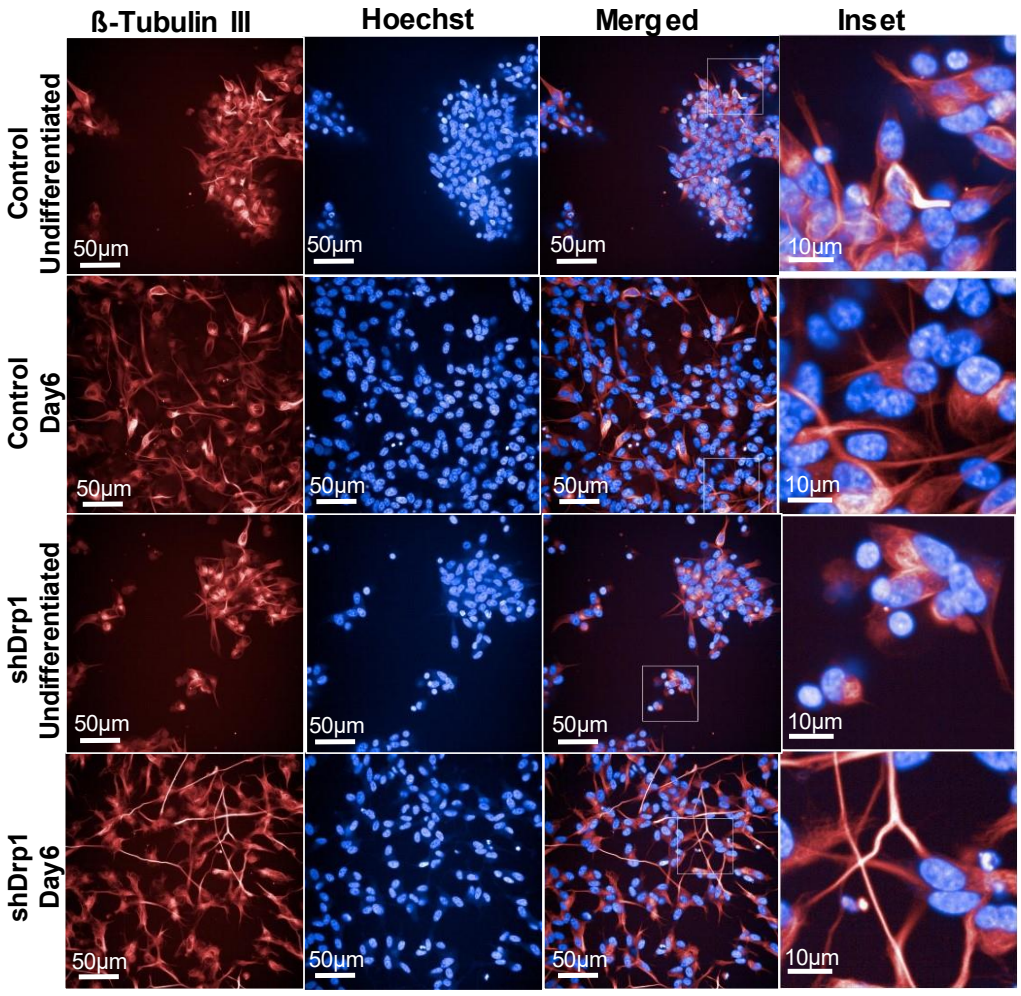
ß-Tubulin III
Hoechst
Merged
Inset
Control Undifferentiated
Control Day6
shDrp1 Undifferentiated
shDrp1 Day6
50µm
10µm

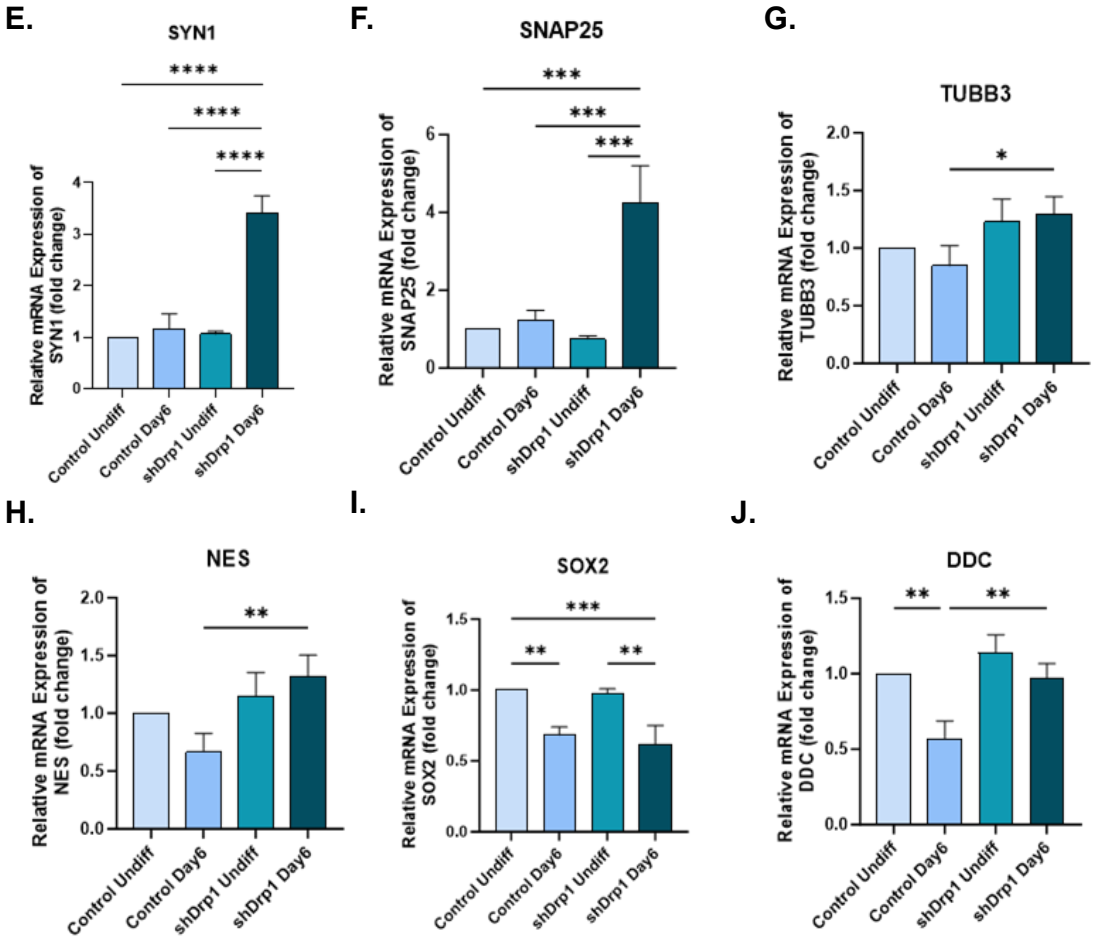

Fig. 10: ***shDrp1 showed longer neurite length and a more interconnected neuronal network than the control, indicating more neuronal differentiation.*** *Control and shDrp1 cells were differentiated by treating cells with 10 uM RA in phase 1 (Day 0-3) differentiation and with 1% N2 supplement and 50 ng/ml BDNF in phase 2 (Day 3-6) differentiation. Images were taken using a High-Content Screening confocal microscopy of an Opera Phenix. Image-acquisition settings were as follows: 40× water objective, filters for Hoechst, and tubulin tracker were selected. (A-B) Using a fluorescence and brightfield microscope, representative images of differentiated and undifferentiated control and shDrp1 cells. Images were taken on Day 3 and Day 6. (C) Representative images of differentiated control and shDrp1 cells. Images were taken using a confocal microscope. The cells were fixed with 4% PFA, stained with Tuj1 (β- tubulin III), and counterstained with Alexa 568. (D) Representative live confocal images of differentiated and undifferentiated control and shDrp1cells are shown. Cells were stained with Hoechst 33342 and neurons specific β-tubulin III tracker for nuclei and neurites, respectively. Inset shows that neuronal outgrowth and interconnected branches were significantly increased in differentiated cells compared to undifferentiated cells. The scale bar is 50 μm. (E-J) RT-qPCR determined the mRNA expression level of some neuronal marker genes in differentiated and undifferentiated cells. (E) Synapsin 1 (SYN1) (F) Synaptosomal-associated protein 25 (SNAP25), (G) Tubulin*

beta-3 chain (TUBB3), (H) Nestin (NES), (I) Transcription factor SOX-2 (SOX2), and (J) Aromatic-L-amino-acid decarboxylase (DDC). The mRNA expression level of differentiated control and shDrp1 cells normalized to their corresponding undifferentiated pairs using the $2^{-\Delta\Delta Ct}$ *method. Data are presented as the mean ± SD of n=3 separate experiments. Groups were compared using ordinary one-way ANOVA following multiple comparison tests where (* indicates p< 0.05, ** indicates p< 0.01, *** indicates p< 0.001, and **** indicates p< 0.0001).*

Neurite outgrowth analysis is a critical factor for the assessment of CNS development. To quantify the difference between neurite morphology in our differentiated samples, we used a High-Content Analysis system (OperaTM PerkinElmer). CSIRO neurite analysis algorithm, a built-in function of HCA, was used to measure neurite outgrowth and neurite branches. Multiple parameters for the neurite analysis were assessed in live cells to evaluate the nervous system's development critically. We found that maximum and total neurite length parameters were significantly higher in both control and shDrp1 compared to their undifferentiated cells. However, differentiated shDrp1 cells have substantially higher neurite lengths than differentiated control cells to connect to other neuron-like cells synaptically (**Fig. 11A and B**). We found a significantly higher number of extremities (**Fig. 11C**), number of extremities per cell (**Fig. 11 D**), number of segments (**Fig. 11E**), and number of roots (**Fig. 11F**) in both control and shDrp1 differentiated cells vs. their undifferentiated cells. Differentiated shDrp1 cells showed a significant increase in all these parameters compared to the undifferentiated control and shDrp1 and differentiated control groups. The number of nodes type 1 & 2 (**Fig. 11G-H**) were enhanced in differentiated cells compared to undifferentiated cells, but no significant difference was detected. In conclusion, these results indicate that RA-BDNF-induced neuronal differentiation

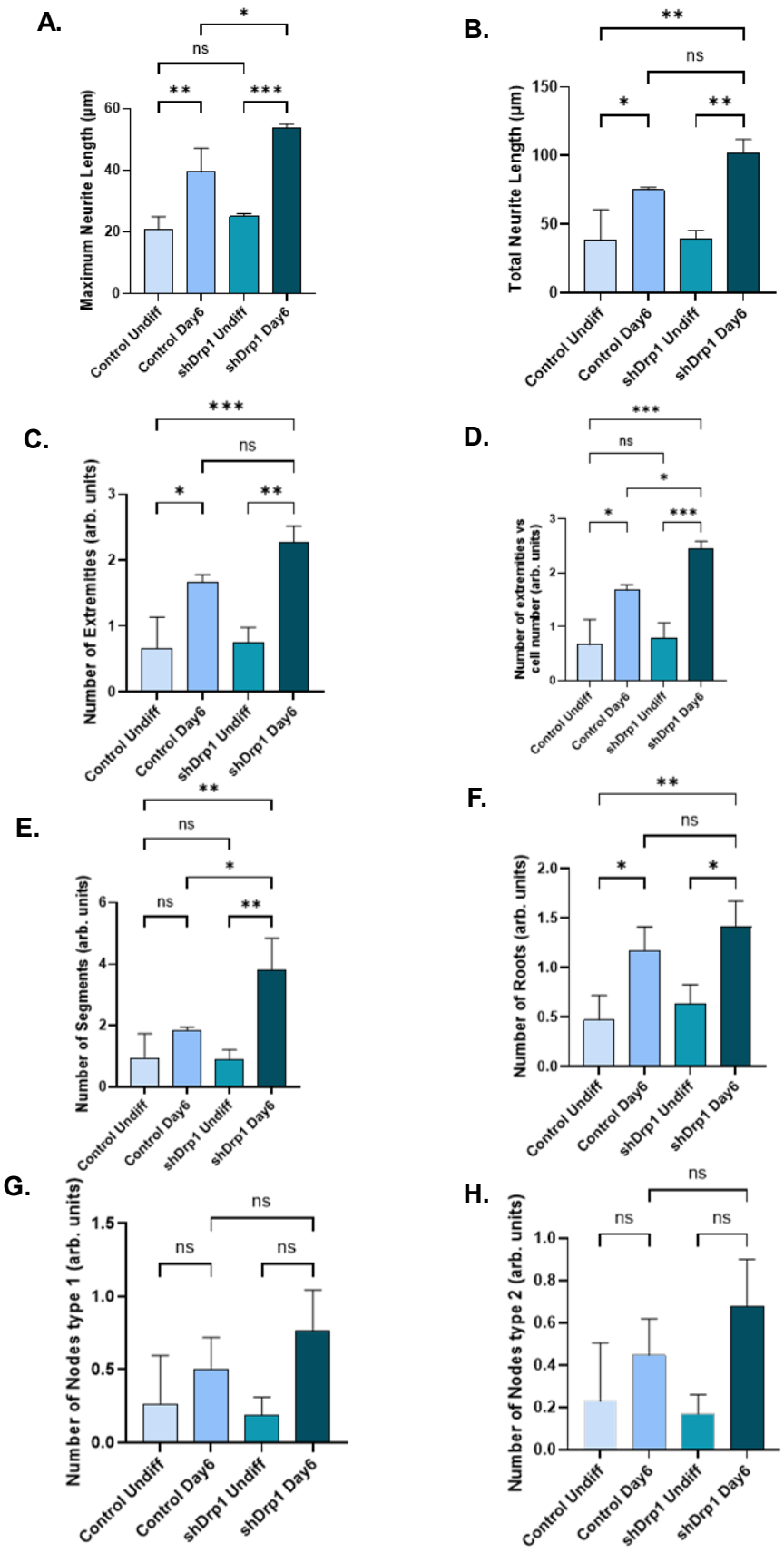
A.
Maximum Neurite Length (µm)
0
20
40
60
*
ns
**
***
Control Undiff
Control Day6
shDrp1 Undiff
shDrp1 Day6
B.
Total Neurite Length (µm)
0
50
100
150
**
ns
*
**
Control Undiff
Control Day6
shDrp1 Undiff
shDrp1 Day6
C.
Number of Extremities (arb. units)
0
1
2
3
***
ns
*
**
Control Undiff
Control Day6
shDrp1 Undiff
shDrp1 Day6
D.
Number of extremities vs cell number (arb. units)
0
1
2
3
***
ns
*
*
***
Control Undiff
Control Day6
shDrp1 Undiff
shDrp1 Day6
E.
Number of Segments (arb. units)
0
2
4
6
**
ns
*
ns
**
Control Undiff
Control Day6
shDrp1 Undiff
shDrp1 Day6
F.
Number of Roots (arb. units)
0.0
0.5
1.0
1.5
2.0
**
ns
*
*
Control Undiff
Control Day6
shDrp1 Undiff
shDrp1 Day6
G.
Number of Nodes type 1 (arb. units)
0.0
0.5
1.0
1.5
ns
ns
ns
Control Undiff
Control Day6
shDrp1 Undiff
shDrp1 Day6
H.
Number of Nodes type 2 (arb. units)
0.0
0.2
0.4
0.6
0.8
1.0
ns
ns
ns
Control Undiff
Control Day6
shDrp1 Undiff
shDrp1 Day6

Fig. 11: ***Quantitative analysis displays a significant increase in neurite outgrowth parameters in shDrp1 cells****. Differentiated (Day 6) and undifferentiated (Day 0) control and shDrp1 cells were quantitatively analyzed for neurite outgrowth parameters through High Content Analysis. On Day 6, cells were stained with Hoechst 33342 for nuclei and tubulin tracker Deep red for neuron-specific β-tubulin III in serum-free media for 30 minutes. Image analysis was done using the "CSIRO neurite analysis" built-in method of Harmony 4.9 software in the High Content Analysis (HCA) system. (A) Maximum neurite length, (B) Total neurite length, (C) Number of extremities, (D) Number of extremities vs cell number, (E) Number of segments, (F) Number of Roots, (G) Number of nodes type 1, and (H) Number of nodes type 2. The units were defined for length, width, and area as µm, µm, and µm², respectively. For all other parameters, the units are arbitrary (arb. Units). Data are presented as mean ± SD of what? (n= 3). For differentiated cells, a total of 45066 and 39677 cells, and for undifferentiated cells, 22568 and 39658 control and shDrp1 cells were analyzed, respectively. The groups were compared using One-way ANOVA using multiple comparisons test where (* indicates p< 0.05, ** indicates p< 0.01, *** indicates p< 0.001).*

enhances the expression of neuronal markers genes and neurite outgrowth parameters in DRP1-depleted SH-SY5Y human neuroblastoma cells *in vitro*.

4.3. Neuronally differentiated shDrp1 cells exhibited low levels of phospho-ERK1/2 after RA-BDNF induction

DRP1 depletion modulates the genetic expression of various pathways, including protein phosphorylation, regulation of MAPK, and downregulation of ERK1/2, as we found in our global transcriptomic analysis of undifferentiated control and shDrp1 cells. RA-induced neuronal differentiation triggers the activation of various signaling pathways. Thus, we screened the control and shDrp1 cells treated with DMSO or RA for 43 phosphorylation sites of kinases. There was a noticeable difference in the phosphorylation of ERK1/2, and no difference was detected in other phospho-proteins (**Fig. 12A**). Based on our transcriptomic data, the reduced DRP1 levels affect the activity of genes related to protein phosphorylation. Additionally, there was a notable decrease in GO terms for genes regulating the MAPK and ERK1/2 signaling pathways following DRP1 knockdown in undifferentiated cells (**Fig. 12B-C**). To check the effect of DRP1 depletion on pathways triggered upon RA and BDNF treatment, we did a western blotting analysis of all major proteins, including MAP kinases and their phosphorylation status. According to our western blotting analysis, JNK, P38, and ERK1/2 showed the same trend in undifferentiated Day3 and Day6 differentiated cells of both control and shDrp1 cells (**Fig. 12D, F, and H**). However, AKT and MEK1/2 were activated upon Day3 and remained same until Day6 (**Fig. E and G**). JNK and AKT phosphorylation increased on Day 3 and remained the same

until Day 6 in both cell lines. BDNF differentiation induced the phosphorylation of JNK and AKT induced by RA on Day 3 (**Fig. 12D-E**). However, P38, MEK1/2, and ERK1/2 phosphorylation were activated on RA treatment but abolished on BDNF treatment. shDrp1 cells compared to control showed reduction in ERK1/2 phosphorylation on Day 3 of differentiation (**Fig. 12F-H**). These results demonstrate that DRP1 knockdown impacts the ERK1/2 phosphorylation during phase 1 of neuronal differentiation.

A.

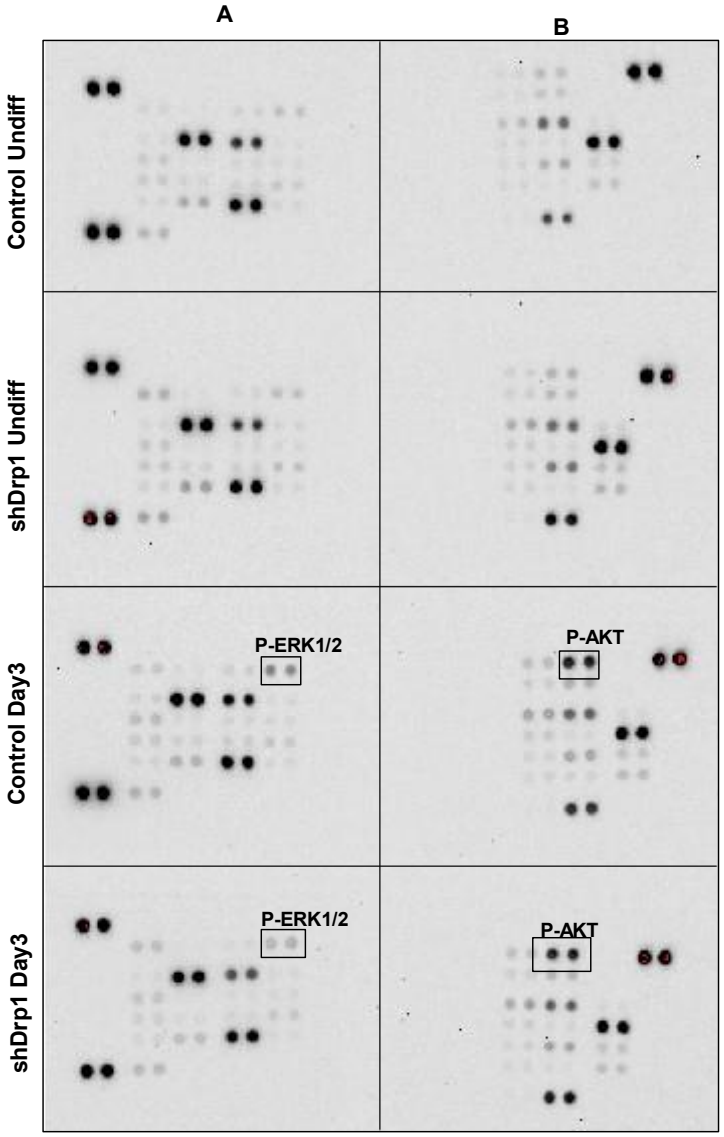

B.

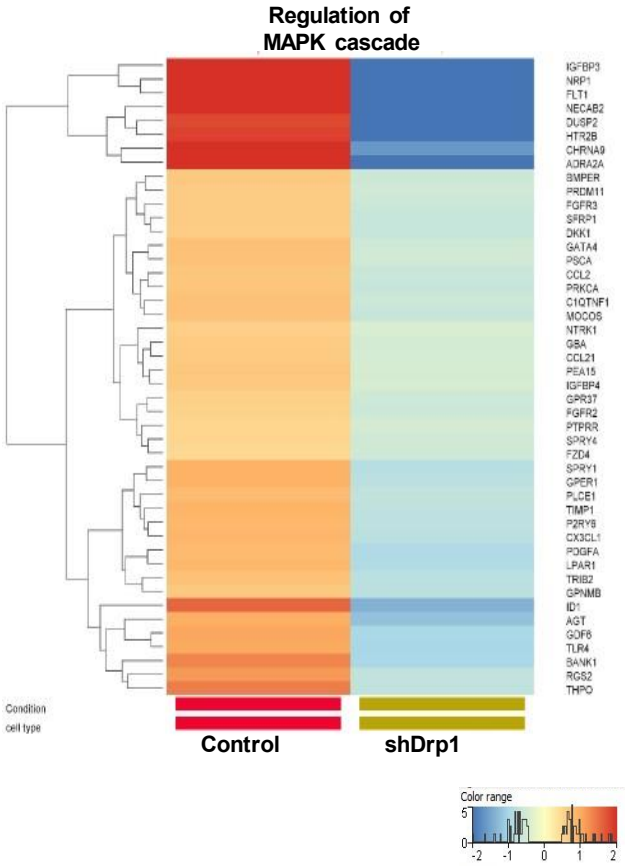
Regulation of MAPK cascade
IGFBP3
NRP1
FLT1
NECAB2
DUSP2
HTR2B
CHRNA9
ADRA2A
BMPER
PRDM11
FGFR3
SFRP1
DKK1
GATA4
PSCA
CCL2
PRKCA
C1QTNF1
MOCOS
NTRK1
GBA
CCL21
PEA15
IGFBP4
GPR37
FGFR2
PTPRR
SPRY4
FZD4
SPRY1
GPER1
PLCE1
TIMP1
P2RY6
CX3CL1
PDGFA
LPAR1
TRIB2
GPNMB
ID1
AGT
GDF6
TLR4
BANK1
RGS2
THPO
Condition
cell type
Control
shDrp1
Color range
5
0
-2
-1
0
1
2

C.

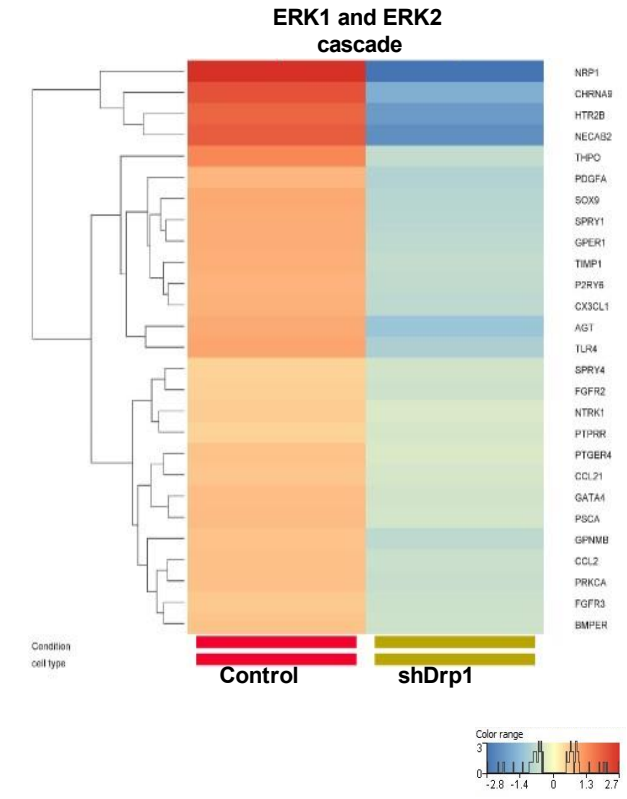
ERK1 and ERK2 cascade
NRP1
CHRNA9
HTR2B
NECAB2
THPO
PDGFA
SOX9
SPRY1
GPER1
TIMP1
P2RY6
CX3CL1
AGT
TLR4
SPRY4
FGFR2
NTRK1
PTPRR
PTGER4
CCL21
GATA4
PSCA
GPNMB
CCL2
PRKCA
FGFR3
BMPER
Condition
cell type
Control
shDrp1
Color range
3
0
-2.8
-1.4
0
1.3
2.7

D.

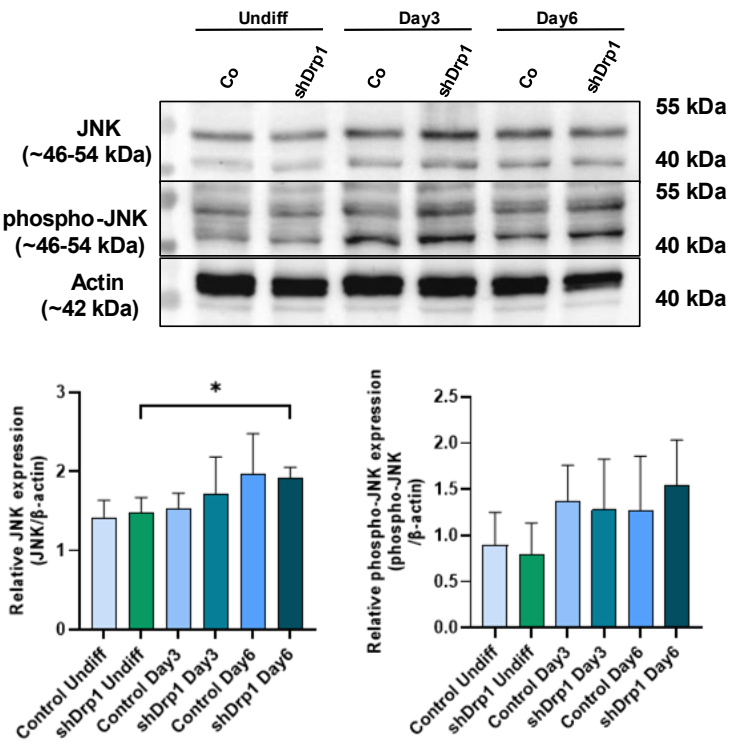
Undiff
Day3
Day6
Co
shDrp1
Co
shDrp1
Co
shDrp1
JNK
(~46-54 kDa)
55 kDa
40 kDa
phospho-JNK
(~46-54 kDa)
55 kDa
40 kDa
Actin
(~42 kDa)
40 kDa
Relative JNK expression
(JNK/β-actin)
*
Relative phospho-JNK expression
(phospho-JNK
/β-actin)
Control Undiff
shDrp1 Undiff
Control Day3
shDrp1 Day3
Control Day6
shDrp1 Day6

E.

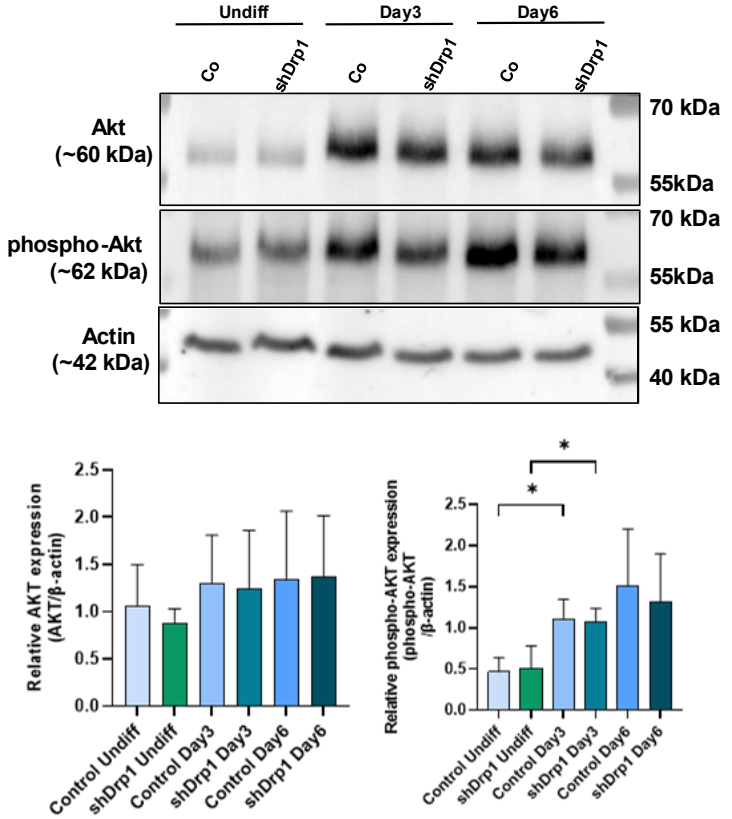
Undiff
Day3
Day6
Co
shDrp1
Co
shDrp1
Co
shDrp1
Akt
(~60 kDa)
70 kDa
55kDa
phospho-Akt
(~62 kDa)
70 kDa
55kDa
Actin
(~42 kDa)
55 kDa
40 kDa
Relative AKT expression
(AKT/β-actin)
Relative phospho-AKT expression
(phospho-AKT
/β-actin)
*
*
Control Undiff
shDrp1 Undiff
Control Day3
shDrp1 Day3
Control Day6
shDrp1 Day6

F.

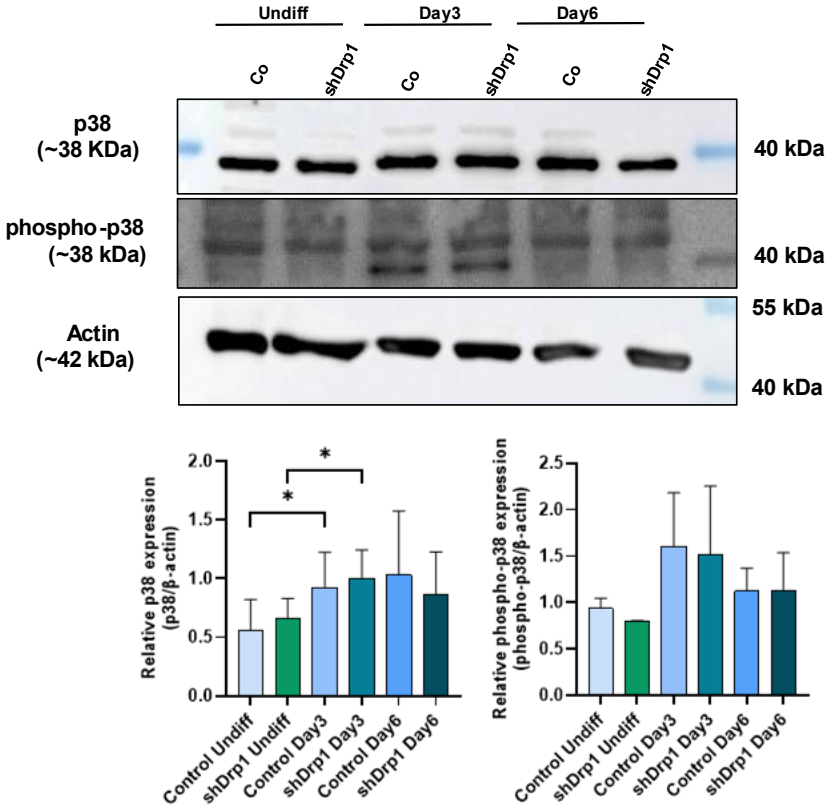
Undiff
Day3
Day6
Co
shDrp1
Co
shDrp1
Co
shDrp1
p38
(~38 KDa)
40 kDa
phospho-p38
(~38 kDa)
40 kDa
55 kDa
Actin
(~42 kDa)
40 kDa
Relative p38 expression
(p38/β-actin)
Relative phospho-p38 expression
(phospho-p38/β-actin)
Control Undiff
shDrp1 Undiff
Control Day3
shDrp1 Day3
Control Day6
shDrp1 Day6

G.

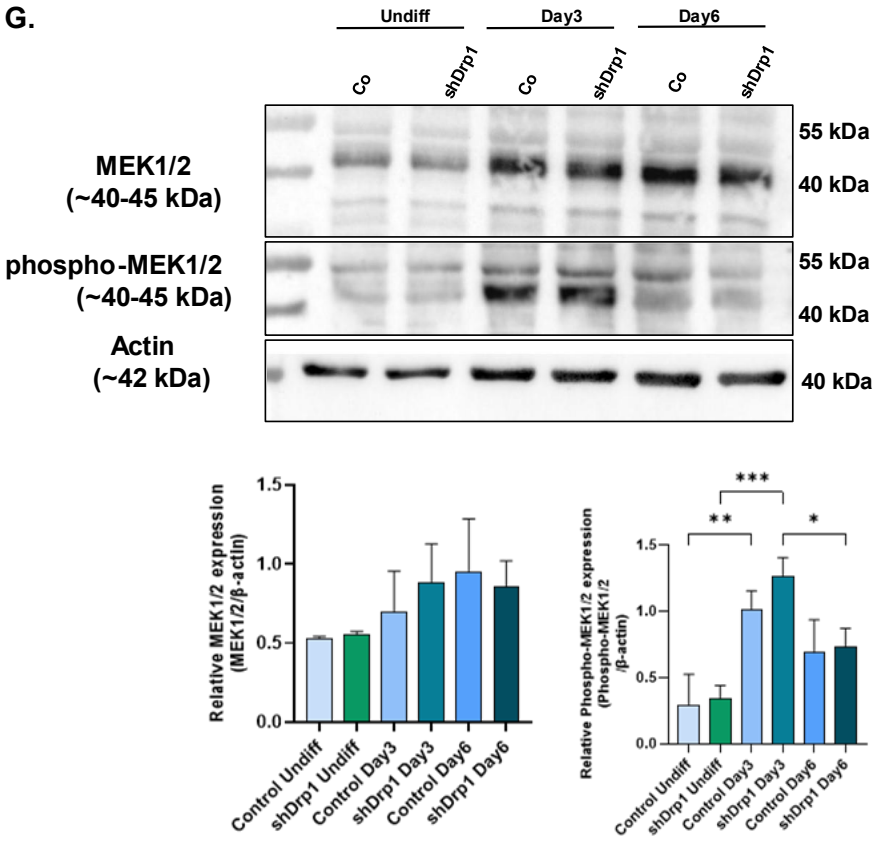
Undiff
Day3
Day6
Co
shDrp1
Co
shDrp1
Co
shDrp1
MEK1/2
(~40-45 kDa)
55 kDa
40 kDa
phospho-MEK1/2
(~40-45 kDa)
55 kDa
40 kDa
Actin
(~42 kDa)
40 kDa
Relative MEK1/2 expression
(MEK1/2/β-actin)
Relative Phospho-MEK1/2 expression
(Phospho-MEK1/2
/β-actin)
Control Undiff
shDrp1 Undiff
Control Day3
shDrp1 Day3
Control Day6
shDrp1 Day6

H.

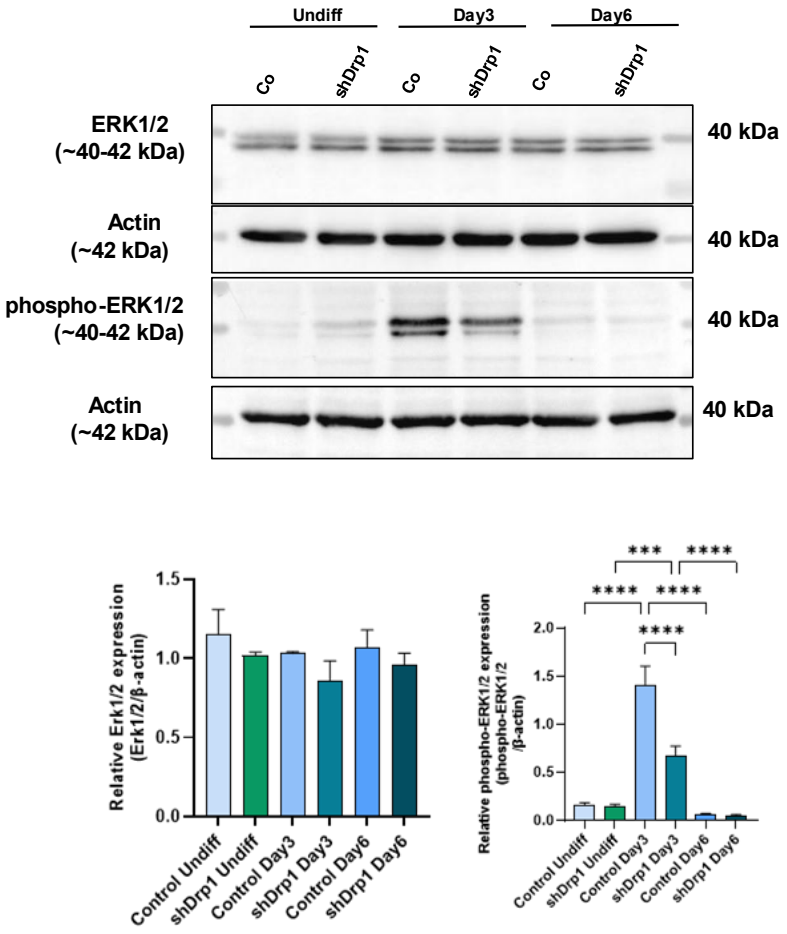

Fig. 12: ***Phosphorylation of ERK1/2 was decreased in shDrp1 cells on Day 3 following the RA-induced differentiation compared to control****. (A) The phospho-kinase assay in control and shDrp1. Cells were treated with DMSO or RA. Cell lysates were incubated with membrane-capturing antibodies (duplicates) of 43 kinase phosphorylation sites, half on one membrane (referred as A) and half on another membrane (referred as B). Subsequently, the membranes were incubated with biotinylated detection antibodies and streptavidin-HRP. Protein detection was done using the ChemiDoc machine's chemiluminescence system. (B) Heatmaps generated by StranNGS represent the MAPK cascade's gene expression pattern (GO:0043408). (C) Heatmaps of ERK1 and ERK2 pathway gene expression (GO:0070371) generated by Ward's lonkage method using hierarchical clustering algorithm and with StranNGS software similarity indexes were measured by Euclidean distance metric. Log2 scale, color scheme, and histogram are normalized gene expression values. (D-H upper panel) AKT and members of the MAP kinase signaling pathways' protein and phospho-protein levels were examined in undifferentiated and differentiated (Day 3 and 6). Cells were kept in 10 µM RA till day 3 and then till day 6 in 1% N2 Supplement and 50 ng/ml BDNF. Lysed the samples using RIPA buffer for SDS-PAGE separation. 20 ug of protein was loaded in each well, and western blot analysis was done to analyze protein*

levels using anti-AKT, anti-P-AKT, anti-JNK, anti-P-JNK, anti-ERK1/2, anti-P-ERK1/2, anti-P38, anti-Phospho-P38, anti-MEK1/2 and anti-phospho-MEK1/2 antibodies. β-actin and GAPDH were used as a loading control. Representative images of the western Blot are shown here. Images were taken using the ChemiDoc Imaging machine. (D-H lower panel) statistical analysis of the relative protein expression of the corresponding protein or phospho-protein is presented. Utilizing ChemiDoc Imager, images were captured, and pixel intensity was measured and standardized to β-actin, the internal loading control. Groups were compared using One-Way ANOVA where (indicates p <0.05, ** indicates p <0.01, *** indicates p< 0.001 and **** indicates p<0.0001). Data are presented as mean values ± SD (n = 4).*

4.4. DUSP1 and DUSP6 has no impact on ERK1/2 dephosphorylation in shDrp1 cells during neuronal differentiation

Dual-specificity mitogen-activated protein kinase 1 and 2 (MEK1/2) regulates the ERK 1/2 phosphorylation. In both cell lines, the MEK1/2 was activated upon RA treatment of neuronal differentiation, and no dissimilarity was observed between the two cell lines. This led us to ask if the difference in the ERK1/2 phosphorylation levels is due to phosphatases. Phosphatases are a group of proteins that dephosphorylate various target proteins. DUSPs or dual specificity phosphatases (DUSP1 and DUSP6) dephosphorylate ERK1/2. Thus, to investigate the role of dual specificity phosphatases on ERK1/2, we treated control and shDrp1 cells with BCI (a specific DUSP1/6 inhibitor) for 24 hrs. First, the cells were treated with RA on Day 0, and on Day 2, they were treated with BCI for 24 hours. After completing the phase 1 differentiation, cells were collected. 1μM treatment of BCI induced a strong level of ERK1/2 phosphorylation in control cells but not in shDrp1 cells (**Fig. 13A**). Therefore, we used 1μM BCI in our subsequent experiments. We compared the ERK1/2 and ERK1/2 phosphorylation levels. We compared with or without BCI treatment in undifferentiated and differentiated control and shDrp1 cells. ERK1/2 remained steady in treated or untreated control or shDrp1 cells (**Fig B-C**). In undifferentiated control and undifferentiated shDrp1 cells, no increase in phospho-ERK1/2 level by BCI treatment was found. However, in phase 1 differentiation, control cells showed significant upregulation in phospho-ERK1/2 level compared to undifferentiated control cells. BCI treatment induced substantial levels of ERK1/2 phosphorylation in control cells on Day 3 differentiation. Still, no significant impact was shown on shDrp1 cells (**Fig. 13B and D**). In transcriptomic data, we detected lower levels of DUSP2 (dual specificity phosphatase 2) in undifferentiated shDrp1 cells. To confirm this, we measured the DUSP2 gene analysis by RT-qPCR in undifferentiated control and shDrp1 and in differentiated control and shDrp1 cells. We found a significant upregulation of DUSP2 in differentiated shDrp1 cells compared to undifferentiated shDrp1 cells

and differentiated control cells. However, a significant decrease was shown in differentiated control cells compared to corresponding undifferentiated cells, indicating that DUSP2 is more active in differentiated shDrp1 cells (**Fig. 13E**). These results suggest that ERK1/2 dephosphorylation by DUSP1/6 might depend on DRP1 and DUSP2 upregulation might play a part in the dephosphorylation of ERK1/2 in shDrp1 cells.

A.

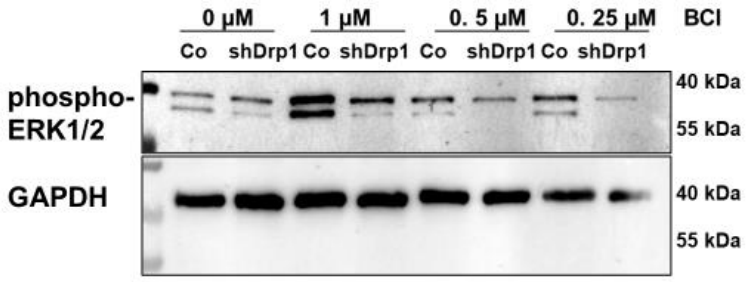
0 μM
1 μM
0. 5 μM
0. 25 μM
BCl
Co shDrp1 Co shDrp1 Co shDrp1 Co shDrp1
phospho-ERK1/2
GAPDH
40 kDa
55 kDa
40 kDa
55 kDa

B.

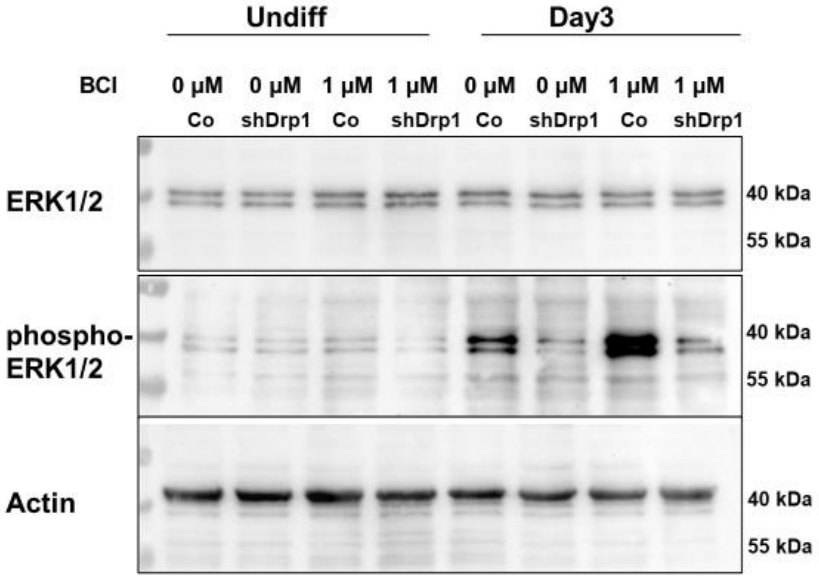
Undiff
Day3
BCl
0 μM 0 μM 1 μM 1 μM 0 μM 0 μM 1 μM 1 μM
Co shDrp1 Co shDrp1 Co shDrp1 Co shDrp1
ERK1/2
phospho-ERK1/2
Actin
40 kDa
55 kDa
40 kDa
55 kDa
40 kDa
55 kDa

C.

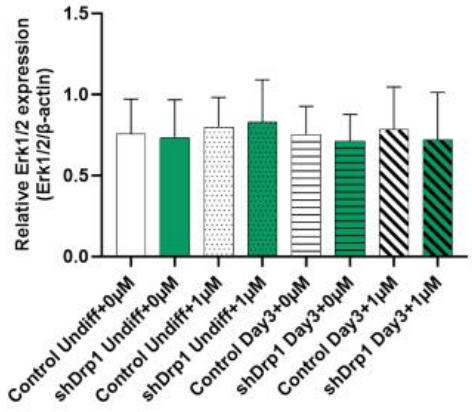
Relative Erk1/2 expression (Erk1/2/β-actin)
1.5
1.0
0.5
0.0
Control Undiff+0μM
shDrp1 Undiff+0μM
Control Undiff+1μM
shDrp1 Undiff+1μM
Control Day3+0μM
shDrp1 Day3+0μM
Control Day3+1μM
shDrp1 Day3+1μM

D.

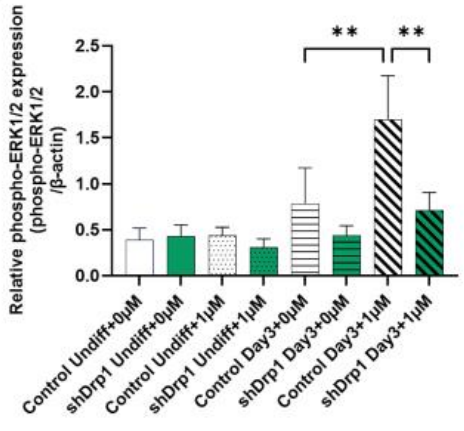
Relative phospho-ERK1/2 expression (phospho-ERK1/2 /β-actin)
**
**
2.5
2.0
1.5
1.0
0.5
0.0
Control Undiff+0μM
shDrp1 Undiff+0μM
Control Undiff+1μM
shDrp1 Undiff+1μM
Control Day3+0μM
shDrp1 Day3+0μM
Control Day3+1μM
shDrp1 Day3+1μM

E.

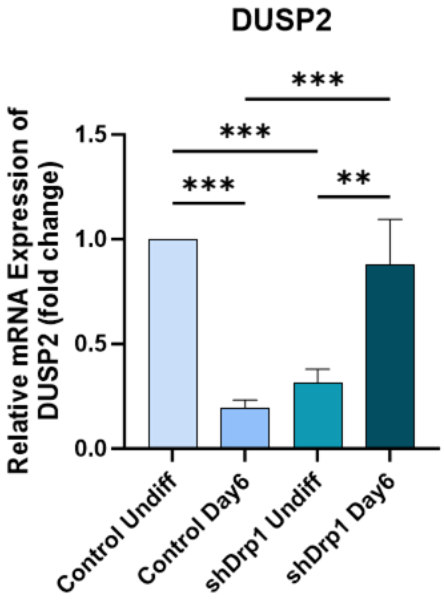

Fig. 13: ***Inhibition of dual specificity phosphatases 1 and 6 does not result in elevated levels of phospho-ERK1/2 in shDrp1 cells.*** *(A) Protein and phosphoprotein levels of ERK1/2 were analyzed using SDS-PAGE and western blotting in undifferentiated and differentiated control and shDrp1 cells. The cells were exposed to DMSO or 10 μM RA for 3 days to initiate phase 1 differentiation. Both control and shDrp1 cells were treated with vehicle and different concentrations of BCI for 24 hrs on Day 2. Cells were lysed using RIPA buffer and an equal amount of protein as separated. GAPDH served as the internal loading control. The representative images are shown. (B) The protein and phospho-protein levels of ERK1/2 were assessed using SD-PAGE and western blotting in undifferentiated and differentiated control and shDrp1 cells. To induce phase 1 differentiation, the cells were treated with DMSO and 10 μM RA for 3 days. On Day 2, both control and shDrp1 cells received treatment with either vehicle or 1μM BCI for 24 hours. Cell lysis was carried out using RIPA buffer, and several proteins were separated. The internal loading control was β-actin. Representative images from the western blots and statistical analysis show relative protein expression of (C) ERK1/2 and (D) phospho-ERK1/2. The images were captured with a ChemiDoc imager; the pixel was measured and standardized to β-actin as the internal loading control. Results are presented as mean values ±SD (n=4). Group comparisons were conducted using One-Way ANOVA (** indicates p < 0.01 and ns indicates not significant). (E). Relative mRNA expression of DUSP2 in differentiated and undifferentiated control and shDrp1 cells. Differentiated samples are normalized to their corresponding undifferentiated cells. The data is analyzed by a* $2^{-\Delta\Delta Ct}$ *method. Data is presented as mean values ±SD (n=3) where ** indicates p <0.01 and *** indicates p< 0.001.*

4.5. During neuronal differentiation control and shDrp1 cells rearrange the mitochondrial morphology and adapt to metabolic changes

DRP1 plays a vital role in controlling mitochondrial dynamics. The mitochondrial morphology depends on its function. In neural stem cells, mitochondria undergo changes during the differentiation in the developing adult brain. This process is governed by mitochondrial fusion/fission cycle proteins. Differentiated neurons display elongated structures in the developing brain and in the adult hippocampus (Beckervordersandforth et al., 2017; Khacho et al., 2016; Khacho & Slack, 2018). We performed live staining in a High Content Analysis imaging system to check the effects of DRP1 depletion on mitochondrial morphology during neuronal differentiation. Mitotracker Red CMXRos was used to stain the mitochondria, and Hoechst was used to stain nuclei. Undifferentiated control cells exhibited dispersed tubular mitochondrial structure. However, differentiated control cells on day 6 contained densely connected elongated tubular and compact mitochondrial structures (**Fig. 14A** upper panel). These changes suggest that mitochondria in control cells underwent remodeling during differentiation. Undifferentiated and differentiated shDrp1 cells showed elongated tubular, compact, and densely packed mitochondrial morphology, implying that the mitochondria in shDrp1 cells do not experience remodeling during differentiation. Comparable results were obtained by (Vantaggiato et al., 2019) in mouse carcinoma P19 cells (**Fig. 14A**, lower panel). We measured the mitochondrial characteristics of undifferentiated and differentiated control and shDrp1 cells using live-cell high-content image analysis with a method established by our group. The quantification confirmed a notable increase in both cell lines' long, elongated, and round compact tubular mitochondrial populations during differentiation. Additionally, there appears to be a morphological transition of mitochondria from short to long tubular structures. Differentiated shDrp1 cells showed significantly higher proportions of extended, elongated, and round compact tubular mitochondria than differentiated control cells (**Fig. 14B**).

A.

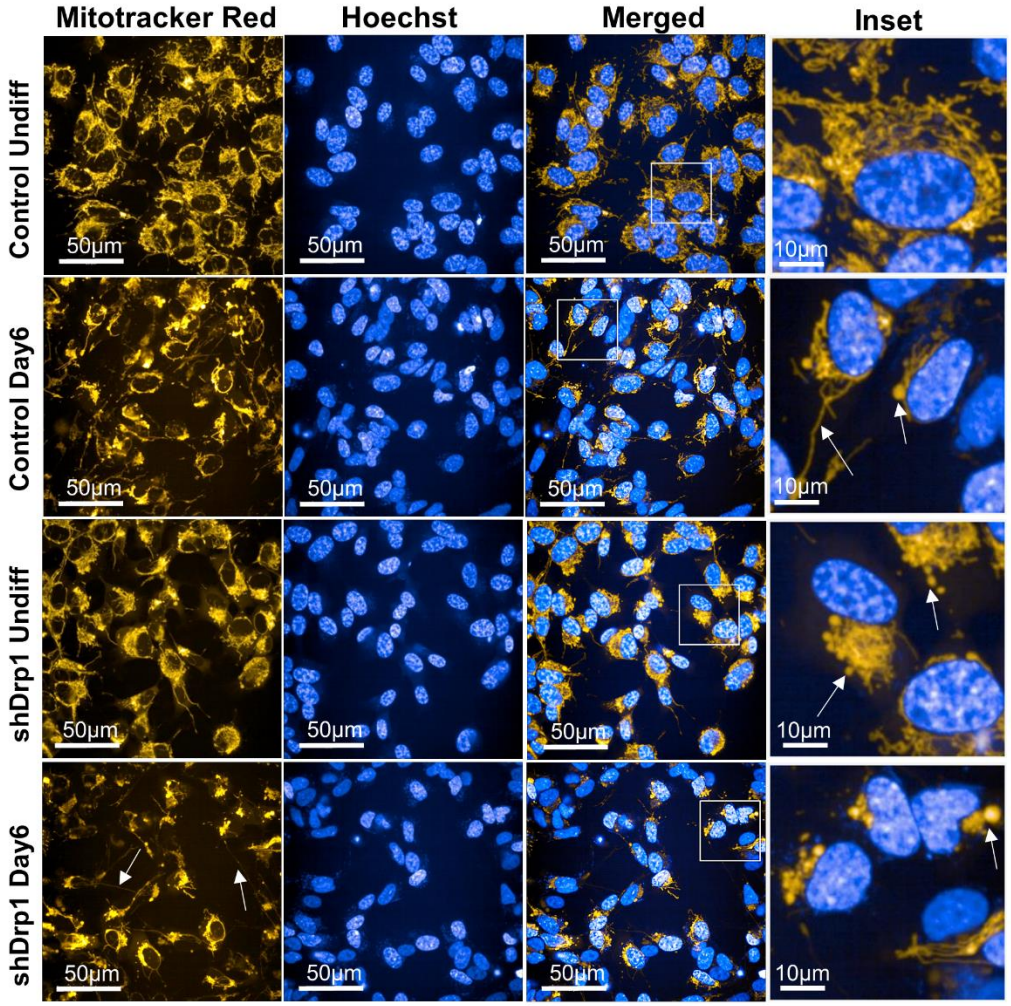
Mitotracker Red
Hoechst
Merged
Inset
Control Undiff
Control Day6
shDrp1 Undiff
shDrp1 Day6
50µm
10µm

B.

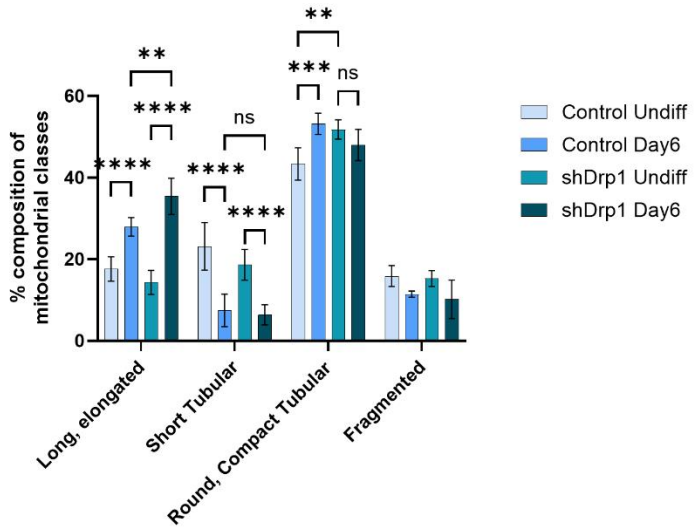
% composition of mitochondrial classes
60
40
20
0
**
****
****
ns
****
****
**
***
ns
Long, elongated
Short Tubular
Round, Compact Tubular
Fragmented
Control Undiff
Control Day6
shDrp1 Undiff
shDrp1 Day6

Fig. 14: ***shDrp1 cells do not experience mitochondrial remodeling during differentiation****. To achieve neuronal differentiation, cells were treated with RA for 3 days (Day 0-3) and 50 ng/ml of BDNF for the additional 3 days (Day 3-6). (A) Automated confocal microscopy was performed on an Opera Phenix high-content screening system. 63× water objective was used to capture images of undifferentiated and differentiated control and shDrp1 cells stained with MitoTracker Red CMXRos for mitochondria and Hoechst for nuclei. (B) Mitochondrial categories were quantified using the built-in software Harmony 4.9 and PhenoLogic machine learning software. The identified classes included long tubular (elongated), short tubular, compact tubular (round), and fragmented mitochondria. The number of mitochondrial populations was assessed in undifferentiated and differentiated control and shDrp1 cells, expressed as a percentage of the total count. More than 300 cells were analyzed per sample for statistical significance using Two-way ANOVA with multiple comparisons (** indicates p <0.01, *** indicates p <0.001 and **** indicates p <0.0001).*

A study detected slightly high DRP1 levels during differentiation (Uo et al., 2009). Similarly, we also checked the DRP1 levels but found no significant changes in our control cells. shDrp1 cells maintained its essential depletion of DRP1 throughout the RA-BDNF-induced differentiation (**Fig. 15A**). Due to their functional importance, S616 and S637 are the two most known phosphorylation sites of DRP1. S616 DRP1 phosphorylation activates mitochondrial fission, while S637 dissociates the DRP1 attachment from mitochondria and activates mitochondrial fusion (Lee & Kim, 2018). We also checked these phosphorylation levels in phase 1 and phase 2 of differentiation in control cells. The S616 phosphorylation gradually increased with RA and BDNF treatments. However, S637 phosphorylation was triggered upon RA treatment and abolished upon BDNF treatment (**Fig. 15B**).

Mitofusins (MFN1 and MFN2) and OPA1 are mitochondrial fusion proteins. Interestingly, reduced levels of DRP1 did not lead to any significant changes in the expression level of OPA1 in both undifferentiated and differentiated control and shDrp1 cells (**Fig. 15C**). Amid differentiation, the MFN1 levels increased significantly in control and not in shDrp1 cells. However, the levels of MFN2 did not change in either of the cell lines. The level of MFN1 increases during the differentiation. In comparing shDrp1 cells to the respective control cells in all phases, the levels of both MFN1 and MFN2 decrease significantly (**Fig. 15D-E**). Reducing mitochondrial fusion proteins is a compensatory mechanism for losing the leading mitochondrial fission protein, i.e., DRP1. Similar results were found by (Wakabayashi et al., 2009) in the MEF

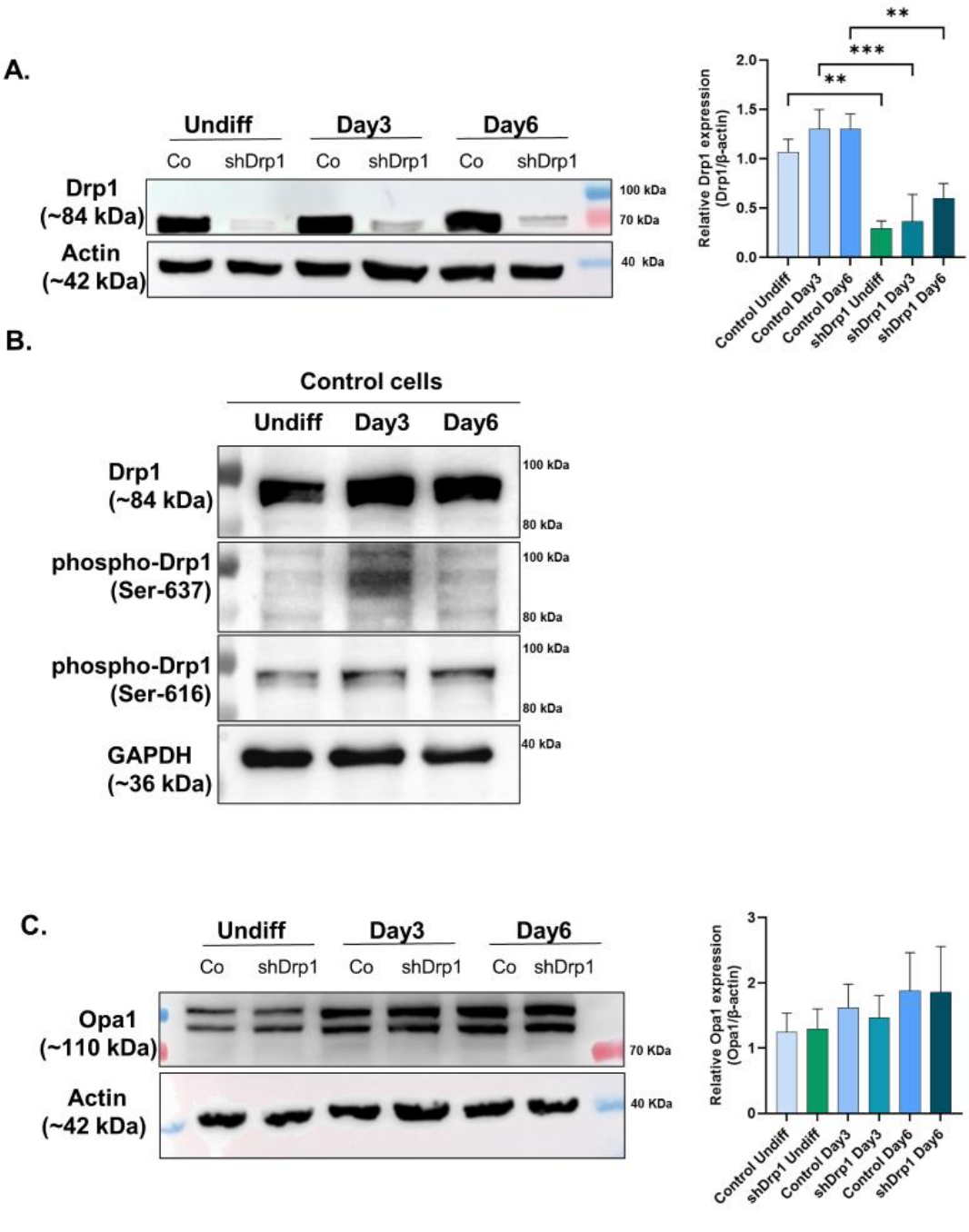
A.
Undiff
Day3
Day6
Co
shDrp1
Co
shDrp1
Co
shDrp1
Drp1
(~84 kDa)
Actin
(~42 kDa)
100 kDa
70 kDa
40 kDa
Relative Drp1 expression
(Drp1/β-actin)
2.0
1.5
1.0
0.5
0.0
**
***
**
Control Undiff
Control Day3
Control Day6
shDrp1 Undiff
shDrp1 Day3
shDrp1 Day6
B.
Control cells
Undiff
Day3
Day6
Drp1
(~84 kDa)
phospho-Drp1
(Ser-637)
phospho-Drp1
(Ser-616)
GAPDH
(~36 kDa)
100 kDa
80 kDa
100 kDa
80 kDa
100 kDa
80 kDa
40 kDa
C.
Undiff
Day3
Day6
Co
shDrp1
Co
shDrp1
Co
shDrp1
Opa1
(~110 kDa)
Actin
(~42 kDa)
70 KDa
40 KDa
Relative Opa1 expression
(Opa1/β-actin)
3
2
1
0
Control Undiff
shDrp1 Undiff
Control Day3
shDrp1 Day3
Control Day6
shDrp1 Day6

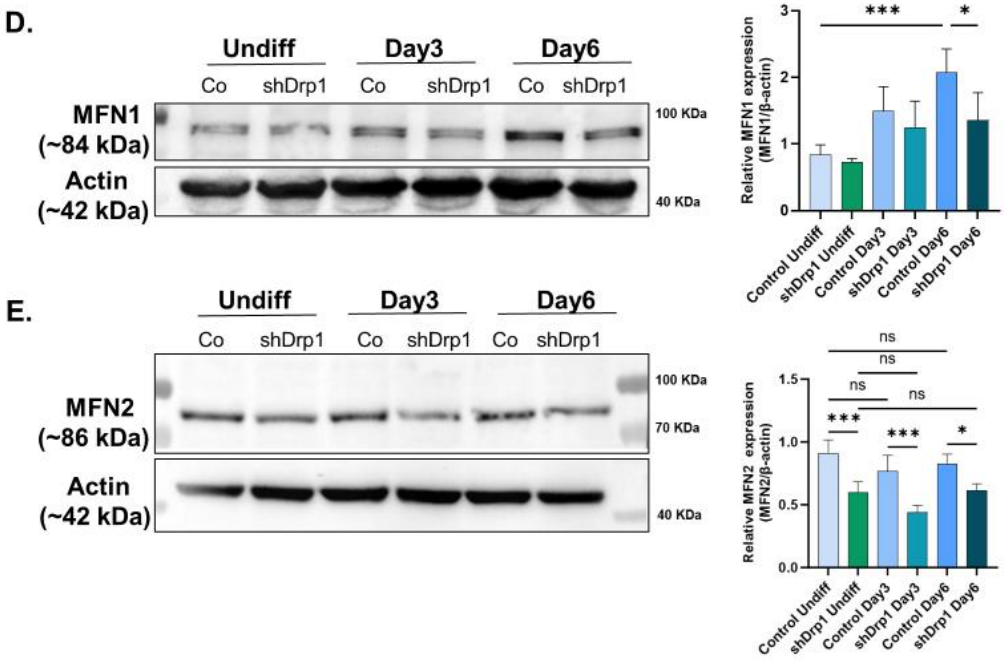

Fig 15: ***Cells with depleted DRP1 show lower mitochondrial proteins MFN1 and MFN2 levels than control cells.*** *(A) The protein level of mitochondrial fission protein was examined using an anti-DRP1 antibody. (B) The phosphorylation status of DRP1 at S637 and S616 was examined using anti-DRP1 and phospho-specific antibodies in undifferentiated and differentiated control cells. The total lysate was lysed using RIPA buffer, and an equal amount of protein was separated. GAPDH was used as an internal loading control. Representative images are shown. (C-E Left panel) The protein levels of mitochondrial fusion proteins were examined using (C) anti-Opa1, (D) anti-MFN1, and (E) anti-MFN2 antibodies in undifferentiated and differentiated control and shDrp1 cells. Cells were lysed with RIPA buffer, and an equal amount of protein was loaded into each well, separated by SDS-PAGE, and analyzed by western blotting using β-actin as a loading internal control. Representative images of the western Blot are shown here. Images were taken using a chemiDoc imaging machine; pixel intensity was quantified and normalized to β-actin. (A, C-E Right panel) Statistical analysis of relative protein expression of DRP1, Opa1, MFN1, and MFN2 was done using One-Way ANOVA. Data are presented as mean values ± SD (n = 4), where (* indicates $p < 0.05$, ** indicates $p < 0.01$, *** indicates $p < 0.001$ and ns indicates not significant).*

single knockout DRP1 (DRP1-/+) cell line. These results indicate that mitochondrial protein reduction is a coping mechanism to ensure the proper functioning of the cells with reduced mitochondrial proteins.

To check the effect of DRP1 absence on cellular bioenergetics during neuronal differentiation, OCR (oxygen consumption rate) was measured in Undifferentiated, phase 1 (Day3) and phase 2 (Day6) of differentiation in both control and shDrp1 cells. OCR was calculated at the basal metabolic rate, and then OCR was calculated after sequentially adding selective mitochondrial inhibitors. At first, oligomycin was added, which blocks the mitochondrial ATP synthase by inhibiting the passing of the proton to the mitochondrial membrane. Secondly, FCCP (cyanide-p-triflouromethoxyphenylhydrazone) was injected, which collapses the proton gradient around the inner mitochondrial membrane, reducing ATP synthesis and uncouples mitochondrial respiration. This uncoupling of mitochondrial respiration, i.e., maximal respiration values, is measured by deducting it from basal respiration values. In the third step, a combination of two drugs, rotenone, and antimycin A, which encumber the respiration by mitochondrial complex I and mitochondrial complex III, respectively, were used to inhibit mitochondrial respiration. This combination (rotenone and Antimycin A) was used to distinguish the difference between mitochondrial and non-mitochondrial respiration. The response to increased energy demands by substrates or electron transport chains is called spare respiratory capacity, measured by subtracting basal respiration from maximal respiration. Coupling efficiency represents the ratio of oxygen consumed for ATP production. It is determined as the portion allocated for the ATP synthesis from basal respiration. Proton leak is the passive movement of the proton back to the matrix despite oligomycin addition (**Fig. 16A**).

The cellular bioenergetics of undifferentiated control and shDrp1 were not significantly different. However, differentiated shDrp1 cells indicated an increasing trend in maximal respiration compared to undifferentiated shDrp1 cells and differentiated control cells. Other parameters such as basal respiration, ATP-linked respiration, proton leak, and spare respiratory capacity also showed an increase but not significant change in differentiated cells (**Fig. 16B**). These results suggest the RA-BDNF-induced neuronal differentiation in SH-SY5Y cells *in vitro* causes functional and morphological reprogramming of mitochondria in control cells and shDrp1 cells, and DRP1 knockdown alter cellular bioenergetics during differentiation.

A.

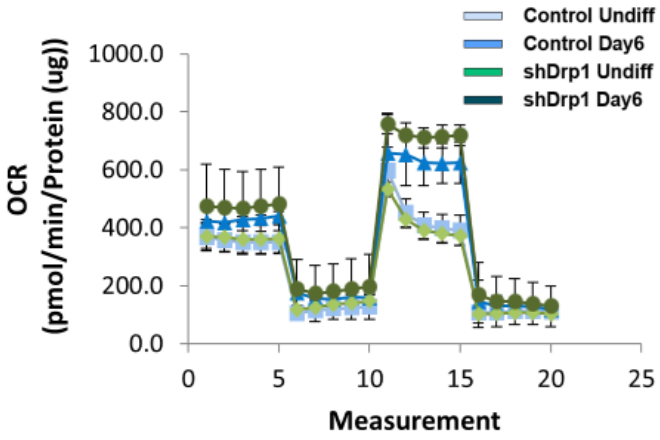
Control Undiff
Control Day6
shDrp1 Undiff
shDrp1 Day6
OCR (pmol/min/Protein (ug))
1000.0
800.0
600.0
400.0
200.0
0.0
0
5
10
15
20
25
Measurement

B.

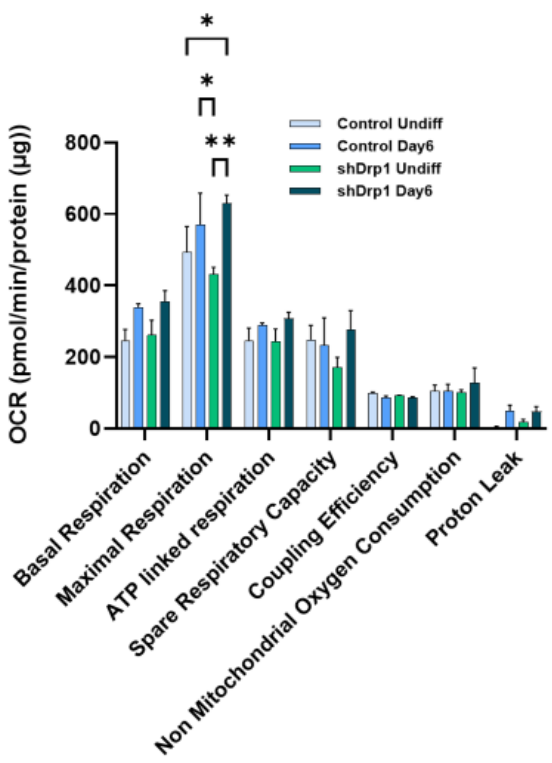
*
*
**
Control Undiff
Control Day6
shDrp1 Undiff
shDrp1 Day6
OCR (pmol/min/protein (µg))
800
600
400
200
0
Basal Respiration
Maximal Respiration
ATP linked respiration
Spare Respiratory Capacity
Coupling Efficiency
Non Mitochondrial Oxygen Consumption
Proton Leak

Fig. 16: ***Bioenergetics remodeling occurs during differentiation in both control and shDrp1 cells with a noticeable change in maximal respiration between the two cell lines****. Oxygen consumption rate (OCR) was measured in undifferentiated and Day 6 differentiated control and shDrp1 cells. (A) Control and shDrp1 cells were seeded 24 hrs before assay in Seahorse XF 96 well-plates. The baseline oxygen consumption rate was calculated 30 minutes before and after the sequential addition of 1.5 μM oligomycin (Olig), 1 μM FCCP, and a cocktail of 1 μM rotenone/Antimycin A (Anti/Rot) mitochondrial inhibitors. (B) The data shows the derived parameters for mitochondrial respiration on OCR measurements, normalized to total protein concentration (pmol/min/μg protein). Data were analyzed using Wave Desktop software and presented as mean values ± SEM (n = 3). Statistical analysis was performed using Two-Way ANOVA using GraphPad Prism v9.5.1 software (* indicates p< 0.05, and ** indicates p< 0.01).*

4.6. RA and mitochondrial inhibitors exposure to DRP1 depleted cells is dispensable for cell death

RA promotes neuronal differentiation in neural stem cells (NSC) (J.-C. Park, Jeong, Kim, Min, & Choi, 2016) in SH-SY5Y human neuroblastoma cells, (Teppola et al., 2016) in mouse embryonic stem cells (Dutta, Pal, & Rao, 2023). RA binds with two different receptors, PPARβ/δ or RAR. The result of the first binding is growth stimulating, while the second binding is the inhibition of cell proliferation, apoptosis, and induction of differentiation. This depends on the binding of the RA with intracellular receptors, which suggests the role of RA in cell growth and death (Noy, 2010; Wolf, 2008).

To check the cell viability of DRP1-depleted cells, we treated both control and shDrp1 cells with 10 μM of RA for three days. Sulphorhodamine B assay (SRB), which measures cellular protein content, was used to check the cellular viability. As anticipated, the RA caused a significant increase in cell death in both control and shDrp1 cells. However, there were no differences between the two cell lines (**Fig. 17A**). Propidium iodide stains, specifically necrotic and late apoptotic cells, excluding live and apoptotic cells. Propidium iodide staining revealed a slight increase in cell death at Day 3 and 6 in both control and shDrp1 cells. A significant increase was found in shDrp1 cells on Day 6, but there was no significant difference between control and shDrp1 cells (**Fig. 17B**). Cells undergo stress when exposed to mitochondrial toxins. To cope with this stress and maintain a quality control mechanism, cells trigger cell death with the assistance of the mitochondrial fission protein DRP1 (Stephan Frank et al., 2001). To carefully monitor the cell death in DRP1-depleted cells, we treated the cells with different mitochondrial inhibitors such as oligomycin (ATP synthase inhibitor), rotenone (complex I inhibitor), and Antimycin A (complex III inhibitor). SRB assay was used to monitor the viability of the cell in

control and shDrp1 cells. The treatment of 100 nM Antimycin and 3 µM oligomycin did not cause any decrease in cell viability of both cell lines. The 10 µM rotenone treatment decreased the cell viability significantly in both cell lines (**Fig. 17C**). These results suggest that DRP1 does not play a role in the modulation of cell death induced either during RA-induced neuronal differentiation or during mitochondrial inhibitor treatment in undifferentiated SH-SY5Y neuroblastoma cells in vitro.

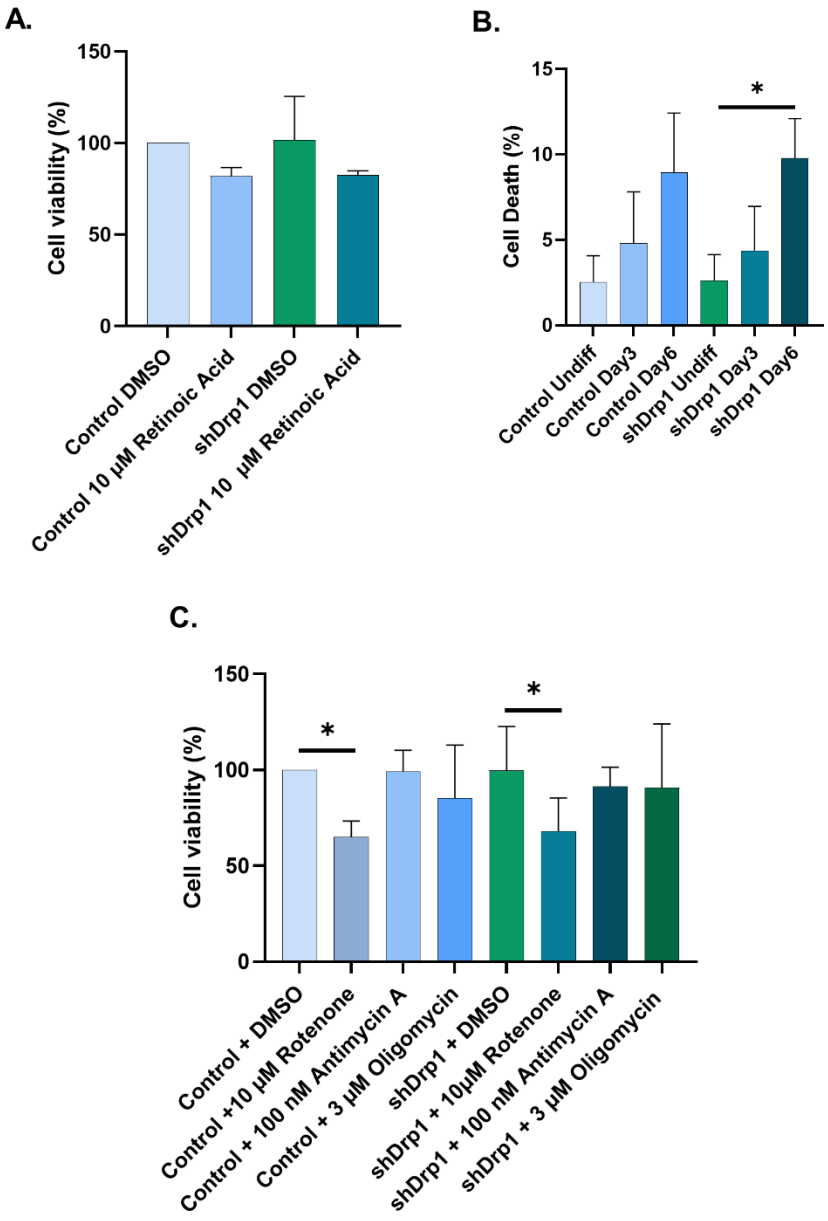

Fig. 17: ***DRP1 depleted cells show minimal cell death when treated with RA and selective mitochondrial inhibitors compared to control.*** *(A) Cell viability of control and shDrp1 cells was*

checked by sulphorhodamine B (SRB) assay. Undifferentiated control and shDrp1 cells were treated with DMSO or 10 μM RA. The results are indicated as ±SD of three independent experiments. Data was analyzed using One-Way ANOVA. (B) The impact of DRP1 reduction following differentiation was also examined. Cell death was assessed through propidium iodide staining in undifferentiated and differentiated control and shDrp1 cells. The results display the means ± SD of three separate experiments. Statistical analysis was done using One-Way ANOVA with GraphPad Prism v9.5.1 software where (indicates p < 0.05, ** indicates p < 0.01, and ns indicates not significant). (C) Cell viability was evaluated using the SRB assay for undifferentiated control and shDrp1 cells treated with DMSO, 10 μM Rotenone, 3 μM Oligomycin, or 100 nM Antimycin A. Data presented as means ±SD of three independent experiments; statistical analysis involved One-Way ANOVA. Only significant differences are displayed (* indicates p <0.05).*

4.7. DRP1 depletion provides protective effects upon overexpression of mutant Huntington protein in SH-SY5Y neuroblastoma cells

Research on neurons of HD patients and transgenic mice models has indicated that the increased mitochondrial fragmentation and abnormal mitochondrial dynamics result from elevated enzymatic activity of DRP1 triggered by mutant huntingtin protein. (Shirendeb et al., 2012). This abnormal interaction of DRP1 and mutant huntingtin protein disrupts mitochondria's fusion and fission balance and causes neuronal cell death (Song et al., 2011). For this purpose, we investigated the role of DRP1 knockdown in the formation of toxic mutant huntingtin protein aggregates. 23 polyQ N-Htt represents the normal length of the protein, and 74 polyQ N-Htt represents the mutant form of the huntingtin protein. Normal and mutant forms of huntingtin or Htt proteins (fused with HA tag) were transiently transfected in the undifferentiated control and shDrp1 cells for 72 hrs. After 72 hrs post-transfection, the fixed cells were monitored using High Content Analysis. The 23 polyQ N-Htt fragments showed cytoplasmic distribution in control and shDrp1 cells (**Fig. 18A-C**). However, 74 polyQ N-Htt fragments depicted a combination of cytoplasmic and aggregated distribution in control and DRP1-depleted cells. The aggregated distribution varied in size, number, and shape (**Fig. 18B-D**). An algorithm was established to assess the mutant huntingtin protein formation quantitatively. The fluorescent intensity of N-Htt/mHtt was normalized to true nuclei using batch analysis in untransfected cells, cells expressing normal N-Htt, and cells expressing mutant N-Htt fragments. There was an increase in the number of aggregates in both control and DRP1 knockdown cells expressing mutant huntingtin proteins compared to their respective untransfected cells or cells expressing 23 polyQ

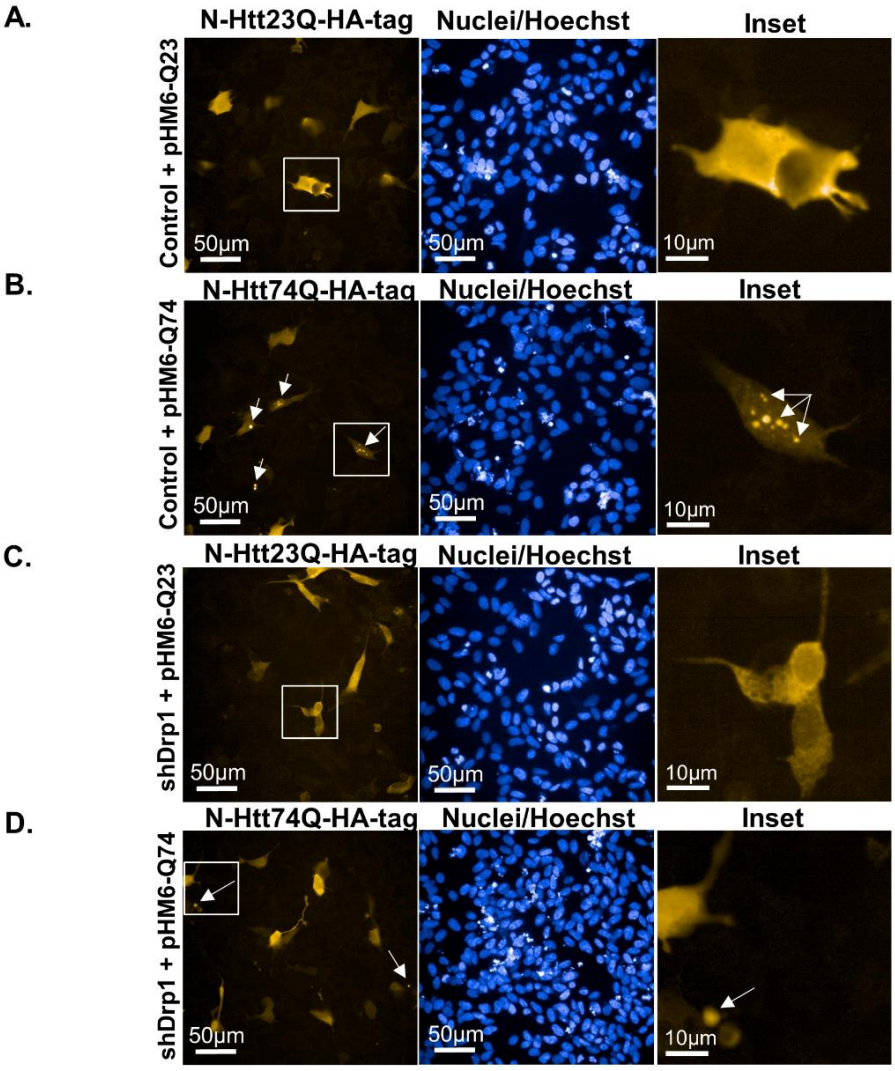
A.
N-Htt23Q-HA-tag
Nuclei/Hoechst
Inset
Control + pHM6-Q23
50µm
50µm
10µm
B.
N-Htt74Q-HA-tag
Nuclei/Hoechst
Inset
Control + pHM6-Q74
50µm
50µm
10µm
C.
N-Htt23Q-HA-tag
Nuclei/Hoechst
Inset
shDrp1 + pHM6-Q23
50µm
50µm
10µm
D.
N-Htt74Q-HA-tag
Nuclei/Hoechst
Inset
shDrp1 + pHM6-Q74
50µm
50µm
10µm

E.

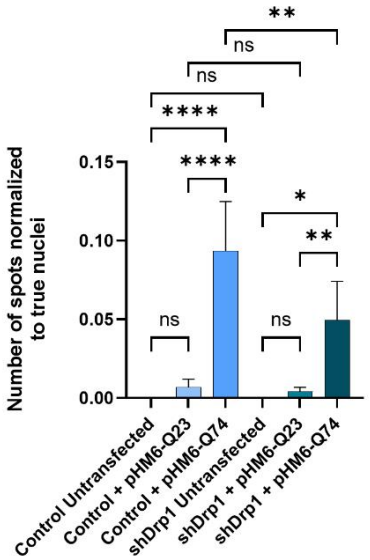
**
ns
ns
****
****
*
**
ns
ns
Number of spots normalized to true nuclei
0.15
0.10
0.05
0.00
Control Untransfected
Control + pHM6-Q23
Control + pHM6-Q74
shDrp1 Untransfected
shDrp1 + pHM6-Q23
shDrp1 + pHM6-Q74

Fig. 18: ***DRP1 depletion delays the progression of mutant huntingtin protein in the SH-SY5Y human neuroblastoma cell line****. Control and shDrp1 cells were either transfected with pHM6-Q23 (wild type N-Htt) or pHM6-Q74 (mutant N-Htt) for 72 hours. (A-D) Representative images of cells overexpressing Q23 and Q74, immunolabeled with anti-HA-tag followed by Alexa 568 secondary antibody. Hoechst was used to stain the nuclei. Images were taken using a 40x water objective using confocal microscopy of a high-content screening system. Arrows indicate toxic N-Htt aggregates. (E) Quantitative analysis of the number of mutant N-Htt aggregates in control and shDrp1 was determined using the built-in "Spot Analysis" module of Harmony 4.9 software. The numbers of shDrp1 analyzed cells were 23351 untransfected, 49701 pHM6-Q23, and 52920 pHM6-Q74 transfected cells. The numbers of control cells analyzed were as follows: 10945 untransfected, 39873 pHM6-Q23, and 43273 pHM6-Q74 transfected cells. Data are presented as mean values ± SD (n = 5) independent experiments. Statistical analysis for the number of aggregates was done by using ordinary One-Way ANOVA where (* indicates p <0.05, ** indicates p <0.01, and **** indicates p< 0.0001).*

N-Htt fragments. However, DRP1 knockdown cells showed a significant reduction in mutant N-Htt aggregate formation compared to control cells expressing mutant N-Htt. (**Fig. 18E**). In conclusion, these results suggest that the DRP1 knockdown causes a reduction in the pathogenic formation of mutant huntingtin proteins in SH-SY5Y cells.

4.8. Mutation at S39 of DRP1 results in cells lacking mitochondrial fission, leading to hyperfused mitochondria

Mitochondria are in constant fusion and fission processes to meet the energy demands and proper functioning of cellular functions. Any mutation or interruption in its fusion/fission machinery hampers its processes (Chan, 2006a; Chang et al., 2010; McBride, Neuspiel, & Wasiak, 2006). X-ray structural analysis of human DRP1 revealed that the S39 amino acid is essential for the backbone interaction of DRP1 with the α-phosphate of GTP, highlighting its critical role in GTP binding (**Fig. 19A**). According to the PhosphoSite database, the S39 residue is not a site for PTM and does not undergo phosphorylation. However, neighboring residues S40 and S44 are documented as PTM sites. These residues can be targeted for phosphorylation by glycogen synthase 3β, leading to mitochondrial fragmentation. The positioning of the S39 residue within the protein structure indicates that it is mainly concealed and, therefore, less accessible for phosphorylation (**Fig 19B-E**).

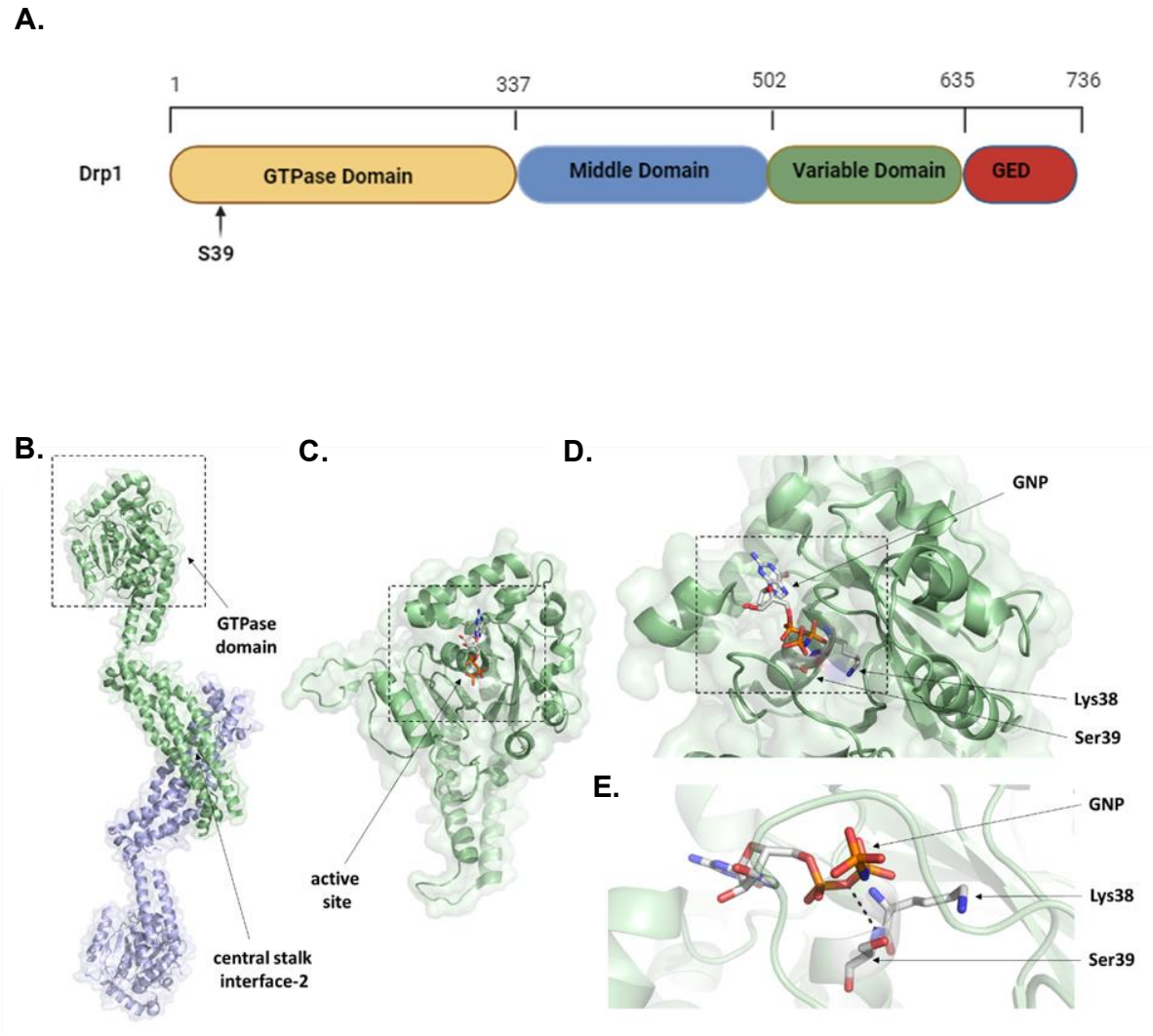

Fig. 19: ***The human DRP1 protein structure is depicted in a diagram.*** *(A) The schematic representation of DRP1 protein with S39 localization. (B) The crystal structure (PDB ID: 4BEJ) (Fröhlich et al., 2013) of the DRP1 dimer shows two monomers labeled with light green and blue colors, highlighting the GTPase domain and the dimer interface (stalk interface 2). (C) A closer look at the GTPase domain binding to 5'-guanylyl-imidodiphosphate, also known as GNP (GMP-PNP), is shown as a ligand (PDBID: AHIV) (Wenger et al., 2013). (D) This active site includes Lys38 and S39 residues (E) with an emphasized view of GNP ligand binding, indicating a hydrogen bond between the phosphate and a backbone atom of S39 alongside a representation of the Lys38 residue.*

Consequently, we created a mutant by introducing the S39A substitution via quick change mutagenesis into the mCherry-DRP1 backbone plasmid obtained from Gia Voeltz (Addgene plasmid # 49152) (J. R. Friedman et al., 2011). Western blot analysis confirmed overexpression of both mCherry-DRP1 S39A and wild-type mCherry-DRP1 in human neuroblastoma SH-SY5Y cells (**Fig. 20A**). Confocal microscopy revealed cytosolic localization with punctate structures in DRP1 S39A mutant when transfected into SH-SY5Y cells (**Fig. 20B**).

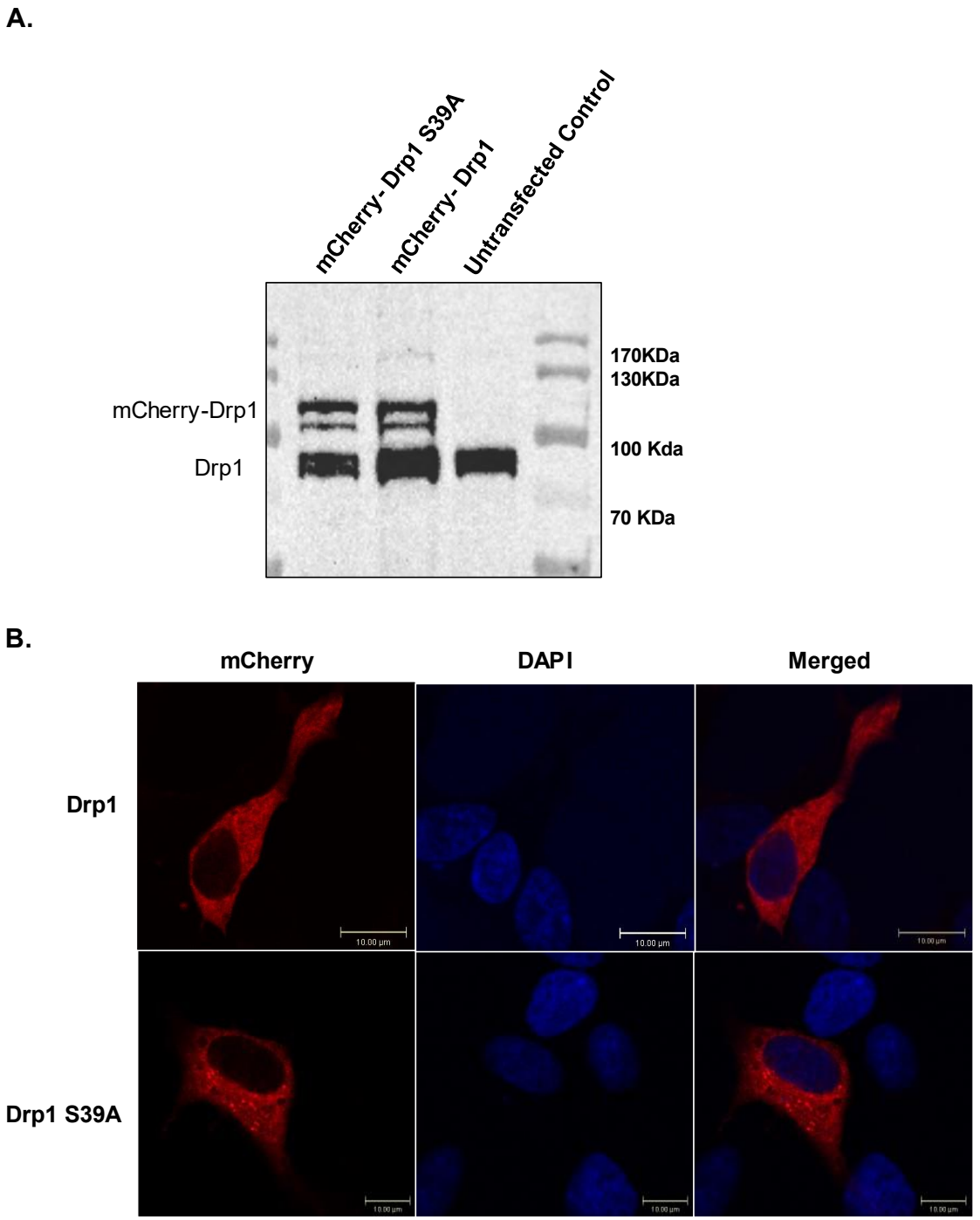

Fig. 20: ***The cytosolic localization of the overexpressed DRP1 S39A mutant is similar to the overexpressed wild-type DRP1****. (A) Western blot analysis indicates the overexpression of mCherry-DRP1 and mCherry-DRP1 S39A proteins in SH-SY5Y neuroblastoma cells. An anti-DNM1L antibody was utilized to identify the endogenous level of DRP1 and overexpressed levels of WT DRP1 and S39A mutant. (B) Cells were transfected with mCherry-DRP1 and mCherry-DRP1 S39A mutant plasmids for 72 hrs. Transfected cells stained with DAP1 to stain nuclei and plasmids were N-terminally fused with mCherry fluorescent proteins for direct monitoring and*

detection. The representative confocal microscopy images for WT mCherry-DRP1 and mCherry-DRP1 S39A mutant are shown.

Following this, we established stable SH-SY5Y neuroblastoma cell lines that expressed the mCherry fusion proteins. These included the mCherry control, mCherry-DRP1 WT, and mCherry-DRP1 S39A variants. We examined the phosphorylation status of DRP1 at S616 and S637 to determine whether the loss of function mutant impacted these two sites. Both endogenous DRP1 and the recombinant proteins were present in both the mCherry-DRP1 WT and mCherry-DRP1 S39A cell lines (**Fig. 21A**). The overexpression of the loss of function S39A mutant did not alter the phosphorylation status of DRP1 at S637 and S616 compared to control (**Fig. 21B-C**). However, it is noteworthy that overexpressing DRP1 WT increased the phosphorylation of S637 compared to both controls and DRP1 mutant S39A. (**Fig 21B-C**).

RCSB protein is a database for the information of protein structure. According to this database, it is unlikely that the S39A mutation directly impacts the phosphorylation status of two sites, S616 and S637, in the monomer structure. The mutation at position 39 might not significantly alter the structural changes that affect these specific sites and vice versa. However, at the oligomeric level, this mutation could indirectly affect the protein phosphorylation. Unfortunately, no data is available on how these amino acids are linked to DRP1 oligomers. The hypothesized effect of the S39A mutation based on structure aligns with western blot results as it does not affect the phosphorylation of other side chains. Nonetheless, structural analysis does not explain why overexpression of DRP1 WT affects S637 phosphorylation. We speculate that overexpression triggers an internal control process related to elevated stress levels and apoptosis response, leading to increased production of DRP1; thus, compensatory phosphorylation may occur to regulate its catalytic activity.

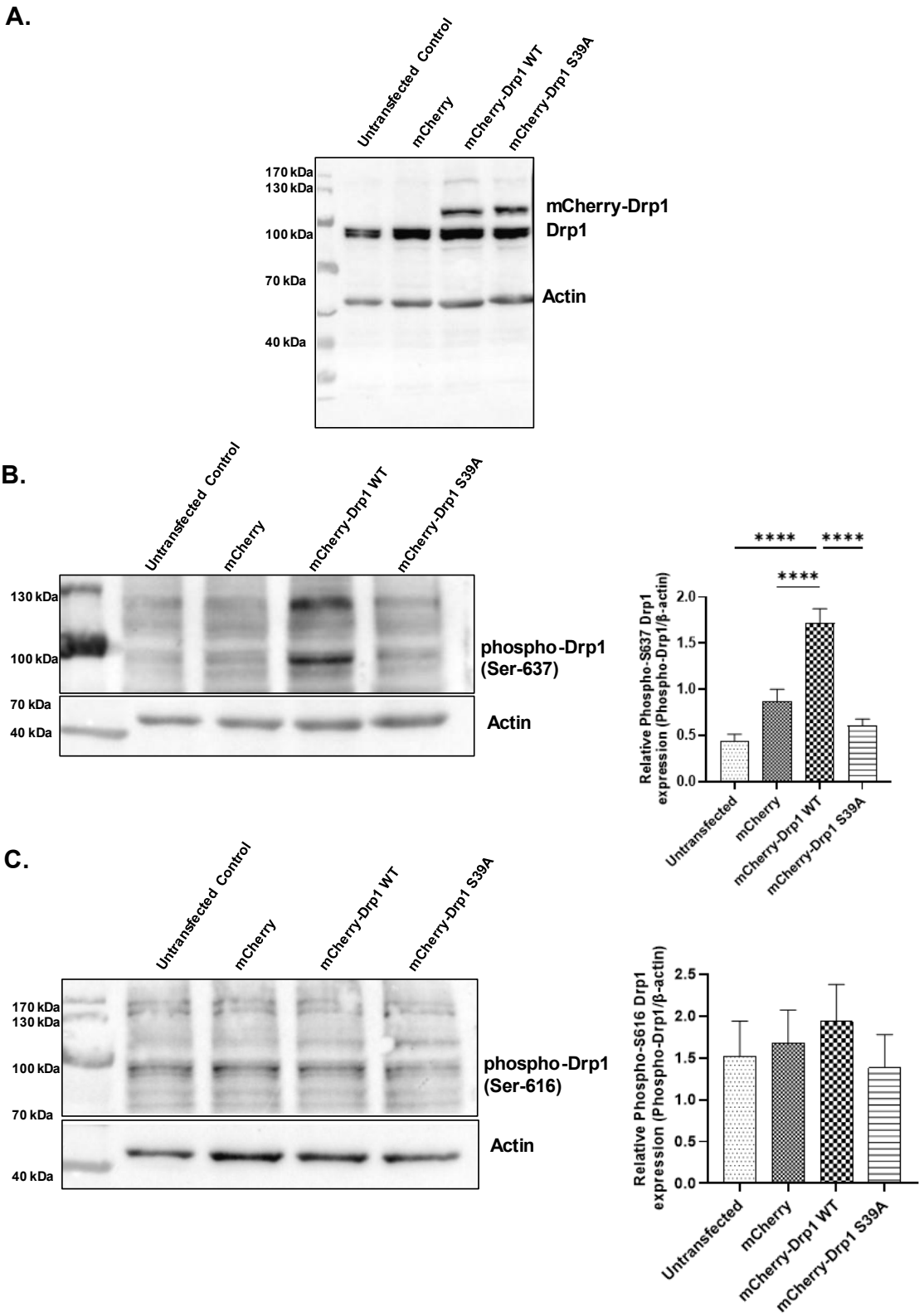
A.
Untransfected Control
mCherry
mCherry-Drp1 WT
mCherry-Drp1 S39A
170 kDa
130 kDa
100 kDa
70 kDa
40 kDa
mCherry-Drp1
Drp1
Actin
B.
Untransfected Control
mCherry
mCherry-Drp1 WT
mCherry-Drp1 S39A
130 kDa
100 kDa
70 kDa
40 kDa
phospho-Drp1 (Ser-637)
Actin
****
****
****
Relative Phospho-S637 Drp1 expression (Phospho-Drp1/β-actin)
2.0
1.5
1.0
0.5
0.0
Untransfected
mCherry
mCherry-Drp1 WT
mCherry-Drp1 S39A
C.
Untransfected Control
mCherry
mCherry-Drp1 WT
mCherry-Drp1 S39A
170 kDa
130 kDa
100 kDa
70 kDa
40 kDa
phospho-Drp1 (Ser-616)
Actin
Relative Phospho-S616 Drp1 expression (Phospho-Drp1/β-actin)
2.5
2.0
1.5
1.0
0.5
0.0
Untransfected
mCherry
mCherry-Drp1 WT
mCherry-Drp1 S39A

Fig. 21: ***The S39A mutation of DRP1 does not affect the phosphorylation status of S616 and S637****. RIPA buffer was used to prepare the cell lysate of cells stably expressing mCherry, mCherry-DRP1 WT, and mCherry-DRP1 S39A. Following protein separation on SDS-PAGE, it was transferred to a nitrocellulose membrane and analyzed using anti-DRP1 and phospho-specific antibodies. (A) unphosphorylated, (B) phosphorylated DRP1 at S637 and (C) phosphorylated DRP1 at S616. Statistical analysis of relative phosphoprotein expressions is presented as mean ±SD (n=3), with groups compared using One-Way ANOVA with multiple comparisons; only significant differences are shown where **** indicates p < 0.0001.*

4.9. Transmission electron microscopy confirms the presence of elongated mitochondrial morphology in cells that express S39A mutant stably

Mitochondrial equilibrium relies on both fusion and fission. Key regulators involved in the division process, such as DRP1, largely influence mitochondrial fission and subsequently impact these organelles' quality, function, and appearance (J. Nunnari & Suomalainen, 2012). We visualized the effects of this mutation on mitochondrial morphology by staining the cells with a TOMM20 (Translocase of outer mitochondrial membrane 20) antibody. This mutation was reported to cause elongated peroxisomes. Overexpression of wild-type DRP1 protein did not alter the mitochondrial morphology as reported by past studies (C.-R. Chang & C. Blackstone, 2007; Chang et al., 2010). The S39A mutation caused a visible difference in the mitochondrial morphology (**Fig. 22A**).

To assess cellular mitochondrial structures in cells overexpressing DRP1 S39A, we established SH-SY5Y neuroblastoma cell lines with stable overexpression of the mCherry fusion protein (referred to as control), mCherry-DRP1 and mCherry-DRP1 S39A. TEM imaging revealed that stable expression of mCherry-DRP1 S39A led to a significant increase in highly elongated giant mitochondria throughout the cells (**Fig. 22B**), indicating that S39 amino acid residue plays a crucial role in initiating GTP hydrolysis for promoting mitochondrial fission. Conversely, cells overexpressing mCherry-DRP1 exhibited more round-shaped, smaller-sized perinuclear-localized mitochondria, suggesting a shift toward increased fission dynamics (**Fig. 22B**). The ultrastructure analysis confirmed that control cells displayed a mixed population of perinuclear mitochondria undergoing continuous balanced fusion-fission processes without affecting morphology significantly whereas S39 mutation had a substantial effect on promoting mitochondrial fusion (**Fig. 22B**).

We conducted measurements of the mitochondria, including mitochondrial number, area, and internal length, using Amira 3D analysis software (Ghani et al., 2024). The number of mitochondria per cell was notably lower in cells expressing the mCherry-S39A mutant compared to the control (**Fig. 22C**). Furthermore, both the average mitochondrial internal length per cell and the average mitochondrial area per cell were significantly higher in cells expressing the mCherry-DRP1 S39A mutant compared to both control and mCherry-DRP1 WT (**Fig. 22D-E**). On another note, the total mitochondrial internal length was significantly reduced in the mCherry-DRP1 S39A cell line compared to the control; however, no significant difference was observed in the total mitochondrial area (**Fig. 22F-G**). In mCherry-DRP1 mutant S39A cells, the total mitochondrial area does not change, but a decrease in the number of mitochondria and an increase in the average inside length due to fusion in cells was observed. These findings indicate that the S39A mutation substantially impacts the mitochondrial morphology as it blocks fission.

A.

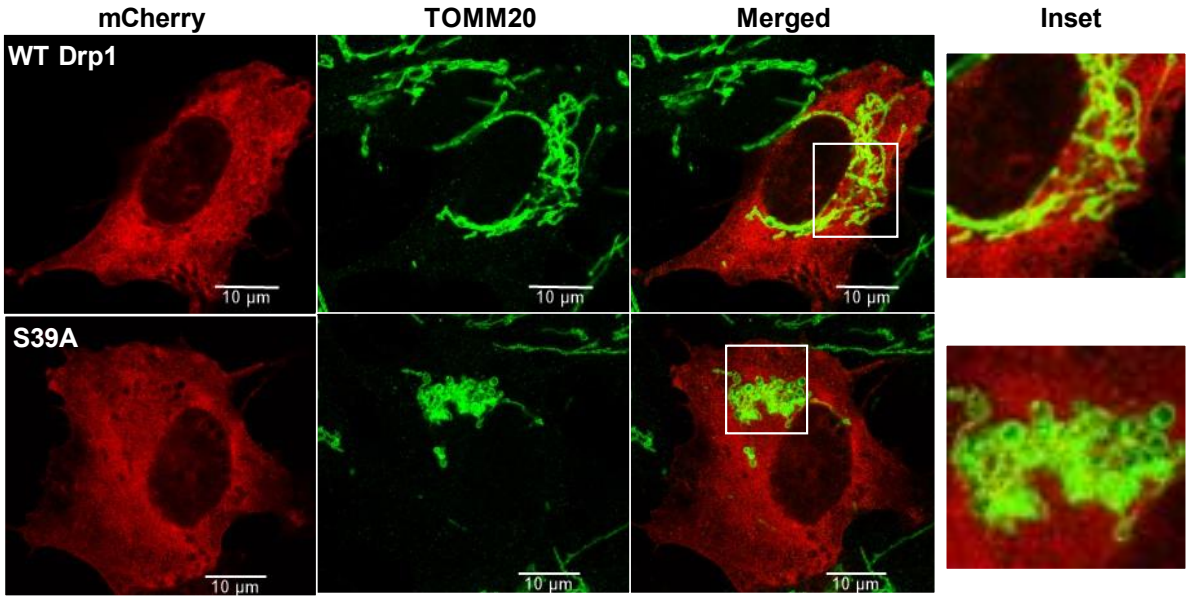

B.

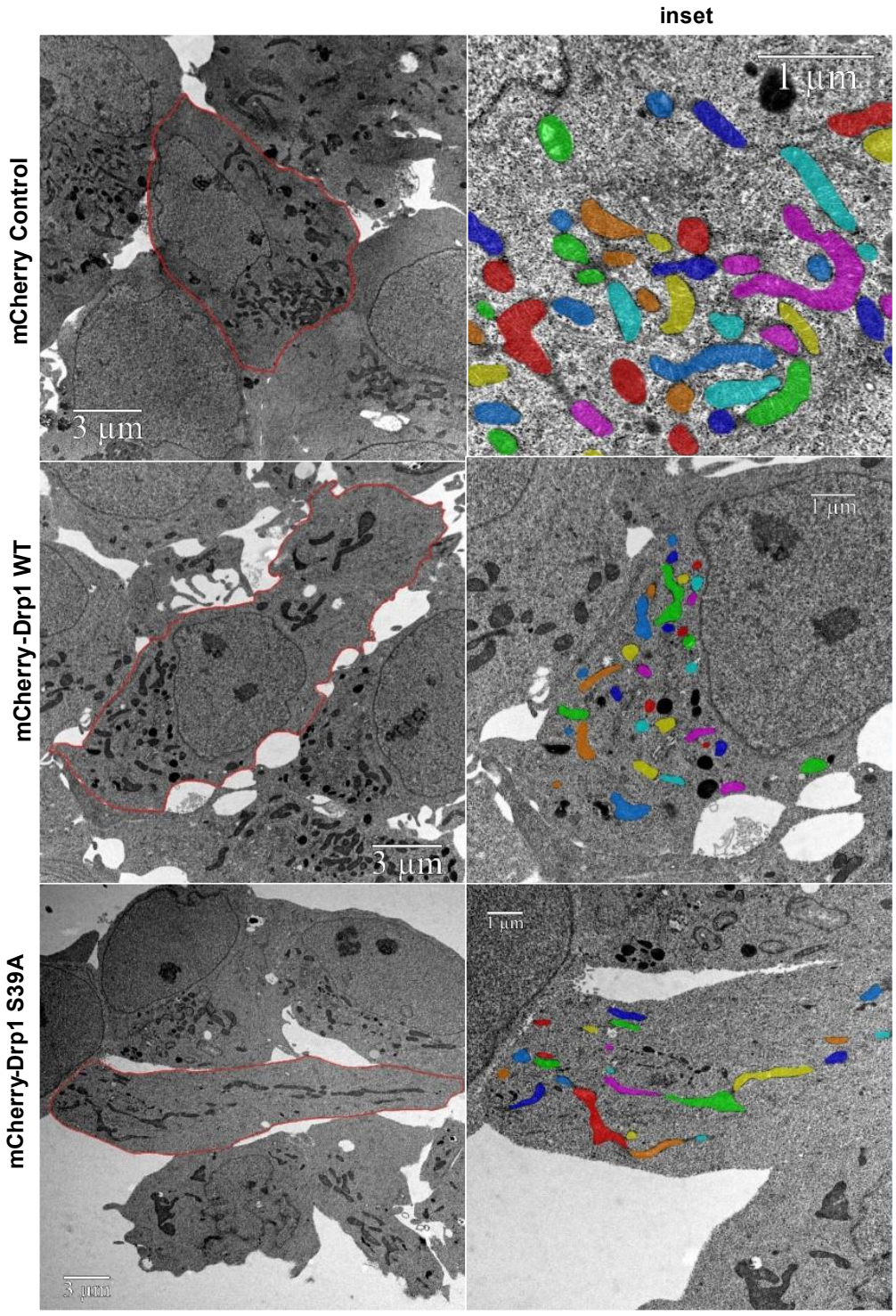
inset
mCherry Control
mCherry-Drp1 WT
mCherry-Drp1 S39A
3 µm
1 µm

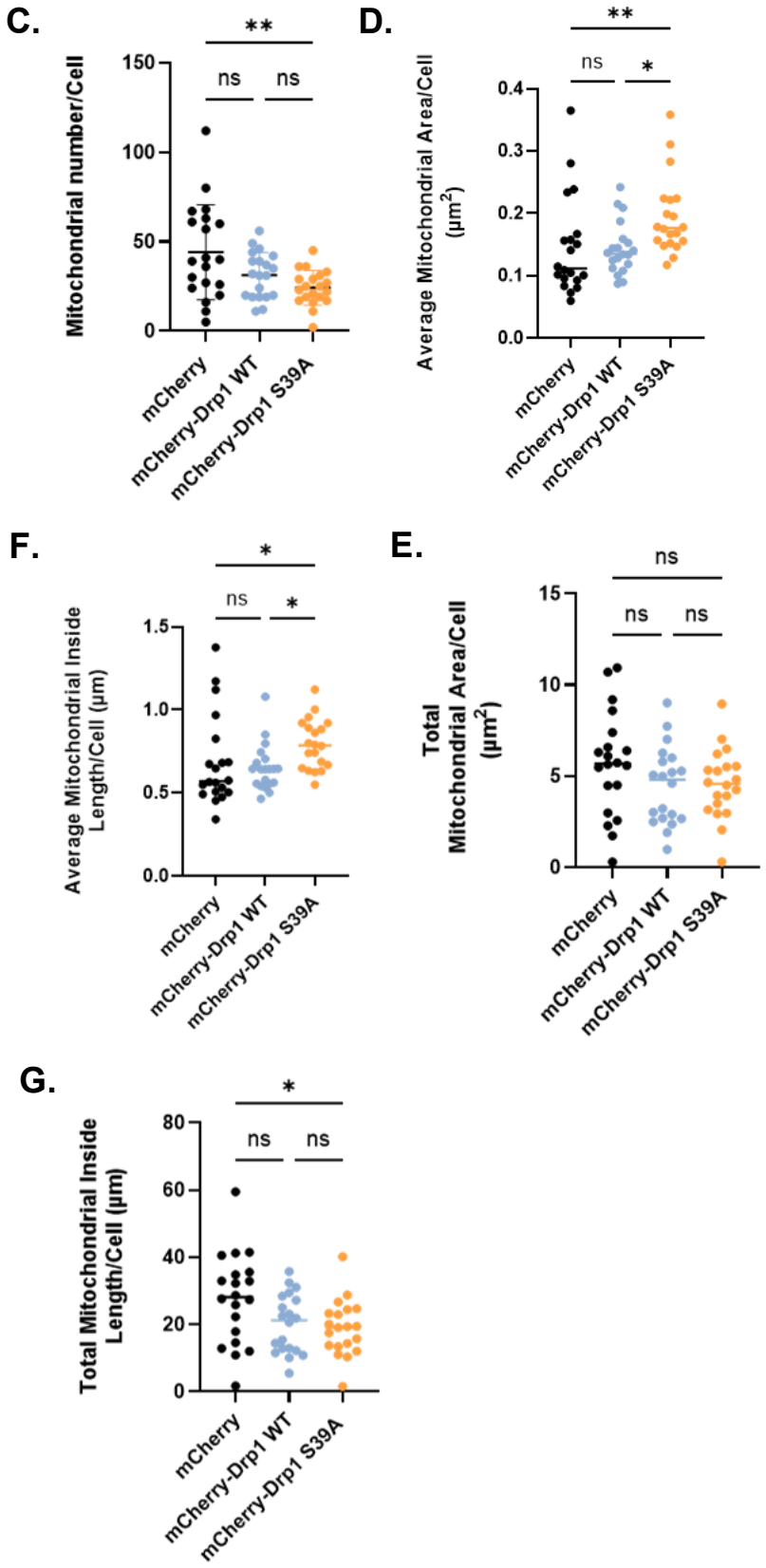
C.
Mitochondrial number/Cell
150
100
50
0
**
ns
ns
mCherry
mCherry-Drp1 WT
mCherry-Drp1 S39A
D.
Average Mitochondrial Area/Cell (μm²)
0.4
0.3
0.2
0.1
0.0
**
ns
*
mCherry
mCherry-Drp1 WT
mCherry-Drp1 S39A
F.
Average Mitochondrial Inside Length/Cell (μm)
1.5
1.0
0.5
0.0
*
ns
*
mCherry
mCherry-Drp1 WT
mCherry-Drp1 S39A
E.
Total Mitochondrial Area/Cell (μm²)
15
10
5
0
ns
ns
ns
mCherry
mCherry-Drp1 WT
mCherry-Drp1 S39A
G.
Total Mitochondrial Inside Length/Cell (μm)
80
60
40
20
0
*
ns
ns
mCherry
mCherry-Drp1 WT
mCherry-Drp1 S39A

Fig. 22: ***Confocal and transmission electron microscopy revealed the elongated mitochondrial morphology in cells expressing DRP1 mutant S39A****. (A) Representative confocal images of Tomm20 mitochondrial staining in mCherry-DRP1 and mCherry-DRP1 S39A. Arrows indicate the fused and compact mitochondrial shapes within the S39A overexpressing cells. (B) Cells stably overexpressing the mCherry, mCherry-DRP1, and mCherry-S39A mutant were sectioned and subjected to transmission electron microscopy (JEOL 1010), and images were taken at the magnification of 5000-30000x. For further analysis, the cell and mitochondria were manually segmented to include only mitochondria with visible and intact internal membranes. Mitochondria images were displayed using the default shared colormaps option of Amira 3D with 8 distinct colors for visualization purposes. Image analysis software from Amira 3D (version 2022.1; Thermofisher Scientific) was utilized to analyze the numerical parameters of the segmented structures, including quantitative analyses of (C) mitochondrial number, (D) average mitochondrial area in* μm^2*, (E) average inside length in* μm *(F) total mitochondrial area in* μm^2*, and (G) Total mitochondrial inside length in* μm*. Statistical significance was determined using One-Way ANOVA with multiple comparison post hoc tests. Only p-values less than 0.05 were considered statistically significant (where * indicates p <0.05 and ** indicates p <0.01).*

4.10. Computational analysis of mitochondrial morphology classification unveils compact hyperfused and compact tubular mitochondria in cells stably expressing DRP1 mutant S39A

Mitochondrial number, structural network, and distribution are subject to change depending on the cell type, cell cycle stage, and response to cellular stress conditions (Rambold et al., 2018). Additionally, morphology is both influenced and affected by the intracellular energy state. In normal circumstances, cells maintain the mitochondria in tubular form, but under cellular perturbations, the mitochondrial morphology is subjected to change (Wasilewski & Scorrano, 2009). During apoptosis, the mitochondria become a dot-like punctate state, indicating fragmented mitochondria (Arnoult, 2007). In necrosis, mitochondria were seen as swollen and distended objects (Laporte et al., 2007), while mitochondria change to elongated shape in autophagy to prevent degradation (X. Liu & Hajnoczky, 2011). There is an increasing demand to assess the different mitochondrial morphologies in different cellular states, such as mutations or pathologies (Giedt et al., 2016; Kumar et al., 2016; Fabiana Longo et al., 2020). Cells with stable expression of mCherry control, mCherry-DRP1, and mCherry-DRP1 S39A were stained with MitoTracker Green and Hoechst for live cell imaging. Both the control and mCherry-DRP1 cells demonstrated an interconnected mitochondrial network primarily located in the perinuclear region, consistent with our observation in TEM and a previous finding (E. Smirnova, L. Griparic, D.-L. Shurland, & A. M. Van Der Bliek, 2001). In contrast, cells overexpressing mCherry-DRP1

S39A exhibited a collapsed mitochondrial network, forming large perinuclear blebby aggregates with the same long retained tubules (**Fig. 23A**).

We categorized mitochondrial objects based on morphology to independently assess morphological differences among the mCherry, mCherry-DRP1, and mCherry-DRP1 S39A expressing cells (**Fig. 23B-C**). We classified and measured the percentage of different mitochondrial classes. An algorithm using Opera Phenix High Content Analysis machine was developed to classify based on morphology and intensity as established previously by our group (A. Douida et al., 2021; Ghani et al., 2024). Five mitochondrial classes were defined by using morphology and intensity properties. These classes are referred to as hyperfused, round/ compact tubular, long tubular, short tubular, and fragmented. Measures were computed for the morphology and intensity of mitochondrial structures across all wells. These measurements encompass total and average values for various morphological parameters of these structures within individual cells, such as area, roundness, spot intensity, width/length ratio, etc. In automating the population sorting process, approximately 1500 mitochondrial objects were manually categorized into five types/classes using this algorithm (**Fig. 23B-C**). The varying proportion of mitochondrial morphologies observed in each cell line reflects the impact of overexpression of the mCherry-DRP1 or mCherry-DRP1 S39A. Several vital parameters and morphological features were selected, such as the baseline cell counts before and after identifying the selected mCherry-expressing population, the number of nuclei, the counts of mitochondrial objects, and the mean and averages of each cell type's number and morphological characteristics. Approximately 269000, 198960, and 116300 cells of mCherry, mCherry-DRP1, and mCherry-DRP1 S39A were analyzed, respectively. Notably, we calculated the percentage of each mitochondrial class using this formula: (mitochondrial class area/ total mitochondrial area) x 100.

The quantitative analysis revealed that mCherry-DRP1 S39A cells exhibited a significantly higher proportion of hyperfused and compact tubular mitochondria than mCherry control (**Fig. 23D-E**). Fragmented mitochondria were lower than mCherry control and mCherry-DRP1 (**Fig. 23F**). Furthermore, we detected no difference in mitochondria's long and short tubular structure in three cell lines (**Fig. 23G-H**). Overexpression of DRP1 led to a shorter tubular rearrangement

compared to the control in TEM observation; however, statistical analysis of High Content Analysis measurement did not validate this observation (**Fig. 23G**).

Here, we combined the hyperfused, round/compact, and long tubular mitochondria into one class as fused mitochondria. The areas of mitochondria in cells expressing the mCherry, mCherry-DRP1, or mCherry mutant S39A were not significantly different (**Fig. 23I**). Additionally, both the mean mitochondrial width (**Fig. 23J**) and mean mitochondrial length (**Fig. 23K**) were considerably higher in cells expressing the mCherry-DRP1 S39A mutant compared to both mCherry control and mCherry-DRP1. These results indicate that while there is a decrease in the number of mitochondria and an increase in average inside length due to fusion in cells expressing the mCherry-DRP1 mutants, the overall mitochondrial area remains unchanged. In conclusion, the S39A mutation significantly impacts the mitochondrial morphology due to neglected fission activity.

A.

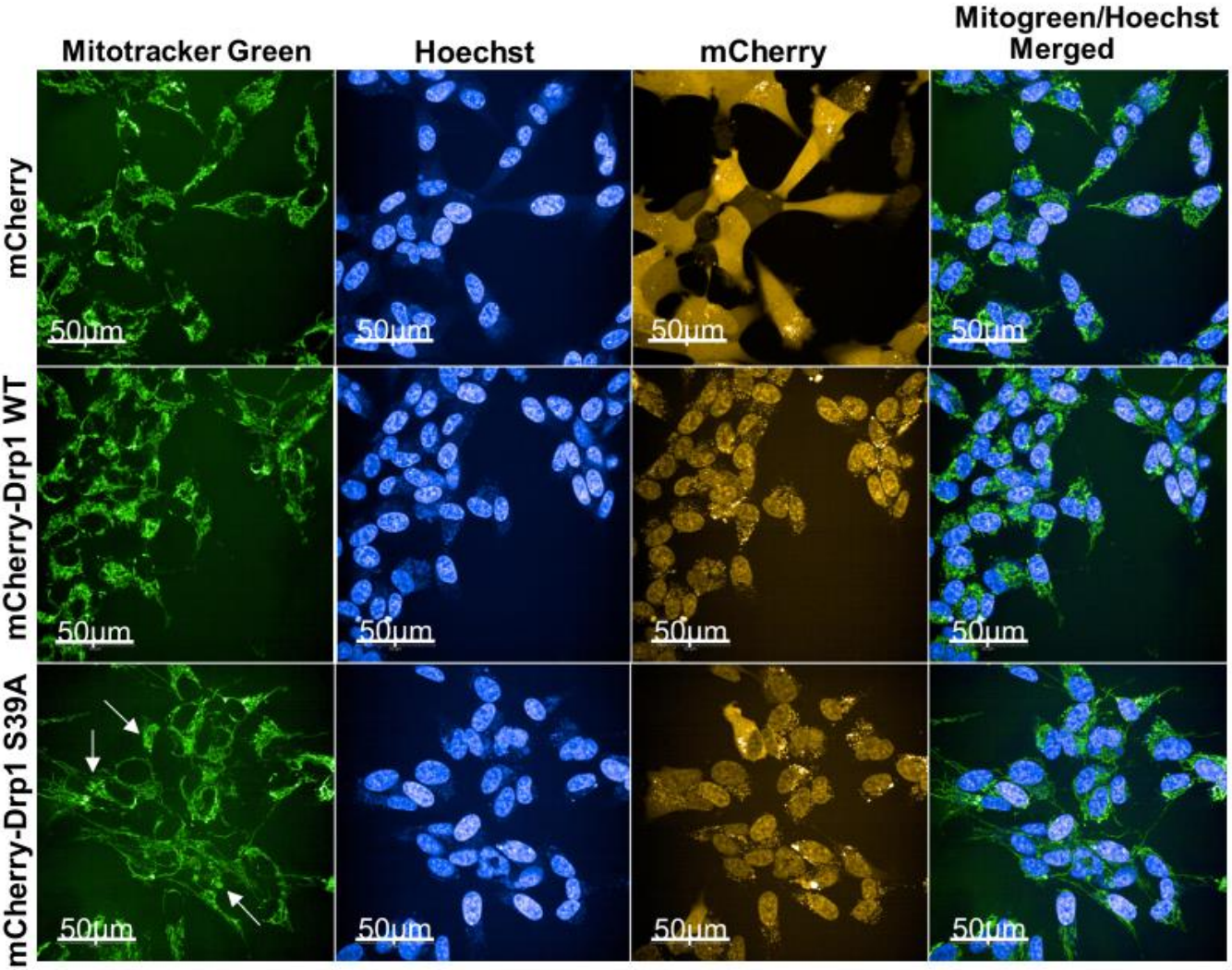
Mitotracker Green
Hoechst
mCherry
Mitogreen/Hoechst Merged
mCherry
mCherry-Drp1 WT
mCherry-Drp1 S39A
50µm

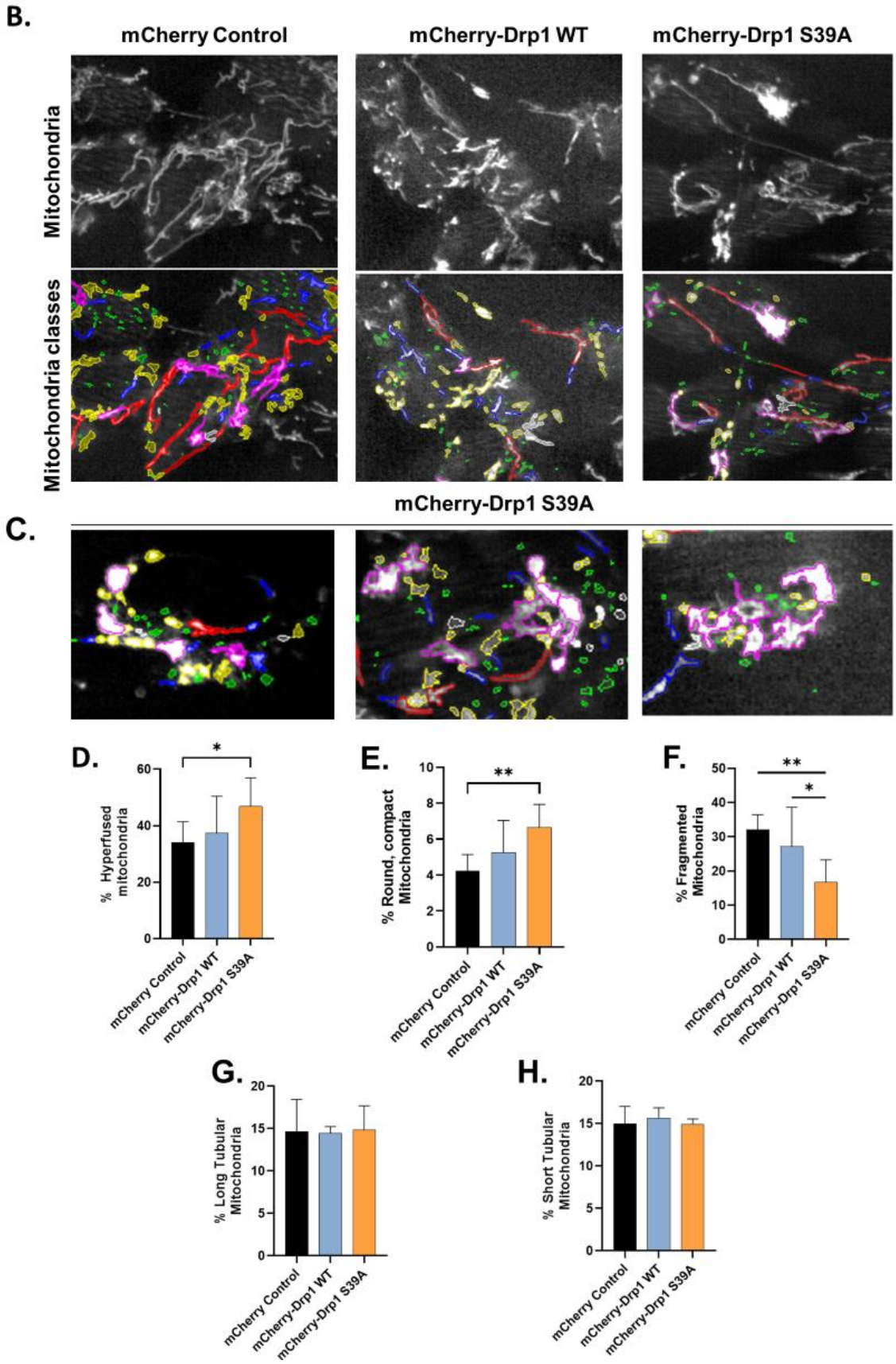
B.
mCherry Control
mCherry-Drp1 WT
mCherry-Drp1 S39A
Mitochondria
Mitochondria classes
C.
mCherry-Drp1 S39A
D.
% Hyperfused mitochondria
E.
% Round, compact Mitochondria
F.
% Fragmented Mitochondria
G.
% Long Tubular Mitochondria
H.
% Short Tubular Mitochondria
mCherry Control
mCherry-Drp1 WT
mCherry-Drp1 S39A

I.

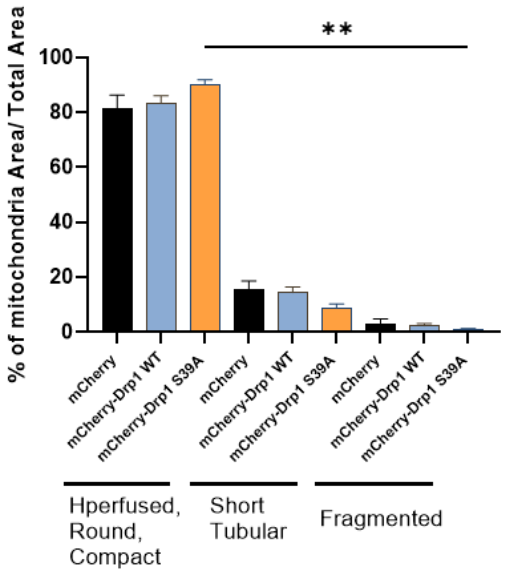
**
% of mitochondria Area/ Total Area
100
80
60
40
20
0
mCherry
mCherry-Drp1 WT
mCherry-Drp1 S39A
mCherry
mCherry-Drp1 WT
mCherry-Drp1 S39A
mCherry
mCherry-Drp1 WT
mCherry-Drp1 S39A
Hperfused, Round, Compact
Short Tubular
Fragmented

J.

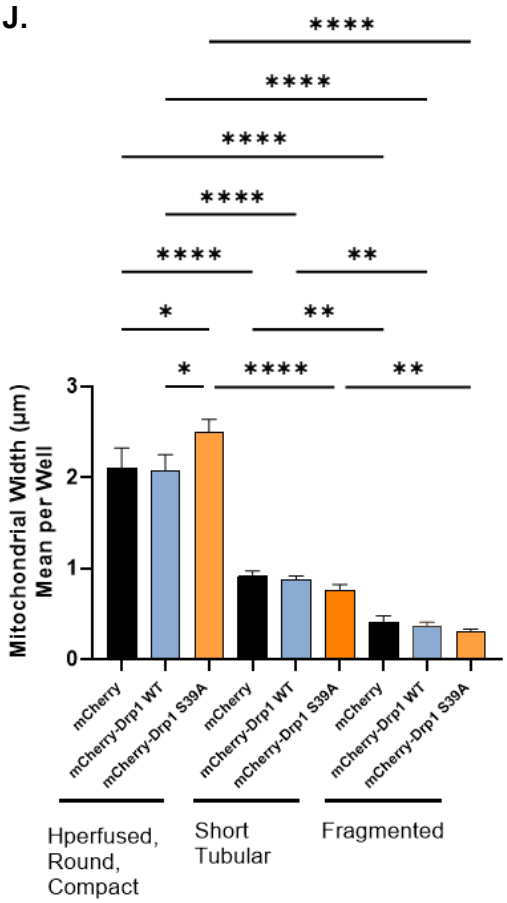
****
****
****
****
****
**
*
**
*
****
**
Mitochondrial Width (µm) Mean per Well
3
2
1
0
mCherry
mCherry-Drp1 WT
mCherry-Drp1 S39A
mCherry
mCherry-Drp1 WT
mCherry-Drp1 S39A
mCherry
mCherry-Drp1 WT
mCherry-Drp1 S39A
Hperfused, Round, Compact
Short Tubular
Fragmented

K.

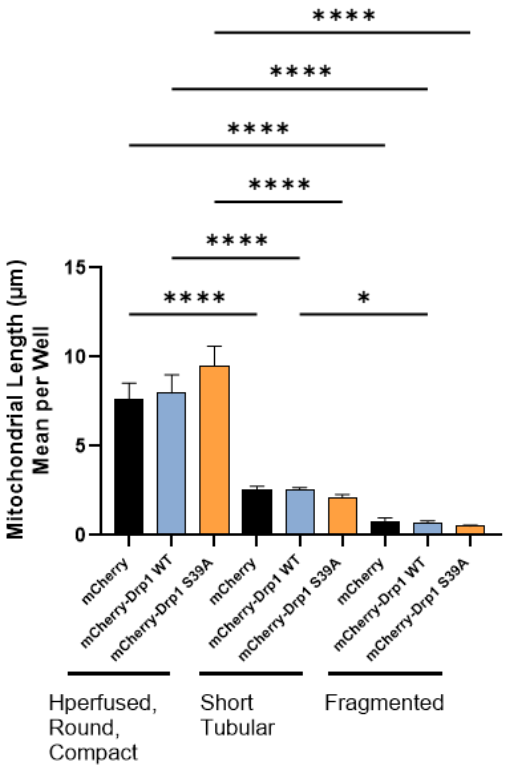
****
****
****
****
****
****
*
Mitochondrial Length (µm) Mean per Well
15
10
5
0
mCherry
mCherry-Drp1 WT
mCherry-Drp1 S39A
mCherry
mCherry-Drp1 WT
mCherry-Drp1 S39A
mCherry
mCherry-Drp1 WT
mCherry-Drp1 S39A
Hperfused, Round, Compact
Short Tubular
Fragmented

Fig. 23: ***Categorization of mitochondrial morphology using high-content analysis validates the presence of compact tubular and highly fused mitochondrial structures in cells overexpressing mCherry-DRP1 S39A****. (A-C) Representative confocal images of live cells where mitochondria stained with MitoTracker Green, nuclei stained with Hoechst, and mCherry expression. All cell lines express mCherry stably (scale bar is 50 μm). The automated confocal microscopy was conducted on an Opera Phenix high-content-screening system by Perkin Elmer, using a 63x water objective (NA=1.15), appropriate lasers, and filters for Hoechst, mCherry, and Mitotracker Green in sequential mode were selected to eliminate spectral overlap. The classification of mitochondrial shapes was conducted through the built-in function of Harmony 4.9 software. Mitochondria were sorted into hyperfused area-pink, compact or round area-yellow, fragmented area-green, long tubular area-red, and short tubular area-blue categories (scale bar=5 μm). (D-H) Quantitative analysis of mitochondrial classes. Data is presented as mean ±SD from three biological replicates. The statistical analysis was performed by One-Way ANOVA using multiple comparison tests where * indicates p < 0.05, ** indicates p < 0.01, and **** indicates p< 0.0001.*

4.11. DRP1 S39A mutation reinstates cellular energy production and cell survival to the same level as control compared to overexpressing DRP1 cells

The mitochondria play a vital role in ATP production in all cells. ATP is an essential energy source for cells and organs with high metabolic activity. Mitochondrial dysfunction can stem from somatic or mitochondrial DNA mutations, disruption in the fusion and fission cycle, as well as inherited mitochondrial dysfunction (Briston & Hicks, 2018). Moreover, studies have indicated that PKCs/DRP1 signaling activation exacerbates diabetic retinopathy through increased rates of mitochondrial fission. Current data suggests a close association between changes in both cellular bioenergetics and dynamics with healthy metabolic adaptation; however, abnormal variations are strongly linked with various diseases, including aging and neurodegenerative disorders (Beal, 2005; Benard et al., 2007).

The cell Mito stress assay by seahorse analysis was utilized to examine the mitochondrial bioenergetics profile. The real-time measurements of oxygen consumption rate were conducted in cells stably expressing mCherry, mCherry-DRP1, and mCherry-DRP1 S39A recombinant proteins. Sequentially, basal OCR and OCR following the addition of selective mitochondrial inhibitors, including Oligomycin, Cyanide-p-trifluoromethoxy hydrazone, as well as a combination of rotenone and Antimycin A were determined (**Fig. 24A**). Oligomycin inhibits ATP synthase and prevents proton entry into mitochondria. At the same time, maximal respiration was induced by FCCP, which reduces ATP synthesis by collapsing the proton gradient across the inner mitochondrial oxygen consumption; complex I inhibitor rotenone and complex III inhibitor

Antimycin A were employed to inhibit mitochondrial respiration—normalization with total protein content allowed for assessment of OCR. The results showed that overexpressing DRP1 significantly increased the OCR-based maximal respiration compared to the control (**Fig. 24B**). Maximal respiration is the maximum rate measurement after FCCP injection – non-mitochondrial respiration (basal + spare capacity). The significant increase in maximal respiration was due to a significantly increased level of spare capacity. The OCR-based calculated ATP production, however, was similar to the control. The increase in spare respiratory reserve is indicative of stress. When cells are subject to stress, energy needs increase, and ATP production increases to maintain cellular homeostasis. Our data suggest that the overexpression of DRP1 triggers a stress response where cells try to cope with increased spare reserve, showing an increasing but insignificant trend of ATP production. Intriguingly, we found that overexpressing the DRP1 S39A mutant reversed the effect of DRP1 overexpression and reduced both the maximal respiration and spare capacity to the control level (**Fig. 24B**).

We did an SRB assay to check the effects of DRP1 WT and DRP1 S39A mutation on cell death. Our results indicate that cells overexpressing DRP1 showed excessive cell death compared to mCherry control and DRP1 S39A cells. However, overexpressing DRP1 mutant S39A cells showed no significant cell death compared to the control. These results demonstrate that DRP1 S39A overexpressing cells are more viable or restore viability than overexpressing DRP1 WT cells (**Fig. 24C**).

A.

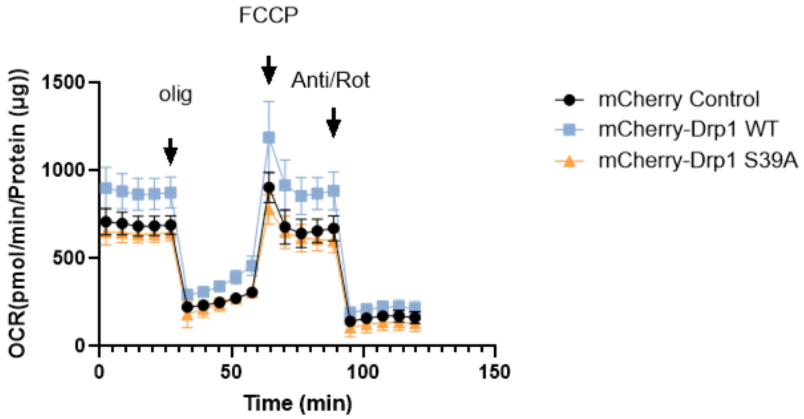
FCCP
olig
Anti/Rot
OCR(pmol/min/Protein (µg))
1500
1000
500
0
0
50
100
150
Time (min)
mCherry Control
mCherry-Drp1 WT
mCherry-Drp1 S39A

B.

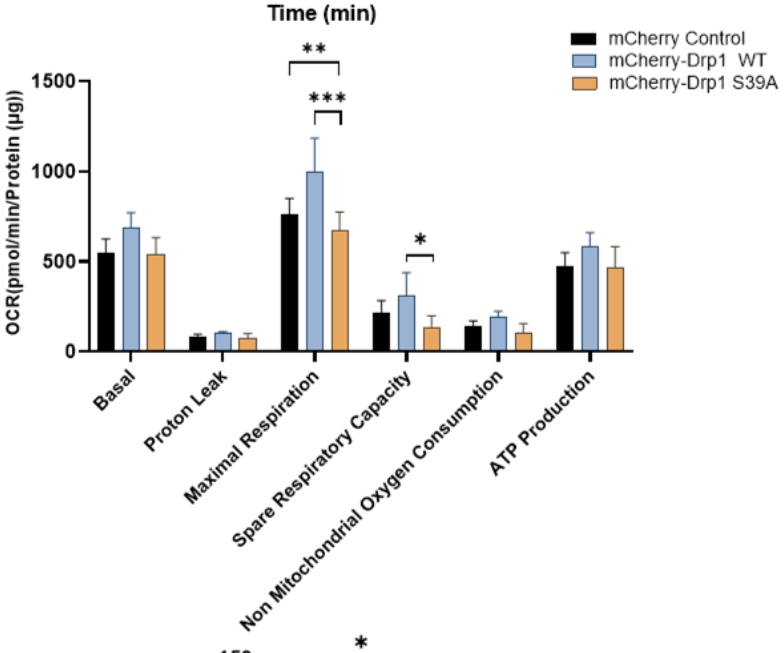
mCherry Control
mCherry-Drp1 WT
mCherry-Drp1 S39A
OCR(pmol/min/Protein (µg))
1500
1000
500
0
**
***
*
Basal
Proton Leak
Maximal Respiration
Spare Respiratory Capacity
Non Mitochondrial Oxygen Consumption
ATP Production

C.

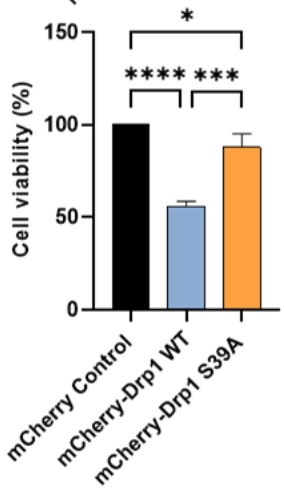
Cell viability (%)
150
100
50
0
*
**** ***
mCherry Control
mCherry-Drp1 WT
mCherry-Drp1 S39A

Fig. 24: ***Overexpressing S39A cells maintained an equal rate of cellular bioenergetics as compared to control and indicated delayed cell death.*** *(A) Oxygen consumption rate was measured in mCherry, mCherry-DRP1, and mCherry-DRP1 S39A overexpressing cells. The cells were seeded in an XF 96 well plate 24 hours before the assay. On the day of the assay, the media was changed to XF DMEM, and appropriate drugs were loaded into each port. After calibration for 30 minutes, the OCR was measured as microgram/pmol/min/µg. The data shown here are mean values ±SD (n=3). The wave desktop software calculated the basal, proton leak, ATP production, spare maximal respiration, and non-mitochondrial oxygen consumption. Data was analyzed by using Two-Way ANOVA using multiple t-tests in GraphPad prism V9.5.1 where * indicates p<0.05, ** indicates p<0.005, and *** indicates p<0.0005 (B) The XY Graph showing the calculated OCR values using wave desktop software (C) Cell viability assay done by SRB assay in cherry, mCherry-DRP1, and mCherry-DRP1 S39A. The values are shown as mean values ±SD (n=3). The data was analyzed using One-Way ANOVA in GraphPad prism V9.5.1 where * indicates p<0.05, and **** indicates p<0.0001.*

5. Discussion

DRP1, a key regulator of mitochondrial dynamics, is critical in maintaining mitochondrial homeostasis and regulation. The role of DRP1 in neuronal differentiation and its potential as a therapeutic target for neurological disorders have garnered significant interest in recent years. The generation of DRP1 complete knockout or tissue-specific knockout mice revealed that these mice die after 11.5 days of embryonic development. Fibroblast and Purkinje cells from these mice showed giant and elongated mitochondria. (Wakabayashi et al., 2009). DRP1 is critical in the development of tissue generation, specifically brain tissue. The neural cell-specific $DRP1^{-/-}$ mice show hypoplasia leading to apoptosis and die just after birth. The primary culture cells from these mice show normal respiration rates. However, severe defects are found in the formation of synapses (Ishihara et al., 2009). Partial reduction of DRP1 or heterozygote knockout of DRP1 shows no defects in the formation of synapses and dendritic spines. $DRP1^{+/-}$ mice show normal expression of mitochondrial proteins (Manczak et al., 2012).

Another study shows that the elongation of mitochondria is crucial for the differentiation of myotubes from myoblasts, and this process is primarily regulated by the phosphorylation of DRP1 by cyclic GMP-dependent nitric oxide through G-kinase (De Palma et al., 2010). The differentiation of induced pluripotent stem cells (iPSC) into cardiac mesodermal cells requires the inhibition of DRP1, a regulatory mitochondrial fission protein. According to this study, the differentiation of iPSC into cardiac cells mainly happens when the mitochondrial equilibrium moves from fission to fusion and bioenergetics alteration from glycolysis to oxidative phosphorylation takes place for energy generation (Hoque et al., 2018). Any disruption in mitochondrial dynamics causes impaired differentiation in neural stem cells. The commitment to the fate of the NSC to either inhibit self-renewal or promote differentiation largely depends on the nuclear transcriptional regulation through mitochondrial dynamics. (Khacho et al., 2016).

Human-induced pluripotent stem cells (iPSCs) are the most relevant model for neuron differentiation. However, their uncertain differentiation efficiency and increased experimental expenses restrict their application to this purpose (B.-Y. Hu et al., 2010). As a result, many researchers opt for neuroblastoma SH-SY5Y cells, an in vitro tool, which provides a perfect model of cellular and molecular biology study of many neurodegenerative diseases. Different protocols have been developed to differentiate SH-SY5Y cells to date. These include serum

deprivation, RA treatment, TPA, dibutyryl cyclic-AMP (dbcAMP), or growth factors such as BDNF, NGF, etc. Depending on the protocol, different types of neuronal cells can be achieved, such as cholinergic, adrenergic, glutaminergic, and dopaminergic. SH-SY5Y cells contain two types of cells from the original biopsy SK-N-SH cells. One is N-type, and the other is S-type. The former is neuroblastic-like, while the latter is epithelial-like cells. Serum or FBS deprivation, along with RA treatment, enhances the N-type phenotype (neuroblastic) and inhibits the growth of S-type cells. According to Encinas et al., exposure to RA acid causes the cells to exit from the cell cycle and enhance the expression of the TrkB receptor. TrkB receptors are essential for the downstream activation of neuronal pathways (Encinas et al., 2000).

Our current study found an extensive alteration in the transcriptomic profile of SH-SH5Y human neuroblastoma cells upon stable knockdown of DRP1. We have also determined that DRP1 stable knockdown leads to enhanced neuronal differentiation *in vitro*. The upregulated GO terms included neurogenesis, neuronal differentiation, synapse formation, and axon development. Several studies have investigated the role of DRP1 in mitochondrial dynamics, but not much is known about the impact of DRP1 depletion on neuronal differentiation. Therefore, this study focused on the role of DRP1 knockdown in cellular and mitochondrial morphology changes upon differentiation induced by RA and BDNF in SH-SY5Y cells. The presence of neuronal markers genes characterizes differentiation induced by RA and BDNF. According to the results of GO terms analysis, there was a significant increase in the expression levels of genes associated with neuronal differentiation in differentiated shDrp1 cells compared to differentiated control cells. This suggests that the knockdown of DRP1 favors SH-SY5Y cell differentiation at the transcriptomic level.

When cells undergo differentiation, specific characteristic morphological changes appear in neurons, such as polarization, axonal growth, neurite outgrowth, and formation of dendrites. According to research, undifferentiated cells are highly proliferative and have no polarization. Differentiated cells show different morphology as compared to undifferentiated cells, which have more cell perimeter, reduction in the cell body, and extensive long neurites with interconnected networks and express specific neuronal markers (Hromadkova et al., 2020; Riegerova et al., 2021). We observed that the characteristics of neuronal differentiation defined by the CSIRO algorithm showed a significant increase in differentiated shDrp1 cells compared to

undifferentiated shDrp1 cells. These traits were also notably higher than those in differentiated control cells, indicating that changes in mitochondrial dynamics can impact neuronal differentiation. DRP1 inhibition by mdivi-1 (a specific DRP1 inhibitor) on hippocampal progenitor cells from Down's syndrome adult mice (DS NPC) demonstrated similar effects on neuronal differentiation. DS NPC exhibits excessive mitochondrial fission and improper neurogenesis. DRP1 inhibition in DS NPC improved neuronal functions, enhanced neurite outgrowth, and increased expression of neuronal markers. This suggests that targeting DRP1 could be a potential therapeutic strategy for improving neuronal differentiation in conditions associated with neurodegeneration, such as Down's syndrome (Valenti et al., 2017). Hereditary spastic paraplegias involve the use of a specific peptide inhibitor P110 or the genetic ablation of DRP1 to prevent axonal and neuronal degeneration in human iPSC-derived patient fibroblast with SPG11 mutation. This suggests the involvement of mitochondrial dynamics in neurodegeneration (Z. Chen et al., 2022).

Studying the signaling molecules and pathways that regulate DRP1 activity in neuronal differentiation could provide valuable insights into the underlying mechanism and potential targets for therapeutic intervention. Various pathways are triggered in DRP1-depleted cells upon RA-BDNF-induced neuronal differentiation, such as MAP kinases. We found a reduced level of ERK1/2 phosphorylation in shDrp1 cells compared to control cells after RA-induced differentiation. However, ERK1/2 levels remained unchanged in both control and shDrp1 cells. MEK1/2, the upstream regulator of ERK1/2, showed no significant differences in phosphorylation levels between control cells and shDrp1 cells. These results suggest that the decreased levels of ERK1/2 phosphorylation in DRP1-depleted cells may be attributed to the enhanced activity of phosphatases. DUSPs control ERK1/2 activity in cells. DUSP1 is known to dephosphorylate ERK1, while DUSP6 dephosphorylates ERK1 and ERK2. ERK1/2 and DUSP1/6 indirectly connect by forming a negative feedback loop in which ERK1/2 phosphorylation levels are regulated. The downregulation of DUSPs renders the activation of ERK1/2 (Prieto et al., 2016). This dysregulation of ERK1/2 phosphorylation in DRP1-depleted cells during neuronal differentiation suggests a potential role of DRP1 in modulating the MAPK/ERK signaling pathway.

Interestingly, our analysis revealed a significant upregulation of ERK1/2 in the absence of DRP1 during neuronal differentiation in control cells but not in DRP1-depleted cells. This upregulation of ERK1/2 could account for the decreased DUSP1/6 in DRP1-depleted cells, indicating a potential role of DUSP1/6 in regulating ERK1/2 signaling in the context of mitochondrial dynamics and neuronal differentiation. The alternate scenario could be that DRP1 depletion leads to the increased expression of several members of DUSPs, leading to the downregulation of ERK1/2 during neuronal differentiation. The upregulation of DUSP2 in DRP1-depleted cells could potentially compensate for the decreased ERK1/2 phosphorylation levels. Aberrant ERK signaling pathway activation is caused by DUSP2 downregulation during neural progenitor cell metastasis (Ding et al., 2022). Also, Kim et al. (S.-C. Kim et al., 1999) found that DUSP2 negatively regulated ERK1/2 in neuronal cells. Our transcriptomic and qPCR data revealed that the expression of DUSP2 was increased in DRP1-depleted cells compared to control cells. However, our analysis did not reveal the DUSP1 and DUSP6 increase, suggesting that there are some other regulators in this context. This mechanism should be further investigated to determine the precise role of DRP1 in modulating the MAPK/ERK signaling pathway during neuronal differentiation, and the role of DUSPs should be given more attention in further studies.

Mitochondrial rearrangement is a continuous process in many different cellular processes, such as in cell cycle progression, apoptosis, or neurite outgrowth (Voccoli & Colombaioni, 2009) to adapt metabolic reprogramming and cytoplasmic rearrangement during differentiation in pluripotent stem cells (H. W. Choi et al., 2015). SH-SY5Y cells, the most widely used model in neuroscience, showed a mitochondrial network rearrangement and a considerable rise in tubular mitochondrial morphology during differentiation (D'Aloia et al., 2024). We now know that DRP1 depletion, which inhibits mitochondrial fission, can positively impact neuronal differentiation. For this purpose, we monitored the mitochondrial morphology and protein level before and after the neuronal differentiation. During the RA-BDNF differentiation protocol, an increase in mitochondrial fusion and a more elongated mitochondrial network were observed in differentiated control and shDrp1 cells. The level of Opa1 showed a slight but not significant increase. However, other mitochondrial proteins, such as MFN2, did not show significant changes during neuronal differentiation in control and shDrp1 cells. However, comparing the MFN1 and MFN2 levels between control to shDrp1, a decrease was observed in shDrp1 cells in the undifferentiated state, Day3 or Day6 and MFN1 increased significantly in control cells

during the differentiation. These results indicate that the cells create a compensatory mechanism in reaction to DRP1 depletion and changes in mitochondria dynamics.

After 6 days of differentiation in shDrp1 cells, we observed a significant rearrangement of the mitochondrial network, with increased interconnected mitochondria. The interconnected mitochondria in shDrp1 cells had a more elongated and tubular morphology than control cells. We also observed the phosphorylation status of DRP1 in control cells. Phosphorylation of DRP1 S616 promotes mitochondrial fission. However, our study found that the level of DRP1 S616 phosphorylation was triggered by RA treatment but remained steady after BDNF treatment in control cells. The phosphorylation of DRP1 at S616, mediated by CDK1, causes DRP1 to localize on microtubule and facilitates the mitochondrial movement, resulting in mitochondrial division in Jurkat 6E.1 cells (Strack, Wilson, & Cribbs, 2013). The phosphorylation at S637 of DRP1 seems to play a role in regulating the phosphorylation of S616 and ultimately influencing mitochondrial fission. This phosphorylation was initiated upon RA but decreased after BDNF treatment, suggesting a shift toward mitochondrial fusion during neuronal differentiation. A typical ratio of these phosphorylation events (S616/S637) is known to regulate the balance between mitochondrial fusion and fission (Ko, Hyun, Min, & Kim, 2016). Our findings suggest that differentiated control and DRP1-depleted cells displayed a shift toward mitochondrial fusion during neuronal differentiation. Similar results were observed in a study by (Jin, Wei, Zhi, Wang, & Meng, 2021). According to this study, DRP1 phosphorylation at S616 alone is insufficient to induce mitochondrial fission, as it requires the balance between phosphorylation at S616 and dephosphorylation at S637 to regulate mitochondrial dynamics. In cardiomyocytes, DRP1 phosphorylation at S637 plays a crucial role in regulating the phosphorylation of S616 to control the division of mitochondria (Jhun et al., 2018).

The active mitochondria were marked with Mitotracker RedCMX Ros after 6 days of inducing differentiation and in undifferentiated cells of both control and DRP1 depleted cells. Significant changes in the arrangement of mitochondrial networks were noted, showing a combination of tubular phenotypes and interconnected tubules. The mitochondrial networks in shDrp1 cells displayed persistent fusion with an asymmetric distribution usually compacted near the nucleus. Additionally, elongated and highly interconnected tubules were observed, indicating the adaptation of mitochondria to neuronal cell morphology. Furthermore, our

investigation into the metabolic activity of control cells during differentiation uncovered a higher energy demand likely due to mitochondrial remodeling and adaptation, which are associated with increased mitochondrial elongation. However, DRP1 depleted cells behaved similarly to the control, except we detected a significant change in maximal respiration on Day 6 of differentiation. This change was significant compared to control and undifferentiated shDrp1 cells, suggesting that shDrp1 cells acquire a high demand for respiratory capacity. Recently published research has mentioned that the SH-SY5Y cells turn into mature neurons at the end of Day 20 (D'Aloia et al., 2024). Probably due to this, we did not see any significant differences in other parameters of bioenergetic measurement, except maximal respiration. A possible scenario to explain these findings is that shDrp1 cells rearrange completely while transitioning from undifferentiated to differentiated cells earlier to attain a neuronal phenotype and adapt to increased respiratory capacity in shDrp1 cells.

Cell death in control and shDrp1 cells remained unaffected by RA or the treatment of mitochondrial inhibitors. Our findings align with earlier research indicating that DRP1 depletion delays apoptosis without inhibiting it and that DRP1-mediated mitochondrial fission is a prerequisite for apoptosis but is not solely dependent on DRP1. DRP1 depletion and apoptosis occur through various pathways and mechanisms; while DRP1 depletion may delay apoptosis, it does not completely inhibit it. DRP1 inhibition partially halts the caspase activation and cytochrome c release but does not prevent the apoptosis-mediated Bax/Bak complex (Estaquier & Arnoult, 2007).

DRP1 and Huntington's disease are closely linked as well. Studies have shown that the dysregulation of mitochondrial dynamics, including excessive mitochondrial fragmentation, can contribute to the pathogenesis of Huntington's disease. Furthermore, modulation of DRP1 activity has been explored as a potential therapeutic target for addressing mitochondrial dysfunction and neurodegeneration in the context of this disease. We have demonstrated that downregulation of DRP1 delays toxic huntingtin protein formation, suggesting a potential therapeutic avenue for Huntington's disease and other proteinopathies. DRP1 knockdown has shown a positive impact on slowing down the formation and aggregation of toxic huntingtin protein. Thus, it protects the cells from neurotoxicity in an *in vitro* model by reducing the burden of protein aggregates.

In the second study, we designed a mutant form of the DRP1 protein mainly involved in GTPase activity. We investigated a mutation site (S39A) in DRP1 that has been studied in peroxisomes. It showed a reduced GTP activity, resulting in giant reticular and elongated peroxisomes (X. Li & Gould, 2003). This work is an extended study of this DRP1 GTPase domain mutation. Substitution of S39A in the DRP1 protein led to a hyperfused mitochondrial morphology. We demonstrate that the DRP1 GTPase domain plays a pivotal role in the maintenance of the morphology of mitochondria. Our results indicated that the cells overexpressing mCherry-DRP1 S39A showed a fused mitochondrion compared to those overexpressing wild-type DRP1. Also, this mutation significantly affects the fission of the mitochondria, leading to very hyperfused, balloon-like, and aggregated structures of mitochondria. This balloon-like mitochondrial structure is also specific when DRP1 is downregulated (Ban-Ishihara, Ishihara, Sasaki, Mihara, & Ishihara, 2013).

Electron microscopy showed more precise insight into the phenotypic changes in cells overexpressing mCherry-DRP1 WT or mCherry-DRP1 S39A. The overexpressing mCherry-DRP1 cells contained more fragmented mitochondria due to the increased activity of DRP1, and overexpressing S39A cells contained a high percentage of fused mitochondria, indicating the importance of this site of DRP1 in mitochondrial fission activity. It is well established that DRP1 is a critical player in mitochondrial fission and dynamics. The GTPase domain of DRP1 is responsible for catalyzing mitochondrial fission, ensuring the organelle maintains a proper balance between fusion and fission. The Dynamin superfamily comprises conserved GTPases and roughly 300 amino acids and contains five conserved GTP binding motifs (GI-5), from which the phosphate binding loop (P-loop) is most important. Mapping of the GTPase of DRP1 protein based on X-ray structure analysis showed that the S39 and S38 form backbone interactions with the α-phosphate of GTP (Wenger et al., 2013) Mutations in the P-loop, such as S39A, hinder the turnover of GTP activity and ultimately cause fused mitochondria.

A five-year-old girl showing severe ataxia, hypotonia, and delay in psychomotor development harboring DRP1 mutation in its GTPase domain. The patient's fibroblast showed giant hyperfused mitochondria confirmed through TEM and live imaging analysis (Fabiana Longo et al., 2020). Another study on retinal ganglion cells found that overexpressing DRP1 increased fission and swollen mitochondrial cristae *in vitro* (K. Kim et al., 2015). A patient with

psychomotor developmental delay was found to have a new p.S36G mutation in the GTPase domain, causing mislocalization of DRP1 and resulting in impaired fission and elongated mitochondria. The loss of interaction at the S36 residue prevents binding to GTP/GDP, impairing cellular function. An equivalent mutation in yeast showed decreased oxygen consumption rate and growth, indicating its detrimental effects (Nasca et al., 2016). A 5-year-old patient was diagnosed with significant delays in psychomotor development delay, muscular atrophy, and uncoordinated movements due to damage to sensory nerves. Clinical exome sequencing identified a missense mutation (p.D146N) in the GTPase domain of DRP1. Analysis revealed excessively fused mitochondria in the patient's fibroblast compared to healthy cells. Introducing the mutant (D146N) into healthy fibroblast cells also resulted in the overly fused mitochondrial network, indicating a dominant-negative characteristic of this mutation. The p.D146N cells showed a significantly reduced rate of mitochondrial turnover and increased oxidative stress (F. Longo et al., 2020).

Mitochondria are highly diverse organelles. It quickly changes its shape according to the requirement. For example, neurons and muscles need to meet the energy requirement. So, in different conditions, mitochondria fuse or divide to dissipate the energy requirement. Live imaging is a new tool. It provides a susceptible platform to perform various functions quantitatively and calculate different parameters at the same time. We have devised a reliable and fast method to classify mitochondria into five classes in this data. It is a powerful way to locate mitochondria within each cell appropriately. Here, we have demonstrated a detailed step-by-step description of the classification of mitochondria. Using mCherry control, mCherry-DRP1 and mCherry-DRP1 S39A stably expressed cells. In this method, we used Hoechst, mCherry, and mitotraker green staining to detect nuclei, cytoplasm, and mitochondria-related to a specific cell. We defined the five different classes of mitochondria based on mitochondrial area: fragmented, compact, short tubular, long tubular, and hyperfused mitochondria based on each mitochondrial shape.

Classification of mitochondria in different shapes is another unique aspect of knowing mitochondrial dynamics. According to a study, mitochondria can adopt various forms, including tubular, donut, or blob shapes, indicative of different cellular shapes and levels of redox states. The study shows that under normal conditions, mitochondria are predominately tubular. However, under mild stress, they transition into a donut-shaped form, while high stress can cause

them to become blob-like structures (Ahmad et al., 2013). In another study, punctate (fragmented), intermediate, and filamentous (elongated) mitochondria were devised based on the mitochondrial shape by using the High Content Analysis (HCA) method in a cancer cell model (Giedt et al., 2016). Our quantitative analysis of HCA data demonstrated that overexpressing mCherry-DRP1 significantly increased fragmented mitochondria compared to control cells. However, Overexpressing S39A cells caused the mitochondria to turn into a hyperfused shape, indicating the highest percentage of them. These findings suggest that DRP1 site S39 plays a crucial role in mitochondrial fission and altering mitochondrial morphology.

Recent studies have uncovered novel and non-canonical functions of DRP1. Mitochondrial morphology and dynamics are not sole functions to be regulated by DRP1. DRP1 can also play a role in mitochondrial respiration. Studies have revealed that genetic and pharmacological alteration of DRP1 can impact mitochondrial respiration in adult cardiomyocytes, highlighting an additional function of this protein beyond its canonical role in fission (H. Zhang et al., 2016). To check whether this mutation alters the overexpressing cell's oxygen consumption rate (OCR). Our data determines that this mutation causes no hindrance in cellular bioenergetics, including all parameters like control cells. Similar results were found by (Fabiana Longo et al., 2020).

Two patients bearing two heterozygous mutations in the DRP1 protein were found to have severe encephalopathy. One patient, a two-year-old child, was presented with chronic seizures and ataxia and later developed significant cerebral and cerebellar atrophy. A specific mutation (p.G223V) in the DRP1 gene was identified through high-throughput sequencing studies. When the cells from the patients were cultured in glucose-containing media, they exhibited swollen and rod-shaped hyperfused mitochondria. However, when grown in galactose-containing media that require oxidative phosphorylation for ATP generation, the mutant mitochondrial network displayed more disorganization with swollen puncta, rings, and chain-like structures. Furthermore, experiments showed that the mutation led to a 60% decrease in OCR in yeast cells expressing the disease variant DRP1 G252V and caused a significant increase (50%) of petite colonies compared to wild type due to structural changes near residues 215-221 affecting GTPase activity because of substitution from glycine to valine (Verrigni et al., 2019).

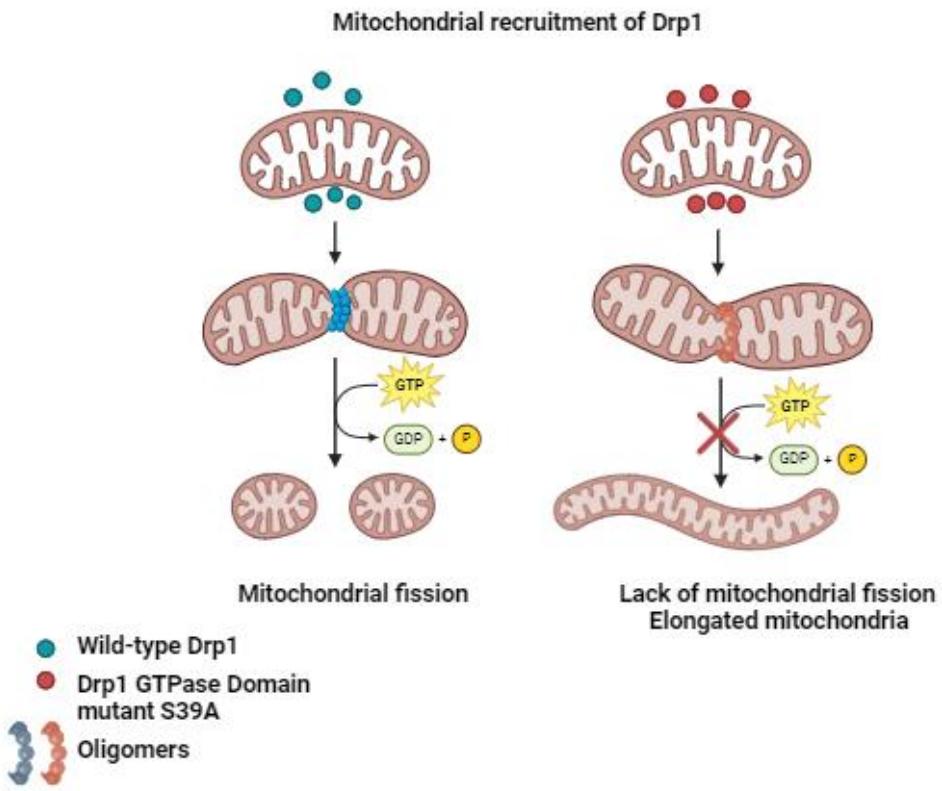

Fig. 25: ***Representative image showing the effects of DRP1 GTPase domain mutation.*** *GTPase domain mutation S39A causes hyperfused or elongated mitochondria by blocking the activity of GTP hydrolysis necessary for mitochondrial division.*

In addition to its role in mitochondrial fission, studies have also implicated DRP1 in other cellular processes, such as apoptosis and necrosis. Our results demonstrated that the overexpression of DRP1 caused excessive cell death. Under oxidative stress conditions, DRP1 stabilizes p53 and causes mitochondrial-associated necrosis (Guo, Sesaki, & Qi, 2014). Various stress conditions induce DRP1 translocation, leading to mitochondrial fragmentation (Pradeep, Sharma, & Rajanikant, 2014). Several research has shown that the overactivation of DRP1 is associated with disordered mitochondrial dynamics and directly exacerbates hepatocellular apoptosis (F. Li, Zhou, Li, Sun, & Chen, 2019). DRP1 dysregulation is linked to cell death in neurodegenerative disorders through excessive mitochondrial fission. For example, in primary cortical neurons, c-Abl-mediated phosphorylated DRP1 is associated with excessive mitochondrial fragmentation and cell death (L. Zhou et al., 2017). Another study highlighted the role of DRP1 inhibition in preventing mitochondrial fission, mitochondrial membrane potential, and cell death induced by glutamate toxicity (Grohm et al., 2012). DRP1 is vital for mitophagy

by inducing fission that generates smaller-sized mitochondria that are targeted for sequestration and degradation by autophagosomes and lysosomes. DRP1 over-expressing cells showed significant cell death compared to mCherry and S39A cells. It is evident from other studies that DRP1 is a mitochondrial fission protein, and overexpression of this protein leads to mitophagy and, ultimately, to cell death (Arnoult et al., 2005)

However, overexpressing S39A in cells significantly increased cell viability compared to overexpressed WT DRP1 cells. In conditions like atherosclerosis vascular disease, impaired mitochondria fail to produce sufficient ATP and cannot effectively neutralize the generated ROS byproducts, leading to toxic accumulation. Deficient mitochondrial dynamic proteins such as DRP1 may contribute to heart failure due to hindered mitophagy process exacerbating mitochondrial dysfunction. Uncontrolled GTPase activity of DRP1 compromises mitochondrial stability, while aberrant activation was observed in pulmonary arterial hypertension, leading to excessive mitochondrial fission. Overexpressing S39A DRP1 mutant cells restored cell death, suggesting the blockage of DRP1 GTPase activity due to the mutation hinders the apoptosis.

In the central nervous system, the PTMs of DRP1 play a crucial role in mitochondrial fission, synaptic injury, and cell death (Cho et al., 2009). In many neurodegenerative diseases, to prevent mitochondrial fission and cell death, DRP1 inhibition through overexpression of DRP1 mutant (K38A) or DRP1 inhibitors such as mdivi-1, p110-TAT are used (Guo et al., 2013; S. W. Park et al., 2011; X. Qi et al., 2013). Similarly, this mutation can be pivotal in reducing excessive mitochondrial fission and correcting the damage caused by DRP1 overexpression as the DRP1 dominant negative K38A (Shirendeb et al., 2012). In many neurodegenerative disorders, DRP1 binds with abnormal/mutant proteins, increasing its GTPase activity, ultimately resulting in the mitochondria's excessive fission (Manczak et al., 2011; Song et al., 2011). Further investigation is needed to determine how this site can be exploited to regulate and inhibit the abnormal binding of mutant neurodegenerative proteins with the DRP1 GTPase domain.

Summary

The study explored the impact of DRP1, an essential protein in splitting mitochondria, on differentiating SH-SY5Y cells into neurons. Decreasing the DRP1 levels led to a reorganization of the mitochondrial network and an increase in the expression of genes related to neuronal development, such as synapse formation, neurogenesis, differentiation, and morphogenesis. The reduction of DRP1 enhanced neuronal differentiation, resulting in longer neurite outgrowth, improved number of segments, and more branch points. Neuronal differentiation induced by RA-BDNF was accompanied by a notable decrease in ERK1/2 phosphorylation, indicating an ERK1/2 independent pathway for neuronal differentiation in shDrp1 cells. Additionally, there was no influence from dual specificity phosphatases DUSP1/6 on the phosphorylation status of ERK1/2 in shDrp1 cells, which maintained highly fused and elongated mitochondrial structures during differentiation while displaying significantly elevated maximal respiration. These findings suggest that lowering DRP1 promotes neuronal maturation through genomic and mitochondria rearrangement in undifferentiated cells. Regarding apoptosis or cell death, the shDrp1 reacted similarly to control when examined in vitro. Several crucially toxic aggregates associated with mutant huntingtin protein (mHtt) were notably reduced following the overexpression within these shDrp1 cells. This implies that lowering DRP1 in a regulated manner can increase several parameters, such as cell viability, neurotoxicity, and cellular bioenergetics. In conclusion, the research findings have shed light on the multifaceted roles of DRP1 in neuronal function. Further research is needed to investigate the mechanisms that can be very helpful in identifying therapeutic targets to treat neurodegenerative diseases.

DRP1 and its function in the GTPase domain are essential for morphology and cellular respiration. S39A mutation of DRP1 caused elongated, fused, and clustered tubular mitochondria compared to normal cells. Despite these changes, the energy remained unchanged, and cell death was reduced in the S39A mutant compared to those with the wild-type DRP1. These findings suggest that S39 plays a crucial role in distributing mitochondria within a cell by regulating GTPase activity and that mutations at this site cause structural abnormalities in the mitochondrial network. This study contributes new insight into understanding how DRP1 functions.

Keywords

Mitochondrial dynamics

Dynamin protein 1/DRP1

Mitochondria morphology

Mitofusin and Opa1

Neurodegeneration

Neuronal differentiation

RA-BDNF differentiation

SH-SY5Y human neuroblastoma cells

Neuronal markers genes

ERK1/2

MAPK signaling

DUSP1/6

DRP1 mutations

ACKNOWLEDGEMENT

I am immensely obliged to God, whose innumerable blessings empowered me to achieve my aims. I thank my supervisor, Dr. Tar Krisztina, an Associate Professor in the Medical Chemistry department, for her kind supervision and inspiring guidance. Her dedication and remarkable suggestions enabled me to complete this tedious task. I want to thank Dr. Virág László, the head of the Medical Chemistry department, for providing the necessary research facilities and constant support.

I want to express my gratitude to all my co-authors for their cooperation. I especially thank my senior lab fellows, Dr. Abdennour Douida and Dr. Azzam Aladdin, for their constant support throughout my research.

I want to acknowledge the Tempus Foundation for providing funds, honorable faculty members, and all the technical staff of the Medical Chemistry department, especially Andrea Tankáné Farkas, Kitti Barta, Dávid Varga, and Vera Szarvas, Prof Péter Szűcs and Gréta Nikoletta Kis for their cooperation during the research experiments.

I owe a debt of gratitude to my affectionate family members for their unflagging love, encouragement, and sacrifices. I also express my deepest gratitude to my loving mother, late father, dearest brothers, and loving sister, who constantly inspired me to pursue higher life ideas and supported and prayed for me to complete my work.

I want to express my deepest gratitude to my friends for their unconditional love and support.

Finally, I would like to thank everybody important to the successful completion of this thesis and express my apologies for not being able to mention myself personally.

This work was supported by Tempus Foundation's Stipendium Hungaricum. The University of Debrecen, Hungary, also supported this research through a Bridging fund (1G3D BKJO BFTK 247) and a fund from the International Education Office. The University of Debrecen catapult program also provided additional support through EPOP-3.6.1-16-2016-00022.

References

Agarwal, Swati, Yadav, Anuradha, Tiwari, Shashi Kant, Seth, Brashket, Chauhan, Lalit Kumar Singh, Khare, Puneet, . . . Chaturvedi, Rajnish Kumar. (2016). Dynamin-related protein 1 inhibition mitigates bisphenol A-mediated alterations in mitochondrial dynamics and neural stem cell proliferation and differentiation. *Journal of Biological Chemistry, 291*(31), 15923-15939.

Agholme, Lotta, Lindström, Tobias, Kågedal, Katarina, Marcusson, Jan, & Hallbeck, Martin. (2010). An in vitro model for neuroscience: differentiation of SH-SY5Y cells into cells with morphological and biochemical characteristics of mature neurons. *Journal of Alzheimer's disease, 20*(4), 1069-1082.

Ahmad, T, Aggarwal, K, Pattnaik, B, Mukherjee, S, Sethi, T, Tiwari, BK, . . . Ghosh, B. (2013). Computational classification of mitochondrial shapes reflects stress and redox state. *Cell death & disease, 4*(1), e461-e461.

Aladdin, Azzam, Yao, Yanhua, Yang, Ciyu, Kahlert, Günther, Ghani, Marvi, Király, Nikolett, . . . Tar, Krisztina. (2020). The proteasome activators Blm10/PA200 enhance the proteasomal degradation of N-terminal huntingtin. *Biomolecules, 10*(11), 1581.

Arnoult, Damien. (2007). Mitochondrial fragmentation in apoptosis. *Trends in cell biology, 17*(1), 6-12.

Arnoult, Damien, Rismanchi, Neggy, Grodet, Alain, Roberts, Roland G, Seeburg, Daniel P, Estaquier, Jérôme, . . . Blackstone, Craig. (2005). Bax/Bak-dependent release of DDP/TIMM8a promotes DRP1-mediated mitochondrial fission and mitoptosis during programmed cell death. *Current biology, 15*(23), 2112-2118.

Baek, Seung Hyun, Park, So Jung, Jeong, Jae In, Kim, Sung Hyun, Han, Jihoon, Kyung, Jae Won, . . . Park, Jin Su. (2017). Inhibition of DRP1 ameliorates synaptic depression, Aβ deposition, and cognitive impairment in an Alzheimer's disease model. *Journal of Neuroscience, 37*(20), 5099-5110.

Ban-Ishihara, Reiko, Ishihara, Takaya, Sasaki, Narie, Mihara, Katsuyoshi, & Ishihara, Naotada. (2013). Dynamics of nucleoid structure regulated by mitochondrial fission contributes to cristae reformation and release of cytochrome c. *Proceedings of the National Academy of Sciences, 110*(29), 11863-11868.

Basu, Kaustuv, Lajoie, Driss, Aumentado-Armstrong, Tristan, Chen, Jin, Koning, Roman I, Bossy, Blaise, . . . Rouiller, Isabelle. (2017). Molecular mechanism of DRP1 assembly studied in vitro by cryo-electron microscopy. *PloS one, 12*(6), e0179397.

Batzir, Nurit Assia, Bhagwat, Pranjali K, Eble, Tanya N, Liu, Pengfei, Eng, Christine M, Elsea, Sarah H, . . . Dhar, Shweta U. (2019). De novo missense variant in the GTPase effector domain (GED) of DNM1L leads to static encephalopathy and seizures. *Molecular Case Studies, 5*(3), a003673.

Beal, M. F. (2005). Mitochondria take center stage in aging and neurodegeneration. *Ann Neurol, 58*(4), 495-505. doi: 10.1002/ana.20624

Beckervordersandforth, Ruth, Ebert, Birgit, Schäffner, Iris, Moss, Jonathan, Fiebig, Christian, Shin, Jaehoon, . . . Stockburger, Carola. (2017). Role of mitochondrial metabolism in the control of early lineage progression and aging phenotypes in adult hippocampal neurogenesis. *Neuron, 93*(3), 560-573. e566.

Benard, Giovanni, Bellance, Nadège, James, Dominic, Parrone, Philippe, Fernandez, Helder, Letellier, Thierry, & Rossignol, Rodrigue. (2007). Mitochondrial bioenergetics and structural network organization. *Journal of cell science, 120*(5), 838-848.

Berman, H. M., Bhat, T. N., Bourne, P. E., Feng, Z., Gilliland, G., Weissig, H., & Westbrook, J. (2000). The Protein Data Bank and the challenge of structural genomics. *Nat Struct Biol, 7 Suppl*, 957-959. doi: 10.1038/80734

Biedler, June L, Roffler-Tarlov, Suzanne, Schachner, Melitta, & Freedman, Lewis S. (1978). Multiple neurotransmitter synthesis by human neuroblastoma cell lines and clones. *Cancer research, 38*(11_Part_1), 3751-3757.

Bleazard, William, McCaffery, J Michael, King, Edward J, Bale, Susan, Mozdy, Amy, Tieu, Quinton, . . . Shaw, Janet M. (1999). The dynamin-related GTPase Dnm1 regulates mitochondrial fission in yeast. *Nature cell biology, 1*(5), 298-304.

Blom, N., Sicheritz-Pontén, T., Gupta, R., Gammeltoft, S., & Brunak, S. (2004). Prediction of post-translational glycosylation and phosphorylation of proteins from the amino acid sequence. *Proteomics, 4*(6), 1633-1649. doi: 10.1002/pmic.200300771

Braschi, Emélie, Zunino, Rodolfo, & McBride, Heidi M. (2009). MAPL is a new mitochondrial SUMO E3 ligase that regulates mitochondrial fission. *EMBO reports, 10*(7), 748-754.

Briston, T., & Hicks, A. R. (2018). Mitochondrial dysfunction and neurodegenerative proteinopathies: mechanisms and prospects for therapeutic intervention. *Biochem Soc Trans, 46*(4), 829-842. doi: 10.1042/BST20180025

Cao, Yu-Lu, Meng, Shuxia, Chen, Yang, Feng, Jian-Xiong, Gu, Dong-Dong, Yu, Bing, . . . Chan, David C. (2017). MFN1 structures reveal nucleotide-triggered dimerization critical for mitochondrial fusion. *Nature, 542*(7641), 372-376.

Chan, David C. (2006a). Mitochondria: dynamic organelles in disease, aging, and development. *Cell, 125*(7), 1241-1252.

Chan, David C. (2006b). Mitochondrial fusion and fission in mammals. *Annu. Rev. Cell Dev. Biol., 22*, 79-99.

Chan, David C. (2020). Mitochondrial dynamics and its involvement in disease. *Annual Review of Pathology: Mechanisms of Disease, 15*, 235-259.

Chang, Chuang-Rung, & Blackstone, Craig. (2007). Cyclic AMP-dependent protein kinase phosphorylation of DRP1 regulates its GTPase activity and mitochondrial morphology. *Journal of Biological Chemistry, 282*(30), 21583-21587.

Chang, Chuang-Rung, Manlandro, Cara Marie, Arnoult, Damien, Stadler, Julia, Posey, Ammon E, Hill, R Blake, & Blackstone, Craig. (2010). A lethal de novo mutation in the middle domain of the dynamin-related GTPase DRP1 impairs higher order assembly and mitochondrial division. *Journal of Biological Chemistry, 285*(42), 32494-32503.

Chang, Chuang-Rung, & Blackstone, Craig. (2007). DRP1 phosphorylation and mitochondrial regulation. *EMBO reports, 8*(12), 1088-1089.

Chen, Hsiuchen, & Chan, David C. (2009). Mitochondrial dynamics–fusion, fission, movement, and mitophagy–in neurodegenerative diseases. *Human molecular genetics, 18*(R2), R169-R176.

Chen, Hsiuchen, Chomyn, Anne, & Chan, David C. (2005). Disruption of fusion results in mitochondrial heterogeneity and dysfunction. *Journal of Biological Chemistry, 280*(28), 26185-26192.

Chen, Hsiuchen, Detmer, Scott A, Ewald, Andrew J, Griffin, Erik E, Fraser, Scott E, & Chan, David C. (2003). Mitofusins Mfn1 and Mfn2 coordinately regulate mitochondrial fusion and are essential for embryonic development. *The Journal of cell biology, 160*(2), 189-200.

Chen, Nengzhou, Guo, Zhenkun, Luo, Zhousong, Zheng, Fuli, Shao, Wenya, Yu, Guangxia, . . . Li, Huangyuan. (2021). DRP1-mediated mitochondrial fission contributes to mitophagy in paraquat-induced neuronal cell damage. *Environmental Pollution, 272*, 116413.

Chen, Zhenyu, Chai, Eric, Mou, Yongchao, Roda, Ricardo H, Blackstone, Craig, & Li, Xue-Jun. (2022). Inhibiting mitochondrial fission rescues degeneration in hereditary spastic paraplegia neurons. *Brain, 145*(11), 4016-4031.

Cherubini, Marta, Lopez-Molina, Laura, & Gines, Silvia. (2020). Mitochondrial fission in Huntington's disease mouse striatum disrupts ER-mitochondria contacts leading to disturbances in Ca2+ efflux and Reactive Oxygen Species (ROS) homeostasis. *Neurobiology of Disease, 136*, 104741.

Chinnery, P, & Schon, E. (2003). Mitochondria. *Journal of neurology, neurosurgery, and psychiatry, 74*(9), 1188.

Cho, Dong-Hyung, Nakamura, Tomohiro, Fang, Jianguo, Cieplak, Piotr, Godzik, Adam, Gu, Zezong, & Lipton, Stuart A. (2009). S-nitrosylation of DRP1 mediates β-amyloid-related mitochondrial fission and neuronal injury. *Science, 324*(5923), 102-105.

Choi, Hyun Woo, Kim, Jin Hoi, Chung, Mi Kyung, Hong, Yean Ju, Jang, Hyun Sik, Seo, Bong Jong, . . . Byun, Sung June. (2015). Mitochondrial and metabolic remodeling during reprogramming and differentiation of the reprogrammed cells. *Stem cells and development, 24*(11), 1366-1373.

Choi, So Yoen, Kim, Joo Yeon, Kim, Hyun-Wook, Cho, Bongki, Cho, Hyo Min, Oppenheim, Ronald W, . . . Sun, Woong. (2013). DRP1-mediated mitochondrial dynamics and survival of developing chick motoneurons during the period of normal programmed cell death. *The FASEB Journal, 27*(1), 51.

Costa, Veronica, Giacomello, Marta, Hudec, Roman, Lopreiato, Raffaele, Ermak, Gennady, Lim, Dmitri, . . . Scorrano, Luca. (2010). Mitochondrial fission and cristae disruption increase the response of cell models of Huntington's disease to apoptotic stimuli. *EMBO molecular medicine, 2*(12), 490-503.

D’Aloia, Alessia, Pastori, Valentina, Blasa, Stefania, Campioni, Gloria, Peri, Francesco, Sacco, Elena, . . . Costa, Barbara. (2024). A new advanced cellular model of functional cholinergic-like neurons developed by reprogramming the human SH-SY5Y neuroblastoma cell line. *Cell Death Discovery, 10*(1), 24.

de Medeiros, Liana M, De Bastiani, Marco A, Rico, Eduardo P, Schonhofen, Patrícia, Pfaffenseller, Bianca, Wollenhaupt-Aguiar, Bianca, . . . Castro, Mauro AA. (2019). Cholinergic differentiation of human neuroblastoma SH-SY5Y cell line and its potential use as an in vitro model for Alzheimer's disease studies. *Molecular Neurobiology, 56*, 7355-7367.

De Palma, C, Falcone, S, Pisoni, S, Cipolat, S, Panzeri, C, Pambianco, S, . . . Cossu, G. (2010). Nitric oxide inhibition of DRP1-mediated mitochondrial fission is critical for myogenic differentiation. *Cell Death & Differentiation, 17*(11), 1684-1696.

Delettre, Cécile, Lenaers, Guy, Griffoin, Jean-Michel, Gigarel, Nadine, Lorenzo, Corinne, Belenguer, Pascale, . . . Perret, Eric. (2000). Nuclear gene OPA1, encoding a mitochondrial dynamin-related protein, is mutated in dominant optic atrophy. *Nature genetics, 26*(2), 207-210.

Ding, Shirong, Gao, Ying, Lv, Dongming, Tao, Yalan, Liu, Songran, Chen, Chen, . . . Chow, Larry Ka-Yue. (2022). DNTTIP1 promotes nasopharyngeal carcinoma metastasis via recruiting HDAC1 to DUSP2 promoter and activating ERK signaling pathway. *EBioMedicine, 81*.

Douida, A., Batista, F., Boto, P., Regdon, Z., Robaszkiewicz, A., & Tar, K. (2021). Cells Lacking PA200 Adapt to Mitochondrial Dysfunction by Enhancing Glycolysis via Distinct Opa1 Processing. *Int J Mol Sci, 22*(4). doi: 10.3390/ijms22041629

Douida, Abdennour, Batista, Frank, Robaszkiewicz, Agnieszka, Boto, Pal, Aladdin, Azzam, Szenykiv, Mónika, . . . Tar, Krisztina. (2020). The proteasome activator PA200 regulates expression of genes involved in cell survival upon selective mitochondrial inhibition in neuroblastoma cells. *Journal of cellular and molecular medicine, 24*(12), 6716-6730.

Dutta, Sangeeta, Pal, Debosree, & Rao, MRS. (2023). Retinoic Acid-Mediated Differentiation of Mouse Embryonic Stem Cells to Neuronal Cells *Stem Cells and Lineage Commitment: Methods and Protocols* (pp. 39-51): Springer.

Duvezin-Caubet, Stéphane, Koppen, Mirko, Wagener, Johannes, Zick, Michael, Israel, Lars, Bernacchia, Andrea, . . . Neupert, Walter. (2007). OPA1 processing reconstituted in yeast depends on the subunit composition of the m-AAA protease in mitochondria. *Molecular biology of the cell, 18*(9), 3582-3590.

Encinas, Mario, Iglesias, Montse, Liu, Yuhui, Wang, Hongyin, Muhaisen, Ashraf, Cena, Valentin, . . . Comella, Joan X. (2000). Sequential treatment of SH-SY5Y cells with retinoic acid and brain-derived neurotrophic factor gives rise to fully differentiated, neurotrophic factor-dependent, human neuron-like cells. *Journal of neurochemistry, 75*(3), 991-1003.

Estaquier, J, & Arnoult, D. (2007). Inhibiting DRP1-mediated mitochondrial fission selectively prevents the release of cytochrome c during apoptosis. *Cell Death & Differentiation, 14*(6), 1086-1094.

Eura, Yuka, Ishihara, Naotada, Yokota, Sadaki, & Mihara, Katsuyoshi. (2003). Two mitofusin proteins, mammalian homologues of FZO, with distinct functions are both required for mitochondrial fusion. *Journal of biochemistry, 134*(3), 333-344.

Ford, Marijn GJ, Jenni, Simon, & Nunnari, Jodi. (2011). The crystal structure of dynamin. *Nature, 477*(7366), 561-566.

Forster, JI, Köglsberger, S, Trefois, C, Boyd, O, Baumuratov, AS, Buck, L, . . . Antony, PMA. (2016). Characterization of differentiated SH-SY5Y as neuronal screening model reveals increased oxidative vulnerability. *Journal of biomolecular screening, 21*(5), 496-509.

Franco-Iborra, Sandra, Vila, Miquel, & Perier, Celine. (2016). The Parkinson disease mitochondrial hypothesis: where are we at? *The Neuroscientist, 22*(3), 266-277.

Francy, Christopher A, Clinton, Ryan W, Fröhlich, Chris, Murphy, Colleen, & Mears, Jason A. (2017). Cryo-EM studies of DRP1 reveal cardiolipin interactions that activate the helical oligomer. *Scientific reports, 7*(1), 10744.

Frank, S., Gaume, B., Bergmann-Leitner, E. S., Leitner, W. W., Robert, E. G., Catez, F., . . . Youle, R. J. (2001). The role of dynamin-related protein 1, a mediator of mitochondrial fission, in apoptosis. *Dev Cell, 1*(4), 515-525. doi: 10.1016/s1534-5807(01)00055-7

Frank, Stephan, Gaume, Brigitte, Bergmann-Leitner, Elke S, Leitner, Wolfgang W, Robert, Everett G, Catez, Frédéric, . . . Youle, Richard J. (2001). The role of dynamin-related protein 1, a mediator of mitochondrial fission, in apoptosis. *Developmental cell, 1*(4), 515-525.

Friedman, J. R., Lackner, L. L., West, M., DiBenedetto, J. R., Nunnari, J., & Voeltz, G. K. (2011). ER tubules mark sites of mitochondrial division. *Science, 334*(6054), 358-362. doi: 10.1126/science.1207385

Friedman, Jonathan R, Lackner, Laura L, West, Matthew, DiBenedetto, Jared R, Nunnari, Jodi, & Voeltz, Gia K. (2011). ER tubules mark sites of mitochondrial division. *Science, 334*(6054), 358-362.

Fröhlich, C., Grabiger, S., Schwefel, D., Faelber, K., Rosenbaum, E., Mears, J., . . . Daumke, O. (2013). Structural insights into oligomerization and mitochondrial remodelling of dynamin 1-like protein. *EMBO J, 32*(9), 1280-1292. doi: 10.1038/emboj.2013.74

Fukushima, Noelle H, Brisch, Ellen, Keegan, Brian R, Bleazard, William, & Shaw, Janet M. (2001). The GTPase effector domain sequence of the Dnm1p GTPase regulates self-assembly and controls a rate-limiting step in mitochondrial fission. *Molecular Biology of the Cell, 12*(9), 2756-2766.

Ghani, M., Zohar, P., Ujlaki, G., Tóth, M., Amsalu, H., Póliska, S., & Tar, K. (2024). Stable knockdown of DRP1 improves retinoic acid-BDNF-induced neuronal differentiation through global transcriptomic changes and results in reduced phosphorylation of ERK1/2 independently of DUSP1 and 6. *Front Cell Dev Biol, 12*, 1342741. doi: 10.3389/fcell.2024.1342741

Ghosh, Rhia, & Tabrizi, Sarah J. (2018). Clinical features of Huntington's disease. *Polyglutamine disorders*, 1-28.

Giedt, Randy J, Fumene Feruglio, Paolo, Pathania, Divya, Yang, Katherine S, Kilcoyne, Aoife, Vinegoni, Claudio, . . . Weissleder, Ralph. (2016). Computational imaging reveals mitochondrial morphology as a biomarker of cancer phenotype and drug response. *Scientific reports, 6*(1), 32985.

Gomes, Ligia C, Benedetto, Giulietta Di, & Scorrano, Luca. (2011). During autophagy mitochondria elongate, are spared from degradation and sustain cell viability. *Nature cell biology, 13*(5), 589-598.

Grohm, J, Kim, SW, Mamrak, U, Tobaben, S, Cassidy-Stone, A, Nunnari, J, . . . Culmsee, C. (2012). Inhibition of DRP1 provides neuroprotection in vitro and in vivo. *Cell Death & Differentiation, 19*(9), 1446-1458.

Guo, Xing, Disatnik, Marie-Helene, Monbureau, Marie, Shamloo, Mehrdad, Mochly-Rosen, Daria, & Qi, Xin. (2013). Inhibition of mitochondrial fragmentation diminishes Huntington's disease–associated neurodegeneration. *The Journal of clinical investigation, 123*(12), 5371-5388.

Guo, Xing, Sesaki, Hiromi, & Qi, Xin. (2014). DRP1 stabilizes p53 on the mitochondria to trigger necrosis under oxidative stress conditions in vitro and in vivo. *Biochemical Journal, 461*(1), 137-146.

Han, Xiao-Jian, Lu, Yun-Fei, Li, Shun-Ai, Kaitsuka, Taku, Sato, Yasufumi, Tomizawa, Kazuhito, . . . Matsushita, Masayuki. (2008). CaM kinase Iα–induced phosphorylation of DRP1 regulates mitochondrial morphology. *The Journal of cell biology, 182*(3), 573-585.

Harder, Zdena, Zunino, Rodolfo, & McBride, Heidi. (2004). Sumo1 conjugates mitochondrial substrates and participates in mitochondrial fission. *Current Biology, 14*(4), 340-345.

Haun, Florian, Nakamura, Tomohiro, Shiu, Alicia D, Cho, Dong-Hyung, Tsunemi, Taiji, Holland, Emily A, . . . Lipton, Stuart A. (2013). S-nitrosylation of dynamin-related protein 1 mediates mutant huntingtin-induced mitochondrial fragmentation and neuronal injury in Huntington's disease. *Antioxidants & redox signaling, 19*(11), 1173-1184.

Hinshaw, JE. (2000). Dynamin and its role in membrane fission. *Annual review of cell and developmental biology, 16*(1), 483-519.

Hollenbeck, Peter J, & Saxton, William M. (2005). The axonal transport of mitochondria. *Journal of cell science, 118*(23), 5411-5419.

Hoque, Ashfaqul, Sivakumaran, Priyadharshini, Bond, Simon T, Ling, Naomi XY, Kong, Anne M, Scott, John W, . . . Wong, Raymond CB. (2018). Mitochondrial fission protein DRP1 inhibition promotes cardiac mesodermal differentiation of human pluripotent stem cells. *Cell death discovery, 4*(1), 39.

Hornbeck, P. V., Zhang, B., Murray, B., Kornhauser, J. M., Latham, V., & Skrzypek, E. (2015). PhosphoSitePlus, 2014: mutations, PTMs and recalibrations. *Nucleic Acids Res, 43*(Database issue), D512-520. doi: 10.1093/nar/gku1267

Hromadkova, Lenka, Bezdekova, Dagmar, Pala, Jan, Schedin-Weiss, Sophia, Tjernberg, Lars O, Hoschl, Cyril, & Ovsepian, Saak V. (2020). Brain-derived neurotrophic factor (BDNF) promotes molecular polarization and differentiation of immature neuroblastoma cells into definitive neurons. *Biochimica et Biophysica Acta (BBA)-Molecular Cell Research, 1867*(9), 118737.

Hu, Bao-Yang, Weick, Jason P, Yu, Junying, Ma, Li-Xiang, Zhang, Xiao-Qing, Thomson, James A, & Zhang, Su-Chun. (2010). Neural differentiation of human induced pluripotent stem

cells follows developmental principles but with variable potency. *Proceedings of the National Academy of Sciences, 107*(9), 4335-4340.

Hu, Chenxia, Huang, Yong, & Li, Lanjuan. (2017). DRP1-dependent mitochondrial fission plays critical roles in physiological and pathological progresses in mammals. *International journal of molecular sciences, 18*(1), 144.

Hutson, Anelise, & Mears, Jason A. (2024). Role of disordered regions on DRP1 structure and function. *Biophysical Journal, 123*(3), 67a.

Ioghen, Octavian Costin, Ceafalan, Laura Cristina, & Popescu, Bogdan Ovidiu. (2023). SH-SY5Y cell line in vitro models for Parkinson disease research—old practice for new trends. *Journal of Integrative Neuroscience, 22*(1), 20.

Ishihara, Naotada, Fujita, Yuu, Oka, Toshihiko, & Mihara, Katsuyoshi. (2006). Regulation of mitochondrial morphology through proteolytic cleavage of OPA1. *The EMBO journal, 25*(13), 2966-2977.

Ishihara, Naotada, Nomura, Masatoshi, Jofuku, Akihiro, Kato, Hiroki, Suzuki, Satoshi O, Masuda, Keiji, . . . Goto, Yu-ichi. (2009). Mitochondrial fission factor DRP1 is essential for embryonic development and synapse formation in mice. *Nature cell biology, 11*(8), 958-966.

James, Dominic I, Parone, Philippe A, Mattenberger, Yves, & Martinou, Jean-Claude. (2003). hFis1, a novel component of the mammalian mitochondrial fission machinery. *Journal of Biological Chemistry, 278*(38), 36373-36379.

Jellinger, Kurt A. (2009). Recent advances in our understanding of neurodegeneration. *Journal of neural transmission, 116*, 1111-1162.

Jenner, Andreas, Peña-Blanco, Aida, Salvador-Gallego, Raquel, Ugarte-Uribe, Begoña, Zollo, Cristiana, Ganief, Tariq, . . . Ries, Jonas. (2022). DRP1 interacts directly with BAX to induce its activation and apoptosis. *The EMBO journal, 41*(8), e108587.

Jhun, Bong Sook, O-Uchi, Jin, Adaniya, Stephanie M, Mancini, Thomas J, Cao, Jessica L, King, Michelle E, . . . Yang, Donqin. (2018). Protein kinase D activation induces mitochondrial fragmentation and dysfunction in cardiomyocytes. *The Journal of physiology, 596*(5), 827-855.

Jin, J. Y., Wei, X. X., Zhi, X. L., Wang, X. H., & Meng, D. (2021). DRP1-dependent mitochondrial fission in cardiovascular disease. *Acta Pharmacol Sin, 42*(5), 655-664. doi: 10.1038/s41401-020-00518-y

Kaplan, David R, Matsumoto, Kazue, Lucarelli, Enrico, & Thielet, Carol J. (1993). Induction of TrkB by retinoic acid mediates biologic responsiveness to BDNF and differentiation of human neuroblastoma cells. *Neuron, 11*(2), 321-331.

Karbowski, Mariusz, Lee, Yang-Ja, Gaume, Brigitte, Jeong, Seon-Yong, Frank, Stephan, Nechushtan, Amotz, . . . Youle, Richard J. (2002). Spatial and temporal association of Bax with mitochondrial fission sites, DRP1, and Mfn2 during apoptosis. *The Journal of cell biology, 159*(6), 931-938.

Karbowski, Mariusz, Neutzner, Albert, & Youle, Richard J. (2007). The mitochondrial E3 ubiquitin ligase MARCH5 is required for DRP1 dependent mitochondrial division. *The Journal of cell biology, 178*(1), 71-84.

Khacho, Mireille, Clark, Alysen, Svoboda, Devon S, Azzi, Joelle, MacLaurin, Jason G, Meghaizel, Cynthia, . . . Harper, Mary-Ellen. (2016). Mitochondrial dynamics impacts stem cell identity and fate decisions by regulating a nuclear transcriptional program. *Cell stem cell, 19*(2), 232-247.

Khacho, Mireille, & Slack, Ruth S. (2018). Mitochondrial dynamics in the regulation of neurogenesis: from development to the adult brain. *Developmental Dynamics, 247*(1), 47-53.

Kim, Boa, Kim, Ji-Seok, Yoon, Yisang, Santiago, Mayra C, Brown, Michael D, & Park, Joon-Young. (2013). Inhibition of DRP1-dependent mitochondrial division impairs myogenic differentiation. *American Journal of Physiology-Regulatory, Integrative and Comparative Physiology, 305*(8), R927-R938.

Kim, Hyun Jung, Shaker, Mohammed R, Cho, Bongki, Cho, Hyo Min, Kim, Hyun, Kim, Joo Yeon, & Sun, Woong. (2015). Dynamin-related protein 1 controls the migration and neuronal differentiation of subventricular zone-derived neural progenitor cells. *Scientific reports, 5*(1), 15962.

Kim, JE, Ryu, HJ, Kim, MJ, & Kang, TC. (2014). LIM kinase-2 induces programmed necrotic neuronal death via dysfunction of DRP1-mediated mitochondrial fission. *Cell Death & Differentiation, 21*(7), 1036-1049.

Kim, KY, Perkins, GA, Shim, MS, Bushong, E, Alcasid, N, Ju, S, . . . Ju, WK. (2015). DRP1 inhibition rescues retinal ganglion cells and their axons by preserving mitochondrial integrity in a mouse model of glaucoma. *Cell death & disease, 6*(8), e1839-e1839.

Kishida, H, & Sugio, Shigetoshi. (2014). *Crystal structure of GTPase domain fused with minimal stalks from human dynamin-1-like protein (Dlp1) in complex with several nucleotide analogues*.

Kitamura, Shinya, Yanagi, Teruki, Imafuku, Keisuke, Hata, Hiroo, Abe, Riichiro, & Shimizu, Hiroshi. (2017). DRP1 regulates mitochondrial morphology and cell proliferation in cutaneous squamous cell carcinoma. *Journal of dermatological science, 88*(3), 298-307.

Ko, Ah-Reum, Hyun, Hye-Won, Min, Su-Ji, & Kim, Ji-Eun. (2016). The differential DRP1 phosphorylation and mitochondrial dynamics in the regional specific astroglial death induced by status epilepticus. *Frontiers in cellular neuroscience, 10*, 124.

Kotiadis, Vassilios N, Duchen, Michael R, & Osellame, Laura D. (2014). Mitochondrial quality control and communications with the nucleus are important in maintaining mitochondrial function and cell health. *Biochimica et Biophysica Acta (BBA)-General Subjects, 1840*(4), 1254-1265.

Kovalevich, Jane, & Langford, Dianne. (2013). Considerations for the use of SH-SY5Y neuroblastoma cells in neurobiology. *Neuronal cell culture: methods and protocols*, 9-21.

Kraus, Felix, Roy, Krishnendu, Pucadyil, Thomas J, & Ryan, Michael T. (2021). Function and regulation of the divisome for mitochondrial fission. *Nature, 590*(7844), 57-66.

Kumar, Rita, Bukowski, Melissa J, Wider, Joseph M, Reynolds, Christian A, Calo, Lesley, Lepore, Bradley, . . . Sanderson, Thomas H. (2016). Mitochondrial dynamics following global cerebral ischemia. *Molecular and Cellular Neuroscience, 76*, 68-75.

Lee, Duk-shin, & Kim, Ji-Eun. (2018). PDI-mediated S-nitrosylation of DRP1 facilitates DRP1-S616 phosphorylation and mitochondrial fission in CA1 neurons. *Cell Death & Disease, 9*(9), 869.

Li, Fangfang, Zhou, Juan, Li, Yi, Sun, Kewei, & Chen, Jun. (2019). Mitochondrial damage and DRP1 overexpression in rifampicin-and isoniazid-induced liver injury cell model. *Journal of Clinical and Translational Hepatology, 7*(1), 40.

Li, Xiao-Jiang, & Li, Shihua. (2011). Proteasomal dysfunction in aging and Huntington disease. *Neurobiology of disease, 43*(1), 4-8.

Li, Xiaoling, & Gould, Stephen J. (2003). The dynamin-like GTPase DLP1 is essential for peroxisome division and is recruited to peroxisomes in part by PEX11. *Journal of Biological Chemistry, 278*(19), 17012-17020.

Li, Zheng, Okamoto, Ken-Ichi, Hayashi, Yasunori, & Sheng, Morgan. (2004). The importance of dendritic mitochondria in the morphogenesis and plasticity of spines and synapses. *Cell, 119*(6), 873-887.

Liu, Raymond, & Chan, David C. (2015). The mitochondrial fission receptor Mff selectively recruits oligomerized DRP1. *Molecular biology of the cell, 26*(24), 4466-4477.

Liu, Tong, Yu, Rong, Jin, Shao-Bo, Han, Liwei, Lendahl, Urban, Zhao, Jian, & Nistér, Monica. (2013). The mitochondrial elongation factors MIEF1 and MIEF2 exert partially distinct functions in mitochondrial dynamics. *Experimental cell research, 319*(18), 2893-2904.

Liu, X, & Hajnoczky, G. (2011). Altered fusion dynamics underlie unique morphological changes in mitochondria during hypoxia–reoxygenation stress. *Cell Death & Differentiation, 18*(10), 1561-1572.

Livak, Kenneth J, & Schmittgen, Thomas D. (2001). Analysis of relative gene expression data using real-time quantitative PCR and the 2− ΔΔCT method. *methods, 25*(4), 402-408.

Longo, F., Benedetti, S., Zambon, A. A., Sora, M. G. N., Di Resta, C., De Ritis, D., . . . Previtali, S. C. (2020). Impaired turnover of hyperfused mitochondria in severe axonal neuropathy due to a novel DRP1 mutation. *Hum Mol Genet, 29*(2), 177-188. doi: 10.1093/hmg/ddz211

Longo, Fabiana, Benedetti, Sara, Zambon, Alberto A, Sora, Maria Grazia Natali, Di Resta, Chiara, De Ritis, Daniele, . . . Previtali, Stefano Carlo. (2020). Impaired turnover of hyperfused mitochondria in severe axonal neuropathy due to a novel DRP1 mutation. *Human Molecular Genetics, 29*(2), 177-188.

López-Carballo, Gracia, Moreno, Lucrecia, Masiá, Susana, Pérez, Paloma, & Barettino, Domingo. (2002). Activation of the phosphatidylinositol 3-kinase/Akt signaling pathway by retinoic acid is required for neural differentiation of SH-SY5Y human neuroblastoma cells. *Journal of Biological Chemistry, 277*(28), 25297-25304.

Losón, Oliver C, Liu, Raymond, Rome, Michael E, Meng, Shuxia, Kaiser, Jens T, Shan, Shu-ou, & Chan, David C. (2014). The mitochondrial fission receptor MiD51 requires ADP as a cofactor. *Structure, 22*(3), 367-377.

Losón, Oliver C, Song, Zhiyin, Chen, Hsiuchen, & Chan, David C. (2013). Fis1, Mff, MiD49, and MiD51 mediate DRP1 recruitment in mitochondrial fission. *Molecular biology of the cell, 24*(5), 659-667.

Lu, Bin, Kennedy, Bridget, Clinton, Ryan W, Wang, Emily Jue, McHugh, Daniel, Stepanyants, Natalia, . . . Ramachandran, Rajesh. (2018). Steric interference from intrinsically disordered regions controls dynamin-related protein 1 self-assembly during mitochondrial fission. *Scientific Reports, 8*(1), 10879.

Manczak, Maria, Calkins, Marcus J, & Reddy, P Hemachandra. (2011). Impaired mitochondrial dynamics and abnormal interaction of amyloid beta with mitochondrial protein DRP1 in neurons from patients with Alzheimer's disease: implications for neuronal damage. *Human molecular genetics, 20*(13), 2495-2509.

Manczak, Maria, Sesaki, Hiromi, Kageyama, Yusuke, & Reddy, P Hemachandra. (2012). Dynamin-related protein 1 heterozygote knockout mice do not have synaptic and mitochondrial deficiencies. *Biochimica et Biophysica Acta (BBA)-Molecular Basis of Disease, 1822*(6), 862-874.

McBride, H. M., Neuspiel, M., & Wasiak, S. (2006). Mitochondria: more than just a powerhouse. *Curr Biol, 16*(14), R551-560. doi: 10.1016/j.cub.2006.06.054

Meeusen, Shelly, McCaffery, J Michael, & Nunnari, Jodi. (2004). Mitochondrial fusion intermediates revealed in vitro. *Science, 305*(5691), 1747-1752.

Michalska, Bernadeta, Duszyński, Jerzy, & Szymański, Jędrzej. (2016). Mechanism of mitochondrial fission-structure and function of DRP1 protein. *Postepy biochemii, 62*(2), 127-137.

Miloso, Mariarosaria, Villa, Daniela, Crimi, Marco, Galbiati, Stefania, Donzelli, Elisabetta, Nicolini, Gabriella, & Tredici, Giovanni. (2004). Retinoic acid-induced neuritogenesis of human neuroblastoma SH-SY5Y cells is ERK independent and PKC dependent. *Journal of neuroscience research, 75*(2), 241-252.

Mils, Valérie, Bosch, Stéphanie, Roy, Julie, Bel-Vialar, Sophie, Belenguer, Pascale, Pituello, Fabienne, & Miquel, Marie-Christine. (2015). Mitochondrial reshaping accompanies neural differentiation in the developing spinal cord. *PLoS One, 10*(5), e0128130.

Nagy, Lilla, Docsa, Tibor, Szanto, Magdolna, Brunyanszki, Attila, Hegedűs, Csaba, Marton, Judit, . . . Gergely, Pal. (2013). Glycogen phosphorylase inhibitor N-(3, 5-dimethyl-

benzoyl)-N'-(β-D-glucopyranosyl) urea improves glucose tolerance under normoglycemic and diabetic conditions and rearranges hepatic metabolism. *PloS one, 8*(7), e69420.

Nakamura, Nobuhiro, Kimura, Yasuo, Tokuda, Masaki, Honda, Shinji, & Hirose, Shigehisa. (2006). MARCH-V is a novel mitofusin 2-and DRP1-binding protein able to change mitochondrial morphology. *EMBO reports, 7*(10), 1019-1022.

Nasca, Alessia, Legati, Andrea, Baruffini, Enrico, Nolli, Cecilia, Moroni, Isabella, Ardissone, Anna, . . . Ghezzi, Daniele. (2016). Biallelic mutations in DNM1L are associated with a slowly progressive infantile encephalopathy. *Human mutation, 37*(9), 898-903.

Niemann, Hartmut H, Knetsch, Menno LW, Scherer, Anna, Manstein, Dietmar J, & Kull, F Jon. (2001). Crystal structure of a dynamin GTPase domain in both nucleotide-free and GDP-bound forms. *The EMBO journal*.

Noy, Noa. (2010). Between death and survival: retinoic acid in regulation of apoptosis. *Annual review of nutrition, 30*, 201-217.

Nunnari, J., & Suomalainen, A. (2012). Mitochondria: in sickness and in health. *Cell, 148*(6), 1145-1159. doi: 10.1016/j.cell.2012.02.035

Nunnari, Jodi, Marshall, Wallace F, Straight, Aaron, Murray, Andrew, Sedat, John W, & Walter, Peter. (1997). Mitochondrial transmission during mating in Saccharomyces cerevisiae is determined by mitochondrial fusion and fission and the intramitochondrial segregation of mitochondrial DNA. *Molecular biology of the cell, 8*(7), 1233-1242.

Oliver, D., & Reddy, P. H. (2019). Dynamics of Dynamin-Related Protein 1 in Alzheimer's Disease and Other Neurodegenerative Diseases. *Cells, 8*(9). doi: 10.3390/cells8090961

Ordonez, Dalila G, Lee, Michael K, & Feany, Mel B. (2018). α-synuclein induces mitochondrial dysfunction through spectrin and the actin cytoskeleton. *Neuron, 97*(1), 108-124. e106.

Ortiz-Sandoval, Carolina G, Hughes, Sarah C, Dacks, Joel B, & Simmen, Thomas. (2014). Interaction with the effector dynamin-related protein 1 (DRP1) is an ancient function of Rab32 subfamily proteins. *Cellular logistics, 4*(4), e986399.

Osellame, Laura D, Blacker, Thomas S, & Duchen, Michael R. (2012). Cellular and molecular mechanisms of mitochondrial function. *Best practice & research Clinical endocrinology & metabolism, 26*(6), 711-723.

Otera, Hidenori, & Mihara, Katsuyoshi. (2011). Discovery of the membrane receptor for mitochondrial fission GTPase DRP1. *Small GTPases, 2*(3), 241-251.

Park, Jong-Chan, Jeong, Woo-Jeong, Kim, Mi-Yeon, Min, DoSik, & Choi, Kang-Yell. (2016). Retinoic-acid-mediated HRas stabilization induces neuronal differentiation of neural stem cells during brain development. *Journal of cell science, 129*(15), 2997-3007.

Park, Sang Woo, Kim, Keun-Young, Lindsey, James D, Dai, Yi, Heo, Hwan, Nguyen, Duy H, . . . Ju, Won-Kyu. (2011). A selective inhibitor of DRP1, mdivi-1, increases retinal ganglion cell survival in acute ischemic mouse retina. *Investigative ophthalmology & visual science, 52*(5), 2837-2843.

Park, So Jung, Bae, Ji-Eun, Jo, Doo Sin, Kim, Joon Bum, Park, Na Yeon, Fang, Jianguo, . . . Cho, Dong-Hyung. (2021). Increased O-GlcNAcylation of DRP1 by amyloid-beta promotes mitochondrial fission and dysfunction in neuronal cells. *Molecular brain, 14*, 1-3.

Pernaute, Barbara, Pérez-Montero, Salvador, Nieto, Juan Miguel Sánchez, Di Gregorio, Aida, Lima, Ana, Lawlor, Katerina, . . . Meier, Pascal. (2022). DRP1 levels determine the apoptotic threshold during embryonic differentiation through a mitophagy-dependent mechanism. *Developmental cell, 57*(11), 1316-1330. e1317.

Pradeep, H, Sharma, B, & Rajanikant, GK. (2014). DRP1 in ischemic neuronal death: an unusual suspect. *Current medicinal chemistry, 21*(19), 2183-2189.

Prieto, Javier, León, Marian, Ponsoda, Xavier, Sendra, Ramón, Bort, Roque, Ferrer-Lorente, Raquel, . . . Torres, Josema. (2016). Early ERK1/2 activation promotes DRP1-dependent mitochondrial fission necessary for cell reprogramming. *Nature communications, 7*(1), 11124.

Prudent, Julien, Zunino, Rodolfo, Sugiura, Ayumu, Mattie, Sevan, Shore, Gordon C, & McBride, Heidi M. (2015). MAPL SUMOylation of DRP1 stabilizes an ER/mitochondrial platform required for cell death. *Molecular cell, 59*(6), 941-955.

Przedborski, Serge, Vila, Miquel, & Jackson-Lewis, Vernice. (2003). Series Introduction: Neurodegeneration: What is it and where are we? *The Journal of clinical investigation, 111*(1), 3-10.

Qi, Xin, Qvit, Nir, Su, Yu-Chin, & Mochly-Rosen, Daria. (2013). A novel DRP1 inhibitor diminishes aberrant mitochondrial fission and neurotoxicity. *Journal of cell science, 126*(3), 789-802.

Qi, Zhihao, Huang, Zhen, Xie, Feng, & Chen, Linxi. (2019). Dynamin-related protein 1: a critical protein in the pathogenesis of neural system dysfunctions and neurodegenerative diseases. *Journal of cellular physiology, 234*(7), 10032-10046.

Reddy, P. H., Reddy, T. P., Manczak, M., Calkins, M. J., Shirendeb, U., & Mao, P. (2011). Dynamin-related protein 1 and mitochondrial fragmentation in neurodegenerative diseases. *Brain Res Rev, 67*(1-2), 103-118. doi: 10.1016/j.brainresrev.2010.11.004

Riegerova, Petra, Brejcha, Jindřich, Bezděková, Dagmar, Chum, Tomáš, Mašínová, Eva, Čermáková, Nikola, . . . Štefl, Martin. (2021). Expression and localization of AβPP in SH-SY5Y cells depends on differentiation state. *Journal of Alzheimer's Disease, 82*(2), 485-491.

Ross, Robert A, Spengler, Barbara A, & Biedler, June L. (1983). Coordinate morphological and biochemical interconversion of human neuroblastoma cells. *Journal of the National Cancer Institute, 71*(4), 741-747.

Ruiz, Asier, Alberdi, Elena, & Matute, Carlos. (2018). Mitochondrial division inhibitor 1 (mdivi-1) protects neurons against excitotoxicity through the modulation of mitochondrial function and intracellular Ca2+ signaling. *Frontiers in Molecular Neuroscience, 11*, 3.

Saitoh, Hisato, & Hinchey, Joseph. (2000). Functional heterogeneity of small ubiquitin-related protein modifiers SUMO-1 versus SUMO-2/3. *Journal of Biological Chemistry, 275*(9), 6252-6258.

Scheel, Hartmut, & Hofmann, Kay. (2005). Prediction of a common structural scaffold for proteasome lid, COP9-signalosome and eIF3 complexes. *BMC bioinformatics, 6*, 1-10.

Sesaki, Hiromi, Adachi, Yoshihiro, Kageyama, Yusuke, Itoh, Kie, & Iijima, Miho. (2014). In vivo functions of DRP1: lessons learned from yeast genetics and mouse knockouts. *Biochimica et Biophysica Acta (BBA)-Molecular Basis of Disease, 1842*(8), 1179-1185.

Shirendeb, Ulziibat P, Calkins, Marcus J, Manczak, Maria, Anekonda, Vishwanath, Dufour, Brett, McBride, Jodi L, . . . Reddy, P Hemachandra. (2012). Mutant huntingtin's interaction with mitochondrial protein DRP1 impairs mitochondrial biogenesis and

causes defective axonal transport and synaptic degeneration in Huntington's disease. *Human molecular genetics, 21*(2), 406-420.

Shutt, Timothy, Geoffrion, Michèle, Milne, Ross, & McBride, Heidi M. (2012). The intracellular redox state is a core determinant of mitochondrial fusion. *EMBO reports, 13*(10), 909-915.

Singh, Ugra S, Pan, Jing, Kao, Yu-Lin, Joshi, Suchitra, Young, Keri L, & Baker, Kenneth M. (2003). Tissue transglutaminase mediates activation of RhoA and MAP kinase pathways during retinoic acid-induced neuronal differentiation of SH-SY5Y cells. *Journal of Biological Chemistry, 278*(1), 391-399.

Smirnova, E., Griparic, L., Shurland, D. L., & van der Bliek, A. M. (2001). Dynamin-related protein DRP1 is required for mitochondrial division in mammalian cells. *Mol Biol Cell, 12*(8), 2245-2256. doi: 10.1091/mbc.12.8.2245

Smirnova, Elena, Griparic, Lorena, Shurland, Dixie-Lee, & Van Der Bliek, Alexander M. (2001). Dynamin-related protein DRP1 is required for mitochondrial division in mammalian cells. *Molecular biology of the cell, 12*(8), 2245-2256.

Song, Wenjun, Chen, Jin, Petrilli, Alejandra, Liot, Geraldine, Klinglmayr, Eva, Zhou, Yue, . . . Hayden, Michael R. (2011). Mutant huntingtin binds the mitochondrial fission GTPase dynamin-related protein-1 and increases its enzymatic activity. *Nature medicine, 17*(3), 377-382.

Stamler, Jonathan S, Lamas, Santiago, & Fang, Ferric C. (2001). Nitrosylation: the prototypic redox-based signaling mechanism. *Cell, 106*(6), 675-683.

Strack, S., Wilson, T. J., & Cribbs, J. T. (2013). Cyclin-dependent kinases regulate splice-specific targeting of dynamin-related protein 1 to microtubules. *J Cell Biol, 201*(7), 1037-1051. doi: 10.1083/jcb.201210045

Taguchi, Naoko, Ishihara, Naotada, Jofuku, Akihiro, Oka, Toshihiko, & Mihara, Katsuyoshi. (2007). Mitotic phosphorylation of dynamin-related GTPase DRP1 participates in mitochondrial fission. *Journal of Biological Chemistry, 282*(15), 11521-11529.

Teppola, Heidi, Sarkanen, Jertta-Riina, Jalonen, Tuula O, & Linne, Marja-Leena. (2016). Morphological differentiation towards neuronal phenotype of SH-SY5Y neuroblastoma cells by estradiol, retinoic acid and cholesterol. *Neurochemical research, 41*, 731-747.

Thapliyal, Shruti, Arendt, Kristin L, Lau, Anthony G, & Chen, Lu. (2022). Retinoic acid-gated BDNF synthesis in neuronal dendrites drives presynaptic homeostatic plasticity. *Elife, 11*, e79863.

Tondera, Daniel, Grandemange, Stéphanie, Jourdain, Alexis, Karbowski, Mariusz, Mattenberger, Yves, Herzig, Sébastien, . . . Merkwirth, Carsten. (2009). SLP-2 is required for stress-induced mitochondrial hyperfusion. *The EMBO journal, 28*(11), 1589-1600.

Uo, Takuma, Dworzak, Jenny, Kinoshita, Chizuru, Inman, Denise M, Kinoshita, Yoshito, Horner, Philip J, & Morrison, Richard S. (2009). DRP1 levels constitutively regulate mitochondrial dynamics and cell survival in cortical neurons. *Experimental neurology, 218*(2), 274-285.

Valenti, Daniela, Rossi, Leonardo, Marzulli, Domenico, Bellomo, Francesco, De Rasmo, Domenico, Signorile, Anna, & Vacca, Rosa Anna. (2017). Inhibition of DRP1-mediated mitochondrial fission improves mitochondrial dynamics and bioenergetics stimulating neurogenesis in hippocampal progenitor cells from a Down syndrome mouse model. *Biochimica et Biophysica Acta (BBA)-Molecular Basis of Disease, 1863*(12), 3117-3127.

Vantaggiato, Chiara, Castelli, Marianna, Giovarelli, Matteo, Orso, Genny, Bassi, Maria Teresa, Clementi, Emilio, & De Palma, Clara. (2019). The fine tuning of DRP1-dependent mitochondrial remodeling and autophagy controls neuronal differentiation. *Frontiers in Cellular Neuroscience, 13*, 120.

Verrigni, D., Di Nottia, M., Ardissone, A., Baruffini, E., Nasca, A., Legati, A., . . . Bertini, E. (2019). Clinical-genetic features and peculiar muscle histopathology in infantile DNM1L-related mitochondrial epileptic encephalopathy. *Hum Mutat, 40*(5), 601-618. doi: 10.1002/humu.23729

Vichai, Vanicha, & Kirtikara, Kanyawim. (2006). Sulforhodamine B colorimetric assay for cytotoxicity screening. *Nature protocols, 1*(3), 1112-1116.

Vonsattel, Jean Paul G, & DiFiglia, Marian. (1998). Huntington disease. *Journal of neuropathology and experimental neurology, 57*(5), 369.

Wakabayashi, Junko, Zhang, Zhongyan, Wakabayashi, Nobunao, Tamura, Yasushi, Fukaya, Masahiro, Kensler, Thomas W, . . . Sesaki, Hiromi. (2009). The dynamin-related GTPase DRP1 is required for embryonic and brain development in mice. *Journal of Cell Biology, 186*(6), 805-816.

Wang, Dadong, Lagerstrom, Ryan, Sun, Changming, Bishof, Leanne, Valotton, Pascal, & Götte, Marjo. (2010). HCA-vision: Automated neurite outgrowth analysis. *Journal of biomolecular screening, 15*(9), 1165-1170.

Wang, Lei, Ye, Xiaoying, Zhao, Qiang, Zhou, Zhongcheng, Dan, Jiameng, Zhu, Yushan, . . . Liu, Lin. (2014). DRP1 is dispensable for mitochondria biogenesis in induction to pluripotency but required for differentiation of embryonic stem cells. *Stem cells and development, 23*(20), 2422-2434.

Wang, Li, Tu, Zhidong, & Sun, Fengzhu. (2009). A network-based integrative approach to prioritize reliable hits from multiple genome-wide RNAi screens in Drosophila. *BMC genomics, 10*, 1-18.

Wasiak, Sylwia, Zunino, Rodolfo, & McBride, Heidi M. (2007). Bax/Bak promote sumoylation of DRP1 and its stable association with mitochondria during apoptotic cell death. *The Journal of cell biology, 177*(3), 439-450.

Wasilewski, Michał, & Scorrano, Luca. (2009). The changing shape of mitochondrial apoptosis. *Trends in Endocrinology & Metabolism, 20*(6), 287-294.

Waterham, Hans R, Koster, Janet, van Roermund, Carlo WT, Mooyer, Petra AW, Wanders, Ronald JA, & Leonard, James V. (2007). A lethal defect of mitochondrial and peroxisomal fission. *New England Journal of Medicine, 356*(17), 1736-1741.

Wenger, Julia, Klinglmayr, Eva, Fröhlich, Chris, Eibl, Clarissa, Gimeno, Ana, Hessenberger, Manuel, . . . Goettig, Peter. (2013). Functional mapping of human dynamin-1-like GTPase domain based on x-ray structure analyses. *PloS one, 8*(8), e71835.

Wolf, George. (2008). Retinoic acid as cause of cell proliferation or cell growth inhibition depending on activation of one of two different nuclear receptors. *Nutrition reviews, 66*(1), 55-59.

Wu, Qiong, Gao, Cheng, Wang, Haochen, Zhang, Xinmu, Li, Qianqian, Gu, Zhiya, . . . Chen, Xiping. (2018). Mdivi-1 alleviates blood-brain barrier disruption and cell death in experimental traumatic brain injury by mitigating autophagy dysfunction and mitophagy activation. *The International Journal of Biochemistry & Cell Biology, 94*, 44-55.

Yang, Xiaoyong, & Qian, Kevin. (2017). Protein O-GlcNAcylation: emerging mechanisms and functions. *Nature reviews Molecular cell biology, 18*(7), 452-465.

Yaworsky, Paul J, & Kappen, Claudia. (1999). Heterogeneity of neural progenitor cells revealed by enhancers in the nestin gene. *Developmental biology, 205*(2), 309-321.

Yu, Rong, Lendahl, Urban, Nistér, Monica, & Zhao, Jian. (2020). Regulation of mammalian mitochondrial dynamics: opportunities and challenges. *Frontiers in endocrinology, 11*, 534124.

Yu, Young-Mi, Han, Pyung-Lim, & Lee, Ja-Kyeong. (2003). JNK pathway is required for retinoic acid-induced neurite outgrowth of human neuroblastoma, SH-SY5Y. *Neuroreport, 14*(7), 941-945.

Zerihun, Mulate, Sukumaran, Surya, & Qvit, Nir. (2023). The DRP1-mediated mitochondrial fission protein interactome as an emerging core player in mitochondrial dynamics and cardiovascular disease therapy. *International Journal of Molecular Sciences, 24*(6), 5785.

Zhang, Bing, Zhang, Yuwei, Zuo, Zhenzi, Xiong, Guiya, Luo, Huan, Song, Bo, . . . Chang, Xiuli. (2023). Paraquat-induced neurogenesis abnormalities via DRP1-mediated mitochondrial fission. *Ecotoxicology and Environmental Safety, 257*, 114939.

Zhang, Huiliang, Wang, Pei, Bisetto, Sara, Yoon, Yisang, Chen, Quan, Sheu, Shey-Shing, & Wang, Wang. (2016). A novel fission-independent role of dynamin-related protein 1 in cardiac mitochondrial respiration. *Cardiovascular research*, cvw212.

Zhao, Yuanyuan, Sun, Xiaoyan, & Qi, Xin. (2018). Inhibition of DRP1 hyperactivation reduces neuropathology and behavioral deficits in zQ175 knock-in mouse model of Huntington's disease. *Biochemical and biophysical research communications, 507*(1-4), 319-323.

Zhou, Lujun, Zhang, Qiang, Zhang, Peng, Sun, Lei, Peng, Can, Yuan, Zengqiang, & Cheng, Jinbo. (2017). c-Abl-mediated DRP1 phosphorylation promotes oxidative stress-induced mitochondrial fragmentation and neuronal cell death. *Cell death & disease, 8*(10), e3117-e3117.

Zhou, Xiangyue, Chen, Hanmin, Wang, Ling, Lenahan, Cameron, Lian, Lifei, Ou, Yibo, & He, Yue. (2021). Mitochondrial dynamics: a potential therapeutic target for ischemic stroke. *Frontiers in Aging Neuroscience, 13*, 721428.

Zhu, Peng-Peng, Patterson, Andrew, Stadler, Julia, Seeburg, Daniel P, Sheng, Morgan, & Blackstone, Craig. (2004). Intra-and intermolecular domain interactions of the C-terminal GTPase effector domain of the multimeric dynamin-like GTPase DRP1. *Journal of Biological Chemistry, 279*(34), 35967-35974.

Zunino, Rodolfo, Schauss, Astrid, Rippstein, Peter, Andrade-Navarro, Miguel, & McBride, Heidi M. (2007). The SUMO protease SENP5 is required to maintain mitochondrial morphology and function. *Journal of cell science, 120*(7), 1178-1188.

Appendix

This thesis is based on the following publications:

UNIVERSITY AND NATIONAL LIBRARY
UNIVERSITY OF DEBRECEN
H-4002 Egyetem tér 1, Debrecen
Phone: +3652/410-443, email: publikaciok@lib.unideb.hu

Registry number: DEENK/323/2024.PL
Subject: PhD Publication List

Candidate: Marvi Ghani
Doctoral School: Doctoral School of Molecular Medicine

List of publications related to the dissertation

1. **Ghani, M.**, Szabó, B., Alkhatibe, M., Amsalu, H., Zohar, P., Janka, E. A., Mótyán, J. A., Tar, K.: Serine 39 in the GTP-binding domain of Drp1 is involved in shaping mitochondrial morphology.
   FEBS Open Bio. [Epub ahead of print], 2024.
   DOI: http://dx.doi.org/10.1002/2211-5463.13820
   IF: 2.6 (2022)
2. **Ghani, M.**, Zohar, P., Ujlaki, G., Tóth, M., Amsalu, H., Póliska, S., Tar, K.: Stable knockdown of Drp1 improves retinoic acid-BDNF-induced neuronal differentiation through global transcriptomic changes and results in reduced phosphorylation of ERK1/ 2 independently of DUSP1 and 6.
   Front. Cell. Dev. Biol. 12, 1-25, 2024.
   DOI: http://dx.doi.org/10.3389/fcell.2024.1342741
   IF: 5.5 (2022)

List of other publications

3. Ullah, H., Ihsan, J., Mohamed, R. M. K., Khan, M. A., **Ghani, M.**, Rauf, N., Ullah, S., Javed, A., Farooq, M.: Bionanocomposite scaffolds based on MnS-nanorods loaded acacia-Senegal-gum hydrogels: Fabrication, characterization and biological evaluation.
   Bioactive Carbohydrates and Dietary Fibre. 30, 1-9, 2023.
   DOI: http://dx.doi.org/10.1016/j.bcdf.2023.100368
4. Khalil, I., **Ghani, M.**, Khan, M. R., Akbar, F.: Evaluation of biological activities and in vivo amelioration of CCl4 induced toxicity in lung and kidney with Abutilon pannosum (G.Forst.) Schltdl. in rat.
   J. Ethnopharmacol. 249, 1-14, 2020.
   DOI: http://dx.doi.org/10.1016/j.jep.2019.112395
   IF: 4.36

UNIVERSITY of DEBRECEN

UNIVERSITY AND NATIONAL LIBRARY
UNIVERSITY OF DEBRECEN
H-4002 Egyetem tér 1, Debrecen
Phone: +3652/410-443, email: publikaciok@lib.unideb.hu

5. Aladdin, A., Yao, Y., Yang, C., Kahlert, G., **Ghani, M.**, Király, N., Boratkó, A., Uray, K., Dittmar, G., Tar, K.: The Proteasome Activators Blm10/PA200 Enhance the Proteasomal Degradation of N-Terminal Huntingtin.
Biomolecules. 10 (11), 1-33, 2020.
DOI: http://dx.doi.org/10.3390/biom10111581
IF: 4.879

6. Khalil, I., Khan, M. R., **Ghani, M.**, Akbar, F.: Abutilon pannosum stem bark enhances the aphrodisiac activities and spermatogenesis in rat.
Andrologia. 51 (10), 1-11, 2019.
DOI: http://dx.doi.org/10.1111/and.13404
IF: 1.951

Total IF of journals (all publications): 19,29
Total IF of journals (publications related to the dissertation): 8,1

The Candidate's publication data submitted to the iDEa Tudóstér have been validated by DEENK on the basis of the Journal Citation Report (Impact Factor) database.

30 May, 2024

DEBRECENI EGYETEM * Egyetemi és Nemzeti Könyvtár *